

Acid Sulfate Soils Research Program

Lower Lakes Hydro-Geochemical Model Development
and Assessment of Acidification Risks

Report 6 | Part 1 of 4 | October 2010



For further information please contact:

Email: customerservice@sawater.com.au
Phone: 1300 650 950
Post: SA Water
GPO Box 1751
ADELAIDE SA 5001
Website: <http://www.sawater.com.au>

Permissive licence

© State of South Australia through SA Water.

Apart from fair dealings and other uses permitted by the *Copyright Act 1968* (Cth), no part of this publication may be reproduced, published, communicated, transmitted, modified or commercialised without the prior written approval of SA Water.

Written requests for permission should be addressed to:

SA Water
GPO Box 1751
ADELAIDE SA 5001
customerservice@sawater.com.au

Disclaimer

This report has been prepared by consultants for SA Water and views expressed do not necessarily reflect those of SA Water. SA Water cannot guarantee the accuracy of the report, and does not accept liability for any loss or damage incurred as a result of relying on its accuracy.

Printed on recycled paper
October 2010
ISBN 978-1-921735-13-4

Citation

This report should be cited as:
Hipsey, M.R., Bursch, B.D., Coletti, J. and Salmon, S.U. 2010, *Lower Lakes hydro-geochemical model development and assessment of acidification risks*. Prepared by University of Western Australia for SA Water, Adelaide.

Cover image

Boggy Lake, March 2009 (DENR 2009)

Lower Lakes Hydro-geochemical Model Development and Assessment of Acidification Risks

M. Hipsey, B. Bursch, J. Coletti, and S. Salmon

Prepared by University of Western Australia for SA Water. Part of the South Australian Government's \$610 million Murray Futures program funded by the Australian Government's Water for the Future initiative, and the Murray-Darling Basin Authority

October 2010



Executive Summary

It is now well established that acid sulfate soils around the margin of the River Murray Lower Lakes (Lake Alexandrina and Lake Albert, South Australia) are extensive and that the risk of damage to the ecosystem is being exacerbated by continued low flow conditions. The aim of this study was to undertake spatially-resolved hydro-geochemical modelling of historical conditions and various future scenarios related to the drying and rewetting of acid sulfate soils throughout the Lower Lakes region. This was conducted in order to better understand the key dynamics of acid sulfate soil material and its influence on lake biogeochemistry, and to assess the potential benefit of water level stabilisation and/or flooding by supplementing with freshwater or seawater.

Whilst acidification of lake ecosystems has been previously documented around the world, and attributed to various underlying mechanisms, the present case of acidification of the Murray Lower Lakes is unprecedented. The rate of water level change and amount of potentially oxidisable sulfidic minerals have meant that to date no comprehensive model of acid sulfate soils relevant to lake ecosystems has been developed. The challenges of the present project were to develop such a model, which is able to spatially resolve acid sulfate soil dynamics whilst also accounting for lake hydrodynamics and key biogeochemical processes, and for the coupled model to be able to simulate multiple years of management scenarios.

To meet this aim, an existing three-dimensional (3D) lake hydrodynamic-biogeochemical model (ELCOM-CAEDYM) was coupled with a soil hydro-geochemical model suited to simulation of acid sulfate soils. The newly developed soil hydro-geochemical model adopts a simplified vertical representation, but is computationally efficient and therefore able to be applied spatially, and dynamically linked with the 3D lake hydrodynamic-biogeochemical model. Since the vertical structure of acid sulfate soils can not be overly simplified due to the importance of the unsaturated zone soil moisture profiles and the variability of pyrite with depth on acidity dynamics, the present approach does not entirely lump vertical processes into an averaged unit, but instead resolves the vertical profile in a simplified manner that avoids the full Richard's equation solution. Horizontal processes are also simplified by adopting a simple conceptual model that is built from the results of a more detailed 2D Richard's equation model (HYDRUS-2D). The model geochemical parameterisations and parameter values were developed based around data and process information generated from concurrently run Lower Lakes acid sulfate soil research projects. These provided necessary information on the spatial variability of soil properties and actual and net acidity, oxidation rates, moisture content of exposed sediment, acid flux mechanisms and rates, and neutralisation processes.

The model presented here is therefore unique in its ability to meet the project objectives and is able to resolve:

- 3D hydrodynamics, including prediction of circulation patterns, inflows (including pumping and seawater entrance), wetting and drying, temperature, salinity, surface thermodynamics and evaporation;
- 2D spatially variable specification of soil texture and geochemistry, which allows for heterogeneity in soil hydraulic properties, pyrite content, and acid neutralising capacity at high-resolution (100–250m);
- Vertically resolved pyrite oxidation reaction kinetics in exposed cells based on dynamically predicted moisture content profiles, and subsequent neutralisation kinetics;
- Estimation of acidity flux to the surface water following re-wetting of exposed cells, and also from overland flow and seepage processes;
- Buffering of water pH by lake and river alkalinity, and approximation of alkalinity generation by organic matter decomposition in submerged sediments.

The coupled model, termed ELCOM-CAEDYM-ASS, was configured on a range of model sub-domains, representing Lake Alexandrina, Lake Albert and also a high-resolution domain for the Currency Creek, Finniss River and Goolwa Channel region. The simulated variables in all domains were identical and included velocity, temperature, salinity, nutrients, algae, major ions, pH and alkalinity, and solid phase precipitates. The acid sulfate soil module parameters were defined, where possible, based on the associated research programs, or otherwise literature or assumed values were adopted. The model was validated for the period from Jan 2008 – Sept 2009 against a large variety

of parameters, most of which were available for the water column, and to a lesser extent for the soil conditions.

Generally, the model performed well against lake physical properties (water level, temperature and salinity) in each of the domains, and the behaviour of oxygen and conservative ions were also accurately captured. The nutrients and chlorophyll-a values were reasonably well predicted although there were seasonal or site-specific errors that could be improved given continued calibration. The pH and alkalinity dynamics were also well predicted in cases where no acidification was reported. In areas where acidification has been reported, the model was competent in predicting when and where pH would fall, particularly in the main Currency Creek tributary area in 2009. There were some areas that were predicted to acidify in the model that were not observed to acidify in reality, and this highlights the uncertainty in the model predictions and that the application of the model should be applied within an adaptive monitoring framework, and not used in isolation.

Further qualitative information is presented where possible to support the model results, in an attempt to limit uncertainty. Aside from the model structural uncertainty and uncertainty in defining the key parameters, the model is also highly sensitive to the spatial data on soil type and chemistry that is used to drive the predictions. Significant error or simplification in representing these properties needs to also be considered when interpreting the results. Nonetheless, the model predictions are considered reasonably accurate and provide a significant improvement on previous estimates of risk the lakes face due to acid sulfate soils.

To investigate the different future states of the lake for a range of drying-flooding cycles, the model has then been used to forecast the lake conditions from Oct 2009 – Jan 2013. The results were used to recommend a water management target level for both Lake Alexandrina and Lake Albert. The scenarios included sourcing extra water (above the minimum flow allocation to the lakes) from either increased freshwater allocation to the lakes, or alternatively from the Coorong and Murray Mouth region by opening part of Tauwitchere barrage. Although the acid sulfate soil module is sensitive to variations in salinity due to its effect on acidity diffusion during re-flooding, the impact of flooding with seawater as opposed to freshwater did not greatly increase the risk of acidification, but did lead to high salinities, often above that of seawater.

The outputs of the model suggest that the amount of pyrite in exposed soil that is able to oxidise is potentially orders of magnitude larger than that able to cause water body acidification, however limitations on the oxidation rate, and transport of acidity to the lakes introduce complexities in interpreting the time, or water level, where acidification risk becomes unacceptably high.

In this study the rate of oxidation was generally found to be high enough to generate ample acidity to create management problems, however the dominance of vertical transport processes and the slowly moving groundwater meant that the dynamics of the soil hydrology are of critical importance in determining the predicted outcome. In particular, it is predicted that large threshold rain events overwhelm the vertical percolation rate, which generates temporary ponding and throughflow processes and lead to delivery of large loads of acidity to the lake boundaries. These large events typically occur infrequently, and since they are the dominant mechanisms controlling the acidity flux to the lake, it implies that that acidification is very much related to the time of year that the acidity is flushed from the exposed soil by rainfall, regardless of the water level at that time. The role of acidity diffusion into the water column following re-flooding of acidified clays, particularly in Lake Albert, was also identified as a potentially significant loading mechanism, and therefore assessment of trigger levels must not only consider the dynamics during drawdown, but also during refill.

For Lake Albert, the lake became acidic for all model simulations where the water level went below -1.0 m AHD. Sensitivity testing of the model did not significantly change this outcome. Stabilisation at -0.75m AHD and -0.5m AHD appeared to prevent any large scale deterioration until the end of 2012. However, pH instabilities at the lake margins were observed even at -0.5m AHD. This is also reflected in the observational record of soil and water acidification in localised areas around the lake margins over the winter of 2009. Based on these modelling results the key management recommendation to prevent lake acidification is to maintain water levels above -0.75m AHD in Lake Albert.

For Lake Alexandrina, the main lake body maintained neutral pH and sufficient alkalinity until the end of 2012 for all stabilisation and drawdown scenarios. However, the model did indicate several issues that need to be considered in forming an appropriate management strategy:

1. The northern region shows temporary acidification during continued lake drawdown beginning in May 2010, (this has since been confirmed to occur through EPA monitoring);
2. Seawater entrance does create some minor acidification in the southern reach of the lake around Point Sturt, and alkalinity declined over the whole lake area more than during

freshwater stabilisation. Seawater salinities are rapidly established across the whole lake area in the -1.0m AHD water level stabilisation scenario and areas of hyper-salinity develop.

3. A high accumulation of acidic material in the soil occurs with a lag in delivery of the acidity in shallow groundwater becoming a possibility. This indicates that water quality in longer simulations beyond 2012 may eventually deteriorate if levels were maintained below -1.75m. Longer term simulations that were run as part of the seawater Environmental Impact Statement (reported separately) confirm this.

Based on these considerations, the key management recommendation to prevent large-scale whole lake acidification is to maintain water levels above -1.75m AHD in Lake Alexandrina. However, fringing waterbody regions above this level with poor connection to the lake will potentially continue to acidify in response to rainfall.

In all simulations conducted, the area of sulfuric soil continues to expand until stabilisation and acidity levels in the soil remain very high despite ongoing fluxes to the lake due to a large reservoir of accumulated acidity in the oxidised soil profile. There is therefore likely to be a soil hazard that will continue to remain around the margins of the lake with significant impacts on lake ecology.

Further, while the focus of this report has been towards acidity/alkalinity and pH, traditional water quality problems such as elevated nutrients, very high algal concentrations, and reduced clarity will become a persistent feature even at the recommended management levels.

Recommendations for future monitoring, model development and further research into key acid sulfate soil processes are also discussed.

Table of Contents

Executive Summary	ii
1 Project overview	1
2 Aims	1
3 Introduction and background	1
3.1 Introduction	1
3.2 Overview of factors affecting acidity flux to surface waters	2
Definition of solution acidity	3
Soil Acid Base Accounting (ABA)	3
3.3 Controls on acid sulfate soil dynamics	4
O ₂ diffusion limitation on oxidation rates (Figure 3.1, Process 1)	4
Acid-generating oxidation reactions (Figure 3.1, Process 2)	4
Acidity neutralisation (Figure 3.1, Process 3 and 4)	5
Solubility controls	5
Interactions between the soil and the water body	6
3.4 Review of models and modelling approaches for simulation of acid sulfate soils	6
Theoretical basis for unsaturated zone model framework	6
HP1	8
LEACHM	10
UZFL & MODFLOW	11
ACID3D	11
SMASS	11
CAEDYM geochemical & diagenetic model	13
4 Model description	16
4.1 Model platform	16
4.2 Acid sulfate soil model and parameterisation	17
Overview and assumptions	17
Soil hydrology	20
Acidity generation	23
Fluxes	25
4.3 2D lake cross section HYDRUS model	26
Model Approach:	27
Validation	28
Seepage Rate	28
Seepage relationship to soil water storage	30
5 Model setup and application to the Lower Lakes	33
5.1 Model configuration and simulated variables	33
5.2 Application to Lake Albert	39
5.3 Application to Lake Alexandrina	43
5.4 Application to Currency Creek and Finniss River region	46
6 Model validation	50
6.1 Lake Albert: validation (Jun 2008 – Sep 2009)	50
Lake physical properties	50
Nutrients and Chl-a	51
Lake geochemistry	51
6.2 Lake Alexandrina (River Murray-Clayton): validation (Jan 2008 – Sep 2009)	63
Lake physical properties	63
Nutrients and Chl-a	63
Lake Geochemistry	63

6.3	Lake Alexandrina (Clayton-Goolwa): validation (Jan 2008 – Sep 2009)	87
	Hydrodynamics	87
	Nutrients and Chl-a	87
	Lake Geochemistry	87
	Soil Dynamics.....	99
7	Scenario analysis.....	108
7.1	Lake Albert: drawdown scenarios and analysis (Sep 2009 – Sep 2013)	108
	Lake Albert water quality forecast	108
	Lake Albert acid sulfate soil dynamics.....	118
7.2	Lake Alexandrina: drawdown scenarios and analysis (Sep 2009 – Sep 2013)	130
	Lake Alexandrina water quality forecast	130
	Lake Alexandrina acid sulfate soil analysis.....	144
7.4	Recommendations for water level stabilisation	155
	Lake Albert.....	155
	Lake Alexandrina.....	155
8	Conclusions.....	157
8.1	Model development and validation.....	157
8.2	Recommendations for management.....	158
8.3	Recommendations for further research.....	159
9	References.....	160
A1	Appendix 1: Sensitivity analysis of key model processes.....	163

List of Tables

Table 3.1: Summary of important processes to be considered within the acid sulfate soil modelling framework and methods required to generate the necessary data required for model parameterisation.	7
Table 4.1: Overview of literature pyrite oxidation rates	24
Table 4.2: Summary of seepage rates and flow parameters for different model configurations	31
Table 5.1: Simulated variable list and descriptions.	34
Table 5.2: Overview of acid sulfate soil model parameters and justifications.....	36
Table A1.1: Summary of simulations run for sensitivity testing and uncertainty estimation. In this table '0' implies a median parameter value used and '+' / '++' / '+++' indicates successive increases and conversely '-' indicates a decrease.....	163

List of Figures

Figure 3.1: a) Processes involved in acidity generation and fate as lake water levels recede, b) additional process upon re-wetting of previously exposed sediments: diffusive transport of stored acidity back into the water column.	3
Figure 3.2: Schematic of the sequential modelling approach used by HP1 (taken from Jacques and Simunek, 2005). Symbols: n the nth time step, H variables related to water flow (pressure heads, fluxes), T variables concerning heat transport (temperature), C variables dealing with components and species in the system, G variables concerning the solid phase (mineralogical composition, exchange site, surface site, reactive surfaces), p^w vector of parameters needed to solve the water flow equation, p^h vector of parameters needed to solve the heat transport equation, p^s vector of parameters needed to solve the solute transport equation, p^{gc} vector of parameters needed to solve the geochemical reactions.	10
Figure 3.3: Example of a simulated two dimensional steady-state oxygen concentration profile in a structured acid sulphate soil; C_w = oxygen concentration in water ($\text{kg O}_2 \text{ m}^{-3}$ water), C_a = concentration of oxygen in air-filled macropores ($\text{m}^3 \text{ O}_2 \text{ m}^{-3}$ air), $r\phi$ = thickness of the anaerobic zone (m) (taken from Bronswijk and Groenenberg, 2004).	12
Figure 3.4: Overview of the operation of the SMASS model (taken from Bronswijk and Groenenberg, 1993).	12
Figure 3.5: Conceptual view of ELCOM-CAEDYM simulation run to include the dynamic diagenesis model (taken from Hipsey and Hamilton, 2008).	14
Figure 3.6: Conceptual ASS model of acid generation and transport (taken from Hipsey and Salmon, 2008).	15
Figure 4.1: Conceptual model of acid generation and transport processes for the drying phase (top) and the wetting phase (bottom). Notation: E = evaporation; R = rainfall; Q = general inflows coming to the lake; SO_4 = dissolved sulfate concentration; OM = organic matter; Fe_{d} = dissolved iron; Mn_{d} = dissolved manganese; θ = soil moisture; O_2 = oxygen concentration; Q_{se} = saturation excess flow; Q_{ss} = seepage flow; R_{SO_4} = acidity consumption via SO_4 reduction; R_{ox} = pyrite oxidation; F_{SO_4} = acidity consumption by SO_4 reduction in lake sediments; λ_{rw} = flux of acidity from acidified sediment following rewetting.	19
Figure 4.2: Soil unit hydro-geochemical model. Notation: E = evaporation; R = rainfall; UZ = unsaturated zone; SZ = saturated zone; h_{sat} = depth of unsaturated zone, h_{ep} = depth of influence of evaporation; Z_{lake} = lake water level; Q_{se} = saturation excess flow; Q_{ss} = seepage flow; PASS = potential acid sulfate soil material (χ); θ = soil moisture; θ_{fc} = soil field capacity; ϕ_{UZ} = unsaturated zone available acidity (UZAASS); ϕ_{SZ} = saturated zone available acidity (SZAASS).	20
Figure 4.3: Conceptual basis (a & b) of vertical moisture profile (taken from Lu and Likos, 1994), and outline of vertical moisture profile model implementation (c) that is used to resolved vertical moisture dynamics in the soil hydrology model.	22
Figure 4.3: Range of pyrite oxidation rates from literature laboratory weathering experiments on acid sulfate soils and sediments (see Table 4.1 for details), vs. the sulfide content of the material. Red box indicated approximate range originally tested in Hipsey and Salmon (2008) Lower Lakes acid sulfate soil model.	24
Figure 4.4: Schematic diagram outlining hydro-geological setting of lake shore zone on which the numerical domain was configured.	27
Figure 4.5: Boundary conditions (lake level at -1m).	28
Figure 4.6: Soil material distribution throughout the cross section area.	28
Figure 4.7: Location of moisture content and pressure head calibration points in the domain (red dots).	29
Figure 4.8: Field data and predicted moisture content (% volume).	29
Figure 4.9: Field data and predicted soil pressure head. In the model, the observation points were located at 3, 2.1 and 2.6m below the initial water table.	29
Figure 4.10: Seepage flow ($\text{m}^2 \text{ day}^{-1}$) and pressure head (m) calculated for the period between January 1 st (day 0) and September 2009 (day 250). The rate is $\text{m}^3 \text{ day}^{-1}$ if a 1m width cross-section is assumed.	30
Figure 4.11: Reference point for pressure head when lake level is constant and equal to -1m.	30

Figure 4.12: Relationship between seepage flow ($\text{m}^2 \text{ day}^{-1}$) and pressure head (m) taken from a single point calculated for the period between January 1 st (day 0) and September 2009 (day 250). The rate is $\text{m}^3 \text{ day}^{-1}$ if a 1m width cross-section is assumed.	31
Figure 4.13: Relationship between seepage fraction (day^{-1}) and non-dimensional storage capacity of the sand above the clay lens for points taken in the period between January 1 st (day 0) and September 2009 (day 250), assuming $K_s = 1.0 \text{ m day}^{-1}$	32
Figure 4.14: Relationship between seepage fraction (day^{-1}) and non-dimensional storage capacity of the sand above the clay lense for points taken in the period between January 1 st (day 0) and September 2009 (day 250), assuming $K_s = 0.5 \text{ m day}^{-1}$	32
Figure 4.15: Relationship between seepage fraction (day^{-1}) and non-dimensional storage capacity of the sand above the clay lense for points taken in the period between January 1 st (day 0) and September 2009 (day 250), assuming $K_s = 1.5 \text{ m day}^{-1}$	32
Figure 5.1: Conceptual outline of the coupled hydrodynamics-biogeochemical-acid sulfate soil model as configured to the Lower Lakes simulations.	33
Figure 5.2: Lake Albert ELCOM bathymetry, pixel size is the grid resolution of 200x200m.	40
Figure 5.3: Comparison of wind direction data between weather stations located at a) Pelican Point (south of Lake Albert) and b) Narrung (north-west of Lake Albert).	40
Figure 5.4: Comparison of wind speed data between weather stations located at a) Pelican Point (south of Lake Albert) and b) Narrung (north-west of Lake Albert). Mean values for the two wind stations were 3.91 and 3.43 m/s respectively over the time period Jun 2008 – Sept 2009.	41
Figure 5.5: Solar radiation and net radiation data from Hindmarsh Valley (top panels) and air temperature and relative humidity from the SA MDB NRM Narrung weather station from January 2008 – September 2009.	41
Figure 5.6: Comparison of model soil classification map.	42
Figure 5.7: Vertical profiles of acid generating potential (AGP, left) and acid neutralising capacity (ANC, right) estimated from available core information from Lake Albert. Data compiled by Earth Systems (2010).	42
Figure 5.8: Time-series of pumping rate between Lake Alexandrina and Lake Albert, conducted at Narrung.	43
Figure 5.9: ELCOM bathymetric grids configured (a-c) and soil property specifications (d-f).	44
Figure 5.10: Vertical profiles of acid generating potential (AGP, left) and acid neutralising capacity (ANC, right) estimated from averaging available soil core information from Lake Alexandrina. Data compiled by Earth Systems (2010).	45
Figure 5.11: Inflow and outflow boundary condition time-series used in the Lake Alexandrina hindcast (before dashed grey line) and forecast (after dashed grey line) simulations.	45
Figure 5.12: Model bathymetry for high-resolution (100 × 100m) Currency Creek and Finniss River domain, showing the boundary forcing locations, the open boundary connection point with the main Lake Alexandrina domain, and the sampling locations (●) used to validate the model.	46
Figure 5.13a: Time-series water quality attributes used for the Finniss River boundary condition. Note a lack of data prior to Jan 2009 and constant values used for 2008.	47
Figure 5.13b: Time-series of water quality attributes used for the Currency Creek boundary condition. Note a lack of data prior to Jan 2009 and constant values used for 2008.	47
Figure 5.13c: Time-series of water quality attributes used for the open boundary connection with the main lake. Data extracted from profile output point from the Lake Alexandrina (AA) model simulation.	48
Figure 5.14: Currency Creek meteorological station data used in the validation sub-domain.	48
Figure 5.15: Soil property specifications.	49
Figure 5.16: Vertical profiles of acid generating potential (AGP, left) and acid neutralising capacity (ANC, right) estimated from available core information from Lake Albert. Data compiled by Earth Systems (2010).	49
Figure 6.1: Locations of various output reporting locations in Lake Alexandrina and Lake Albert. The EPA points (19 circles) are routine sampling locations for water quality parameters by the South Australian Environmental Protection Authority (EPA) which are the focus of this assessment. The DENR points (squares) are additional output points not presented in this report but have been provided for further ecological risk assessment. Plot adapted from BMTWBM (2010).	50
Figure 6.1: Comparison of modelled (yPP and nPP) and measured (EPA and DFW) water temperature and salinity (expressed as electrical conductivity at 25°C) for four stations within Lake Albert.	52

Figure 6.2: Comparison of modelled (yPP and nPP) and measured (EPA) DO (mg L ⁻¹) and DOC (mg C L ⁻¹) for four stations within Lake Albert.....	53
Figure 6.3: Comparison of modelled (yPP and nPP) and measured (EPA) NH ₄ (mg N L ⁻¹) and NO ₃ (mg N L ⁻¹) for four stations within Lake Albert. Note that the NO ₃ /NH ₄ results were often below detection limit.....	54
Figure 6.4: Comparison of modelled (yPP and nPP) and measured (EPA) TN (mg N L ⁻¹) and PO ₄ (mg P L ⁻¹) for four stations within Lake Albert. Note that the PO ₄ results were often below detection limit.....	55
Figure 6.5: Comparison of modelled (yPP and nPP) and measured (EPA) TP (mg P L ⁻¹) and total Chlorophyll-a (ug Chla L ⁻¹) for four stations within Lake Albert.....	56
Figure 6.6: Comparison of modelled (yPP and nPP) and measured (EPA) DIC (expressed as alkalinity in terms of mg CaCO ₃ L ⁻¹) and Ca (mg L ⁻¹) for four stations within Lake Albert.....	57
Figure 6.7: Comparison of modelled (yPP and nPP) and measured (EPA) Cl (mg L ⁻¹) and Na (mg L ⁻¹) for four stations within Lake Albert.....	58
Figure 6.8: Comparison of modelled (yPP and nPP) and measured (EPA) Mg (mg L ⁻¹) and SO ₄ (mg L ⁻¹) for four stations within Lake Albert.....	59
Figure 6.9: Comparison of modelled (yPP and nPP) and measured (EPA and DFW) pH (-) and CHGBAL for four stations within Lake Albert.....	60
Figure 6.10: Comparison of modelled (yPP and nPP) and measured (EPA) dissolved Al (mg L ⁻¹) and dissolved Mn (mg L ⁻¹) for four stations within Lake Albert.....	61
Figure 6.11: Comparison of modelled (yPP and nPP) and measured (EPA) dissolved Fe (mg L ⁻¹) for four stations within Lake Albert.....	62
Figure 6.12: Plot of modelled surface acidity (mol H ⁺ m ⁻²) taken in Sep 2009. Spatial distribution compares favourably with Fitzpatrick et al. (2010) TAA and surface soil pH maps.....	62
.....	62
Figure 6.13: Comparison of modelled (Val) and measured (DFW) surface water elevation (mAHD) for 15 stations in Lake Alexandrina from the River Murray entrance to Clayton.....	64
Figure 6.14: Comparison of modelled (Val) and measured (DFW and EPA) temperature data (°C) for 15 stations in Lake Alexandrina from the River Murray entrance to Clayton.....	65
Figure 6.15: Comparison of modelled (Val) and measured (DFW and EPA) salinity/EC data (uS cm ⁻¹) for 15 stations in Lake Alexandrina from the River Murray entrance to Clayton.....	66
Figure 6.16: Comparison of modelled (Val) and measured (SAWater profile data, PRO) dissolved oxygen data (mg L ⁻¹) for 15 stations in Lake Alexandrina from the River Murray entrance to Clayton.....	67
Figure 6.17: Comparison of modelled (Val) and measured (EPA) dissolved organic carbon (DOCL) data (mg C L ⁻¹) for 15 stations in Lake Alexandrina from the River Murray entrance to Clayton.....	68
Figure 6.18: Comparison of modelled (Val) and measured (EPA) ammonium (NH ₄) data (mg N L ⁻¹) for 15 stations in Lake Alexandrina from the River Murray entrance to Clayton.....	69
Figure 6.19: Comparison of modelled (Val) and measured (EPA) nitrate+nitrite (NO ₃) data (mg N L ⁻¹) for 15 stations in Lake Alexandrina from the River Murray entrance to Clayton. Note that the NO ₃ results were often below detection limit.....	70
Figure 6.20: Comparison of modelled (Val) and measured (EPA) total nitrogen (TN) data (mg N L ⁻¹) for 15 stations in Lake Alexandrina from the River Murray entrance to Clayton.....	71
Figure 6.21: Comparison of modelled (Val) and measured (EPA) ortho-phosphate (PO ₄) data (mg P L ⁻¹) for 15 stations in Lake Alexandrina from the River Murray entrance to Clayton. Note that the PO ₄ results were often below detection limit.....	72
Figure 6.22: Comparison of modelled (Val) and measured (EPA) total phosphorus (TP) data (mg P L ⁻¹) for 15 stations in Lake Alexandrina from the River Murray entrance to Clayton.....	73
Figure 6.23: Comparison of modelled (Val) and measured (EPA) chlorophyll-a (TCHLA) data (µg chl-a L ⁻¹) for 15 stations in Lake Alexandrina from the River Murray entrance to Clayton.....	74
Figure 6.24: Comparison of modelled (Val) and measured (EPA) dissolved carbonate alkalinity (DIC) data (mg CaCO ₃ L ⁻¹) for 15 stations in Lake Alexandrina from the River Murray entrance to Clayton.....	75
Figure 6.25: Comparison of modelled (Val) and measured (EPA) calcium (Ca) data (mg L ⁻¹) for 15 stations in Lake Alexandrina from the River Murray entrance to Clayton.....	76
Figure 6.26: Comparison of modelled (Val) and measured (EPA) chloride (Cl) data (mg L ⁻¹) for 15 stations in Lake Alexandrina from the River Murray entrance to Clayton.....	77

Figure 6.27: Comparison of modelled (Val) and measured (EPA) magnesium (Mg) data (mg L ⁻¹) for 15 stations in Lake Alexandrina from the River Murray entrance to Clayton.....	78
Figure 6.28: Comparison of modelled (Val) and measured (EPA) sodium (Na) data (mg L ⁻¹) for 15 stations in Lake Alexandrina from the River Murray entrance to Clayton.....	79
Figure 6.29: Comparison of modelled (Val) and measured (EPA) sulphate (SO ₄) data (mg SO ₄ L ⁻¹) for 15 stations in Lake Alexandrina from the River Murray entrance to Clayton.....	80
Figure 6.30: Comparison of modelled (Val) and measured (EPA) pH data for 15 stations in Lake Alexandrina from the River Murray entrance to Clayton.....	81
Figure 6.31: Comparison of modelled (Val) and measured (EPA) dissolved aluminium (Al) data (mg L ⁻¹) for 15 stations in Lake Alexandrina from the River Murray entrance to Clayton.....	82
Figure 6.32: Comparison of modelled (Val) and measured (EPA) dissolved ferrous iron (FeII) data (mg L ⁻¹) for 15 stations in Lake Alexandrina from the River Murray entrance to Clayton. Note that the FeII results were often below detection limit.....	83
Figure 6.33: Comparison of modelled (Val) and measured (EPA) reduced manganese (MnII) data (mg L ⁻¹) for 15 stations in Lake Alexandrina from the River Murray entrance to Clayton. Note that the MnII results were mostly below detection limit.....	84
Figure 6.34: Comparison of modelled (Val) and measured (EPA & DFW) pH for 8 stations in Lake Alexandrina from within the Clayton to Goolwa sub-region. Note that this is modelled using the coarse Lake Alexandrina domain (AA) and the high resolution Currency Creek validation is presented in Section 6.3.....	85
Figure 6.35a: Plot of modelled surface soil acidity (mol H ⁺ m ⁻²) taken in Dec 2009. Spatial distribution qualitatively compares favourably with Fitzpatrick et al. (2010) TAA and surface soil pH maps.....	85
Figure 6.35b: Plot of modelled pH taken in May 2010. The water was observed to acidify (to ~pH=2.5) in the northern region (Boggy Lake) in May 2010, one week after this predicted occurrence by the model. Note that this plot is from the continued drawdown scenario simulation that extended beyond the September 2009 simulations reported throughout this section and therefore has assumed flow and meteorological conditions for 8 months prior to this plot.....	86
Figure 6.36: Comparison of modelled (23f) and measured (LWA, EPA & CCF) water level for 8 stations between Clayton and Goolwa (refer to Figure 5.10 for locations).....	88
Figure 6.37: Comparison of modelled (23f) and measured (LWA, EPA & CCF) temperature (°C) for 8 stations between Clayton and Goolwa (refer to Figure 5.10 for locations).....	89
Figure 6.38: Comparison of modelled (23f) and measured (LWA, EPA & CCF) salinity (as EC, uScm ⁻¹) for 8 stations between Clayton and Goolwa (refer to Figure 5.10 for locations).....	89
Figure 6.39: Comparison of modelled (23f) and measured (LWA, EPA & CCF) dissolved oxygen (DO, mg L ⁻¹) for 8 stations between Clayton and Goolwa (refer to Figure 5.10 for locations).....	90
Figure 6.40: Comparison of modelled (23f) and measured (LWA, EPA & CCF) dissolved organic carbon (DOC, mg L ⁻¹) for 8 stations between Clayton and Goolwa (refer to Figure 5.10 for locations).....	90
Figure 6.41: Comparison of modelled (23f) and measured (LWA, EPA & CCF) NO ₃ -N (NO ₃ , mg L ⁻¹) for 8 stations between Clayton and Goolwa (refer to Figure 5.10 for locations).....	91
Figure 6.42: Comparison of modelled (23f) and measured (LWA, EPA & CCF) NH ₄ -N (NH ₄ , mg L ⁻¹) for 8 stations between Clayton and Goolwa (refer to Figure 5.12 for locations).....	91
Figure 6.43: Comparison of modelled (23f) and measured (LWA, EPA & CCF) total nitrogen (TN, mg L ⁻¹) for 8 stations between Clayton and Goolwa (refer to Figure 5.12 for locations).....	92
Figure 6.44: Comparison of modelled (23f) and measured (LWA, EPA & CCF) filterable reactive phosphorus (PO ₄ , mg L ⁻¹) for 8 stations between Clayton and Goolwa (refer to Figure 5.12 for locations).....	92
Figure 6.45: Comparison of modelled (23f) and measured (LWA, EPA & CCF) total phosphorus (TP, mg L ⁻¹) for 8 stations between Clayton and Goolwa (refer to Figure 5.12 for locations).....	93
Figure 6.46: Comparison of modelled (23f) and measured (LWA, EPA & CCF) total chlorophyll-a (TCHLA, µg chl-a L ⁻¹) for 8 stations between Clayton and Goolwa (refer to Figure 5.12 for locations).....	93
Figure 6.47: Comparison of modelled (23f) and measured (LWA, EPA & CCF) Ca (mg L ⁻¹) for 8 stations between Clayton and Goolwa (refer to Figure 5.12 for locations).....	94
Figure 6.48: Comparison of modelled (23f) and measured (LWA, EPA & CCF) Cl (mg L ⁻¹) for 8 stations between Clayton and Goolwa (refer to Figure 5.12 for locations).....	94

Figure 6.49: Comparison of modelled (23f) and measured (LWA, EPA & CCF) Mg (mg L^{-1}) for 8 stations between Clayton and Goolwa (refer to Figure 5.12 for locations).	95
Figure 6.50: Comparison of modelled (23f) and measured (LWA, EPA & CCF) Na (mg L^{-1}) for 8 stations between Clayton and Goolwa (refer to Figure 5.12 for locations).	95
Figure 6.51: Comparison of modelled (23f) and measured (LWA, EPA & CCF) SO_4 (mg L^{-1}) for 8 stations between Clayton and Goolwa (refer to Figure 5.12 for locations).	96
Figure 6.52: Comparison of modelled (23f) and measured (LWA, EPA & CCF) CHGBAL (meq) for 8 stations between Clayton and Goolwa (refer to Figure 5.102for locations).	96
Figure 6.53: Comparison of modelled (23f) and measured (LWA, EPA & CCF) Al (mg L^{-1}) for 8 stations between Clayton and Goolwa (refer to Figure 5.12 for locations).	97
Figure 6.54: Comparison of modelled (23f) and measured (LWA, EPA & CCF) Mn (mg L^{-1}) for 8 stations between Clayton and Goolwa (refer to Figure 5.12 for locations).	97
Figure 6.55: Comparison of modelled (23f) and measured (LWA, EPA & CCF) pH (-) for 8 stations between Clayton and Goolwa (refer to Figure 5.12 for locations).	98
Figure 6.56: Comparison of modelled (23f) and measured (LWA, EPA & CCF) DIC for 8 stations between Clayton and Goolwa (refer to Figure 5.12 for locations).	98
Figure 6.57: Soil profile evolution over the simulation period (vertical scale is depth, m AHD), showing a) soil moisture content, b) PASS concentration ($\text{mol H}^+ \text{kg}^{-1}$) and c) ANC ($\text{mol H}^+ \text{kg}^{-1}$) evolution.	99
Figure 6.58: Plots of pH and dissolved carbonate alkalinity (DIC, mg C L^{-1}) at intervals through 2008-2009.	101
Figure 6.59: Plots of water table depth (PHREATIC, m) and exposed PASS ($\text{mol H}^+ [10000\text{m}^2]^{-1}$) at intervals through 2008-2009.	102
Figure 6.60: UZAASS ($\text{mol H}^+ [10000\text{m}^2]^{-1}$) and SZAASS ($\text{mol H}^+ [10000\text{m}^2]^{-1}$) at intervals through 2008-2009.	103
Figure 6.61: Plots of acidity flux rate during inundation (ASSRWET, $\text{mol H}^+ \text{m}^{-2} \text{day}^{-1}$; negative implies alkalinity) and acidity flux rate via seepage (ASSBFLW, $\text{mol H}^+ \text{day}^{-1}$) at intervals through 2008-2009.	104
Figure 6.62: Plots of ANC ($\text{mol H}^+ [10000\text{m}^2]^{-1}$) and SO_4 reduction rate (SO4REDN, $\text{x}10^{-3} \text{mol H}^+ \text{m}^{-2} \text{day}^{-1}$) at intervals through 2008-2009.	105
Figure 6.63a: Integrated output from the Currency/Finniss validation simulation showing accumulation of exposed PASS and subsequent AASS production and consumption.	106
Figure 6.63b: Integrated output from the Currency/Finniss validation simulation showing the accumulation of acidity in the unsaturated and saturated zone, and process controlling mobilisation.	106
Figure 6.63c: Integrated output from the Currency/Finniss validation simulation showing the baseflow acidity flux rate, the in-soil neutralisation of acidity by sulfate reduction in the groundwater, and the rewetting flux and in-lake alkalinity flux.	107
Figure 6.64: Annual average budgets of acidity stores and fluxes for Currency Creek acidification event in 2009. Data averaged over Sep 2008-Sep 2009.	107
Figure 7.1: Forecast scenarios of modelled (NoP: no continued pumping; 100: stabilisation at -1.0m AHD; 075: stabilisation at -0.75m AHD; 050: stabilisation at -0.5m AHD) water level (mAHD) and salinity (as expressed by conductivity, uS cm^{-1}) for four stations within Lake Albert.	109
Figure 7.2: Forecast scenarios of modelled (NoP: no continued pumping; 100: stabilisation at -1.0m AHD; 075: stabilisation at -0.75m AHD; 050: stabilisation at -0.5m AHD) dissolved carbonate alkalinity (DIC, as $\text{mg CaCO}_3 \text{L}^{-1}$) and pH (-) for four stations within Lake Albert.	110
Figure 7.3: Forecast scenarios of modelled (NoP: no continued pumping; 100: stabilisation at -1.0m AHD; 075: stabilisation at -0.75m AHD; 050: stabilisation at -0.5m AHD) Ca (mg L^{-1}) and Cl (mg L^{-1}) for four stations within Lake Albert.	111
Figure 7.4: Forecast scenarios of modelled (NoP: no continued pumping; 100: stabilisation at -1.0m AHD; 075: stabilisation at -0.75m AHD; 050: stabilisation at -0.5m AHD) charge imbalance (CHGBAL (meq) and Mg (mg L^{-1}) for four stations within Lake Albert.	112
Figure 7.5: Forecast scenarios of modelled (NoP: no continued pumping; 100: stabilisation at -1.0m AHD; 075: stabilisation at -0.75m AHD; 050: stabilisation at -0.5m AHD) Na (mg L^{-1}) and SO_4 (mg L^{-1}) for four stations within Lake Albert.	113
Figure 7.6: Forecast scenarios of modelled (NoP: no continued pumping; 100: stabilisation at -1.0m AHD; 075: stabilisation at -0.75m AHD; 050: stabilisation at -0.5m AHD) dissolved Fell (mg L^{-1}) and calcite (mol L^{-1}) for four stations within Lake Albert.	114

Figure 7.7: Forecast scenarios of modelled (NoP: no continued pumping; 100: stabilisation at -1.0m AHD; 075: stabilisation at -0.75m AHD; 050: stabilisation at -0.5m AHD) dissolved MnII (mg L ⁻¹) and dissolved Al (mg L ⁻¹) for four stations within Lake Albert.	115
Figure 7.8: Forecast scenarios of modelled (NoP: no continued pumping; 100: stabilisation at -1.0m AHD; 075: stabilisation at -0.75m AHD; 050: stabilisation at -0.5m AHD) DO (mg L ⁻¹) and DOC (mg C L ⁻¹) for four stations within Lake Albert.	116
Figure 7.9: Forecast scenarios of modelled (NoP: no continued pumping; 100: stabilisation at -1.0m AHD; 075: stabilisation at -0.75m AHD; 050: stabilisation at -0.5m AHD) total Chlorophyll-a (ug Chla L ⁻¹) and TN (mg N L ⁻¹) for four stations within Lake Albert.....	117
Figure 7.10: Forecast scenarios of modelled (NoP: no continued pumping; 100: stabilisation at -1.0m AHD; 075: stabilisation at -0.75m AHD; 050: stabilisation at -0.5m AHD) TP (mg P L ⁻¹) for four stations within Lake Albert.	118
Figure 7.11: Hydrology fluxes in Lake Albert -1.0m AHD stabilisation simulation for a boundary clay cell. Refer to Figure 4.2 for symbol definitions and the hydrological conceptual model.	119
Figure 7.12: Vertical soil profile for a single clay cell on the boundary of Lake Albert during the -1.0m temporary stabilisation showing a) moisture content, b) PASS concentration (mol H ⁺ kg ⁻¹) and c) ANC (mol H ⁺ kg ⁻¹) evolution.....	119
Figure 7.13: Plots of pH and DIC (mg C L ⁻¹) for Lake Albert at 12-monthly intervals.	120
Figure 7.14: Plots of water table depth (PHREATIC, m) and exposed PASS (mol H ⁺ [40000m ²] ⁻¹) at 12-monthly intervals.....	121
Figure 7.15: Plots of UZAASS (mol H ⁺ [40000m ²] ⁻¹) and SZAASS (mol H ⁺ [40000m ²] ⁻¹) at 12-monthly intervals.	122
Figure 7.16: Plots of acidity flux rate due ot rewetting (ASSRWET, mol H ⁺ m ⁻² day ⁻¹) and acidity flux rate via baseflow/seepage (ASSBFLW, mol H ⁺ day ⁻¹) at 12-monthly intervals.	123
Figure 7.17: Plots of ANC (mol H ⁺ [40000m ²] ⁻¹) and SO ₄ reduction (SO ₄ REDN, x10 ⁻³ mol H ⁺ m ⁻² day ⁻¹) at 12-monthly intervals.....	124
Figure 7.18a: Integrated output from the Lake Albert simulation showing accumulation of exposed PASS and subsequent AASS production and consumption.....	125
Figure 7.18b: Integrated output from the Lake Albert validation simulation showing the accumulation of acidity in the unsaturated and saturated zone (UZ and SZ respectively), and processes controlling mobilisation.....	125
Figure 7.18c: Integrated output from the Lake Albert simulation showing the baseflow/seepage acidity flux rate, the in-soil neutralisation of acidity by sulfate reduction in the groundwater, and the rewetting flux and in-lake alkalinity flux	126
Figure 7.19a: Comparison of Lake Albert pH (top) and DIC (bottom) for three simulations for the -1.0m AHD stabilisation scenario testing sensitivity to the acid neutralisation and mobilisation rates.	127
Figure 7.19b: Comparison of Lake Albert pH (top) and DIC (bottom) for three simulations for the -0.5m AHD stabilisation scenario testing sensitivity to the acid neutralisation and mobilisation rates.	128
Figure 7.20: Annual average budgets of acidity stores and fluxes for Lake Albert in 2010 and 2012. Data from the -1.0m stabilisation scenario.	129
Figure 7.21: Forecast scenarios of modelled water level (m AHD) (DDN, FWp, FWs, SWs) for four stations within Lake Alexandrina	131
Figure 7.22: Forecast scenarios of modelled (DDN, FWp, FWs, SWs) temperature (°C) and salinity (uS cm ⁻¹) data for four stations within Lake Alex.....	132
Figure 7.23: Forecast scenarios of modelled (DDN, FWp, FWs, SWs) dissolved oxygen (DO, mg L ⁻¹) and dissolved organic C (DOCL, mg L ⁻¹) for four sites in Lake Alex.	133
Figure 7.24: Forecast scenarios of modelled (DDN, FWp, FWs, SWs) nitrate+nitrite (NO ₃ , mg L ⁻¹) and ammonium (NH ₄ , mg L ⁻¹) for four sites in Lake Alexandrina.....	134
Figure 7.25: Forecast scenarios of modelled (DDN, FWp, FWs, SWs) total N (TN, mg L ⁻¹) and ortho-phosphate (PO ₄ , mg L ⁻¹) for four sites in Lake Alexandrina.	135
Figure 7.26: Forecast scenarios of modelled (DDN, FWp, FWs, SWs) total P (TP, mg L ⁻¹) and total chlorophyll-a (TCHLA, ug L ⁻¹) for four sites in Lake Alexandrina.....	136
Figure 7.27: Forecast scenarios of modelled (DDN, FWp, FWs, SWs) calcium (Ca, mg L ⁻¹) and carbonate alkalinity (DIC, mg CaCO ₃ L ⁻¹) for four sites in Lake Alex.	137
Figure 7.28: Forecast scenarios of modelled (DDN, FWp, FWs, SWs) pH and charge imbalance (CHGBAL, meq) for four sites in Lake Alexandrina.....	138

Figure 7.29: Forecast scenarios of modelled (DDN, FWp, FWs, SWs) chloride (Cl, mg L ⁻¹) and sodium (Na, mg L ⁻¹) for four sites in Lake Alexandrina.	139
Figure 7.30: Forecast scenarios of modelled (DDN, FWp, FWs, SWs) magnesium (Mg, mg L ⁻¹) and sulfate (SO ₄ , mg L ⁻¹) for four sites in Lake Alexandrina.	140
Figure 7.31: Forecast scenarios of modelled (DDN, FWp, FWs, SWs) dissolved Al (Al, mg L ⁻¹) and particulate Al (Gibbsite, mol L ⁻¹) for four sites in Lake Alexandrina.	141
Figure 7.32: Forecast scenarios of modelled (DDN, FWp, FWs, SWs) dissolved Mn (MnII, mg L ⁻¹) and particulate Mn (MnO ₂ A, mol L ⁻¹) for four sites in Lake Alexandrina.	142
Figure 7.33: Forecast scenarios of modelled (DDN, FWp, FWs, SWs) dissolved iron (FeII, mg L ⁻¹) and particulate ferric iron (FeOH ₃ A, mol L ⁻¹) data for four stations within Lake Alexandrina.	143
Figure 7.34: Hydrology fluxes in Lake Alexandrina drawdown simulation for a boundary sand cell. Refer to Figure 4.2 for symbol definitions and the hydrological conceptual model.	144
Figure 7.35: Vertical soil profile for a single clay cell on the boundary of Lake Alexandrina during the -1.5m AHD stabilisation showing a) moisture content, b) PASS concentration (mol H ⁺ kg ⁻¹ cell ⁻¹) and c) ANC (mol H ⁺ kg ⁻¹ cell ⁻¹) evolution.	145
Figure 7.36: Plots of pH and dissolved carbonate alkalinity DIC (mg C L ⁻¹) for Lake Alexandrina at annual intervals for the -1.0m AHD water level stabilisation scenario.	146
Figure 7.37: Plots of water table depth (PHREATIC, m from surface) and exposed pyritic material (PASS, mol H ⁺) at annual intervals from 2009-2012 for the lake drawdown scenario (DDN).	147
Figure 7.38: Plots of unsaturated zone acidity (UZAASS, mol H ⁺) and saturated zone acidity (SZAASS, mol H ⁺) at annual intervals from 2009-2012 for the lake drawdown scenario (DDN).	148
Figure 7.39: Plots of acidity re-wetting flux (ASSRWET, mol H ⁺ m ⁻² day ⁻¹) and baseflow/seepage acidity flux (ASSBFLW, mol H ⁺ day ⁻¹) at annual intervals from 2009-2012 for the lake drawdown scenario (DDN).	149
Figure 7.40: Plots of acid neutralising capacity (ANC, mol H ⁺) and submerged sediment alkalinity flux (SO ₄ REDN, mol m ⁻² day ⁻¹) at annual intervals from 2009-2012 for the lake drawdown scenario (DDN).	150
Figure 7.41a: Analysis of spatially-integrated acid sulfate soil model outputs from the base drawdown simulation showing accumulation of exposed PASS and subsequent AASS production and consumption.	151
Figure 7.41b: Analysis of spatially-integrated acid sulfate soil model outputs from the base drawdown simulation showing the accumulation of acidity in the unsaturated and saturated zone, and processes controlling mobilisation.	152
Figure 7.41c: Analysis of spatially-integrated acid sulfate soil model outputs from the base drawdown simulation showing the baseflow/seepage acidity flux rate, the in-soil neutralisation of acidity by sulfate reduction in the groundwater, and the rewetting flux and in-lake alkalinity flux.	152
Figure 7.42: Comparison of pH (top) and DIC (bottom) for three simulations for the lake drawdown scenario (DDN), testing sensitivity to the acid neutralisation and mobilisation parameters.	153
Figure 7.43: Annual average budgets of acidity stores and fluxes for Lake Alexandrina in 2010 and 2012. Data from drawdown (DDN) simulation.	154
Figure A1.1: Time-series of pH at four locations within Lake Alexandrina for a range of drawdown simulation run with different rewetting flux (D02 = RW+; D03 = RW-) parameters.	164
Figure A1.2: Time-series of pH at four locations within Lake Alexandrina for a range of drawdown simulation run with different lake sediment alkalinity generation rate (D08 = SO ₄ +; D09 = SO ₄ -) parameters.	165
Figure A1.3: Time-series of pH at four locations within Lake Alexandrina for a range of drawdown simulation run with different baseflow (BF0, BF+ and BF-) and saturated zone acidity attenuation (SZN) parameters. Top right plot highlights the simulation with 5%, 2%, 1% and 0.5% saturated zone acidity neutralisation (SZN) per day.	165

1 Project overview

It is now well established that acid sulfate soils (ASS) around the margin of the River Murray Lower Lakes (Lake Alexandrina and Lake Albert, South Australia) are extensive and that the risk of damage to the ecosystem is being exacerbated by continued low flow conditions. The aim of this study was to undertake spatially-resolved hydro-geochemical modelling of historical conditions and various future scenarios related to the drying and rewetting of acid sulfate soils throughout the Lower Lakes region. This was conducted in order to better understand the key dynamics of acid sulfate soil material and its influence on lake biogeochemistry, and to assess the potential benefit of water level stabilisation and/or flooding by supplementing with freshwater or seawater.

Following a detailed review of acid sulfate soil models, an existing three-dimensional (3D) lake geochemical model (ELCOM-CAEDYM) was refined using data and process information from several recent acid sulfate soil research projects (e.g. spatial variability of actual and net acidity, oxidation rates, moisture content of sediment, acid flux mechanisms and rates, neutralisation processes) conducted from 2008-2009 in the Murray Lower Lakes. The model was validated for the period from Jan 2008 – Sept 2009 against monitoring data from the various sites in the region, including from the Currency-Finniss region where acid impacts have occurred. The model has then been used to forecast the lake conditions from Oct 2009 – Jan 2013. Various water level management scenarios were run including augmentation of lake volumes with additional freshwater or with seawater, and the critical acidification levels have been revised.

2 Aims

- To develop a new coupled lake and sediment/soil model suitable for the study of drought induced acidification of the Murray Lower Lakes;
- To undertake spatially-resolved hydro-geochemical modelling of various management scenarios associated with the drying and rewetting of acid sulfate soils in the Lower Lakes;
- To validate the model against available soil and water quality data;
- To explore important system dynamics and controls on acidity generation and transport and potential system thresholds.

3 Introduction and background

3.1 Introduction

Widespread decreases in rainfall throughout the Murray-Darling Basin, superimposed on the significant over-allocation of water for irrigation, has resulted in an order of magnitude reduction in flow over the past decade. This has resulted in a dramatic shift in flow regimes and biogeochemical cycling of the Lower River Murray, including significant changes to water quality properties such as salinity, nutrients, algae and turbidity (Hipsey et al., 2009).

Below Wellington, the river enters Lake Alexandrina, which in turn is connected to Lake Albert, collectively referred to as the Lower Lakes. The lakes have been separated from the Coorong, an estuarine-hypersaline coastal lagoon, by barrages since the 1930s, and are listed under the Ramsar Wetland Convention owing to their high natural diversity. A consequence of continued low flow to the Lower Lakes has been exposure of pyrite-bearing lake sediments which has increased the risk of acid sulfate soil impacts. The potential for large-scale acidification of parts of the system due to exposure of acid sulfate soils, both in the Lower Lakes and in wetlands along the river channel, has created a significant management challenge due to the potential for acid and dissolved metal release, and the consequent effects on biodiversity during subsequent re-flooding.

Acidification tends to occur when reduced sulfides are exposed to oxygen (Ahern et al., 2004). While high concentrations of sulfides have been reported to occur in inland water systems (Baldwin et al., 2007), they are typically associated with coastal areas, since high SO_4 concentrations in seawater fuel sulfate reduction in anoxic sediments and promote the subsequent formation of sulfidic materials such as pyrite. Surface waters are at risk of acidification when pyritic material is disturbed and oxidised, for example, as a result of altered drainage or dredging/reclamation activities, and the resulting acidity is transported into the surface waterbody.

The situation in the Lower Lakes is somewhat different since the lakes are now mainly fresh and no drainage actions have occurred to trigger the oxidation process. The lakes have however been

exposed to high sulfate concentrations prior to construction of the barrages, which has led to a build up of pyrite over geological time, and the oxidation process has occurred due to the relatively rapid (and unprecedented) rate of water level decline exposing perimeter regions of the lake sediment to the atmosphere (Fitzpatrick et al., 2008; 2009).

Spatial heterogeneity in soil properties and pyrite content, dynamic water levels and uncertain hydrological behaviour have made it unclear as to the magnitude of the risk being faced. However, to prevent large-scale deterioration of Lake Albert, local agencies initiated pumping across Narrung Narrows as of May 2008 as a solution to keep the sediments submerged. However, continued low flows into the lower Murray River reaches throughout 2009 has meant that the main lake basin is also potentially facing acidification risk. Some areas have shown signs of acidification including the Currency Creek tributary region and Loveday Bay (EPA, 2010). Various management interventions have been undertaken, including pumping to Lake Albert and limestone addition in the Currency Creek region.

Given the environmental significance of the site, the need to plan for potentially major management interventions and engineering works, and the need to focus current and future field monitoring and experimental campaigns aimed at improving our understanding of acidification processes within the lower lakes, an improved numerical model framework is outlined. The need for reduced uncertainty in the model is particularly necessary now that signs of acidification have emerged and the issue has numerous management ramifications. Furthermore, in light of continued low flows there is serious consideration given to stabilisation of lake levels through allowing seawater in to the lake system; there is thus a need for improved ability to predict the geochemical changes that may occur under this scenario.

This report documents a model for exploring potential future lake states given the concerns of acid sulfate soils. The model includes:

- 3D hydrodynamics, including prediction of circulation patterns, inflows (including pumping and seawater entrance), wetting and drying, temperature, salinity, surface thermodynamics and evaporation;
- 2D spatially variable specification of soil texture and geochemistry, which allows for heterogeneity in soil hydraulic properties, pyrite content, and acid neutralising capacity at high-resolution (100–250m);
- Vertically resolved pyrite oxidation reaction kinetics in exposed cells based on dynamically predicted moisture content profiles, and subsequent neutralisation kinetics;
- Estimation of acidity flux to the surface water following re-wetting of exposed cells, and also from overland flow and seepage processes;
- Buffering of water pH by lake and river alkalinity, and approximation of alkalinity generation by organic matter decomposition in submerged sediments.

The model is validated based on available data and other strategic research outputs conducted in relation to this project (Fitzpatrick et al., 2010; Hicks et al., 2009; Sullivan et al., 2009; Earth Systems, 2010). It is then used to identify dominant controls on the acidification process and to understand the sensitivity of the predictions to key soil hydrological and geochemical properties. With this in mind, it is subsequently used to estimate the range of time-frames for large-scale lake acidification, in order to allow for planning mitigation strategies and to highlight targeted areas for further field and laboratory research to help reduce uncertainty. The model is also used to demonstrate the large spatial variability in the manifestations of acid sulfate soils, and the potential for 'hotspot' locations that require priority management.

3.2 Overview of factors affecting acidity flux to surface waters

Acid generation in sediments is predominantly due to the presence of iron sulfide minerals such as pyrite (FeS_2), which react upon exposure to oxygen to produce acid:



Other reactions, such as the dissolution of carbonate minerals if present, may consume some or all of the acidity (e.g. see Ahern et al., 2004). Once net acidity has been generated, it may be stored in soils or transported into the adjacent water body by a number of different mechanisms. A conceptual overview of the main factors contributing to acidity in the Lower Lakes system is presented in Figure 3.1. These are discussed in turn below, and a summary is presented in Table 1. Some background on interpretation of soil biogeochemical data in the context of the model application described later in this report are also described next.

Definition of solution acidity

Components that contribute to acidity are those that can contribute or remove H⁺ from solution (and which are present in significant quantities), such as HCO₃⁻, dissolved Al and Fe. If we chose as our reference ("target" or "ideal") composition a solution of pH 8.3 in equilibrium with the atmosphere (i.e. conditions close to those in the lake), the dominant species under these conditions are HCO₃⁻, Fe(OH)₃, Al(OH)₃, MnO₂, and CaCO₃. For a given solution composition, we can then estimate the H⁺ equivalents that each component will contribute/remove in the process of neutralisation/aeration:

$$\text{Acidity} = 3[\text{Fe(III)}] + 3[\text{Al}^{3+}] + 2[\text{Fe}^{2+}] + 2[\text{Mn}^{2+}] + [\text{H}^+] + [\text{H}_2\text{CO}_3] - [\text{OH}^-] - [\text{CO}_3^{2-}] \quad (3.2)$$

where square brackets indicate molar concentrations. Other species that may contribute to acidity/alkalinity under various circumstances include NH₄⁺/NH₃, H₂S/HS⁻, SO₄²⁻/HSO₄⁻, Cu²⁺/Cu(OH)_{2(s)}, and others. Strict definition should also consider the speciation of each component at the pH of the solution, see for example Blodau (2006). Note that Fe²⁺ contributes two protons as a result of oxidation to Fe³⁺ (-H⁺) and subsequent precipitation (+3H⁺).

Soil Acid Base Accounting (ABA)

Acid base accounting is static laboratory testing of bulk properties of soil samples for the potential for acidity generation and amelioration (see, e.g., Ahern et al., 2004). While the methods do not give any indication of the kinetics of the processes involved, they do provide a relatively simple measure of what the capacity for net acid generation is, e.g.:

$$\text{Net Acidity (NA)} = \text{Potential Sulfide Acidity} + \text{Existing Acidity} - \text{Acid Neutralisation Capacity (ANC)} \quad (3.3)$$

where the Potential Sulfide Acidity is typically estimated from the reduced sulfur content as measure measured by a procedure such as chromium reducible sulfur (CRS, %S). Existing Acidity = Actual acidity + Retained acidity (RA), where the latter is includes relatively insoluble secondary precipitates such as jarosite. The measurement to obtain actual acidity is Titratable Actual Acidity, TAA (if pH in a 1M KCl solution >6.5, TAA=0; otherwise, TAA is the moles required to titrate to value of 5.5). Measurement for retained acidity involves determining SRAS, residual acid soluble sulfur. Acid Neutralising Capacity is defined as the measured ANC corrected by a 'fineness factor' which allows for armouring of large, neutralising soil particles. Net acidity therefore is summarised as:

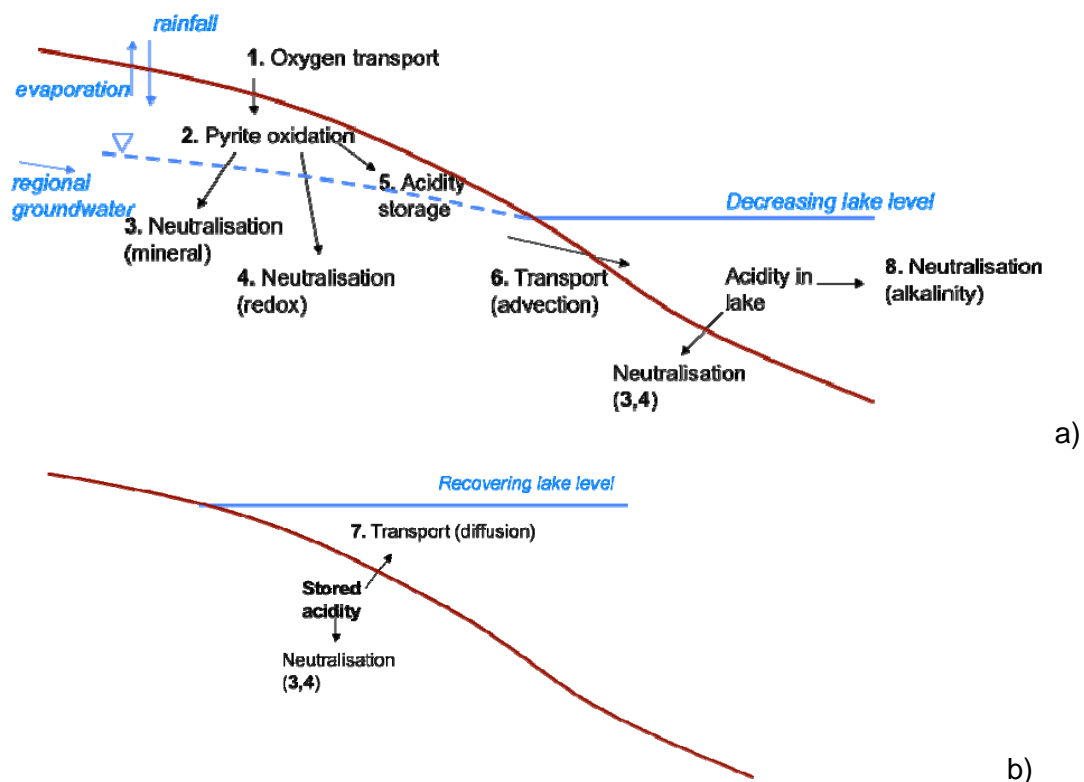


Figure 3.1: a) Processes involved in acidity generation and fate as lake water levels recede, b) additional process upon re-wetting of previously exposed sediments: diffusive transport of stored acidity back into the water column.

$$NA = CRS + TAA + RA - ANC \quad (3.4)$$

where each term is in consistent units. Titratable Peroxide Acidity (TPA) is determined by a similar procedure as TAA, but with an additional step with peroxide to accelerate oxidation of pyrite material. [Note that, as for TAA, this method does not allow for RA; also, acid volatile sulfur (AVS) may be lost during the reaction]. It therefore gives an indication of the terms on the RHS of Eq. 3.4, other than RA, i.e.:

$$TPA = CRS + TAA - ANC \quad (3.5)$$

In the characterisation of Lower Lakes samples (Fitzpatrick et al., 2008), CRS, ANC, TAA, and pH-peroxide were measured. pH-peroxide is the pH resulting from the TPA treatment, prior to titration to the final pH (and may therefore underestimate contributions to acidity from dissolved Al, Fe, and Mn).

3.3 Controls on acid sulfate soil dynamics

O₂ diffusion limitation on oxidation rates (Figure 3.1, Process 1)

The rate of ingress of oxygen into the soil will depend upon factors such as:

- soil porosity, as affected by the soil particle size distribution (including vertical and horizontal heterogeneity), and the presence of cracks and/or macropores;
- the degree of water saturation of the porespace, which is a function of soil properties and the dynamically changing water balance, and;
- the overall rate of oxygen consumption, which will depend upon:
 - amount of pyrite present, in particular, the available reactive surface area of the pyrite crystals;
 - other oxygen sinks, such as aerobic decomposition of organic matter and oxidation of NH₄ and Fe(II).

Acid-generating oxidation reactions (Figure 3.1, Process 2)

Assuming initially saturated conditions in either waterlogged soils or sub-aqueous sediment, oxygen availability will be low, as oxygen is typically consumed at faster rates than it can be replaced by diffusion. With lowering of the water level, oxygen diffusion, now through air-filled porespace instead of saturated media, is greatly enhanced. Generation of acidity is primarily due to oxidation of the sulfide ion in the iron sulfide minerals. For pyrite:



In the continued presence of oxygen, Fe(II) is oxidised to Fe(III):



The Fe(III) produced may also oxidise pyrite (even if oxygen is not present), and in the process is reduced back to Fe(II):



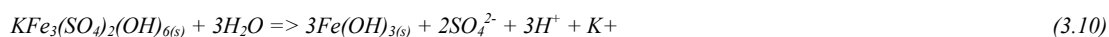
As pyrite oxidation by Fe(III) is faster than the rate of pyrite oxidation by oxygen, the rate of supply of Fe(III) by Fe(II) oxidation has been suggested to be the rate-limiting step in the overall pyrite oxidation rate. The abiotic rate of Fe(II) oxidation is fast at circumneutral pH, but under these conditions the solubility of Fe(III) is low, typically precipitating as hydroxide phases, e.g.:



which may limit the Fe(III) pathway, and hence the overall pyrite oxidation rate. As pH decreases, the rate of abiotic Fe(II) oxidation also decreases, but the reaction may now be accelerated by acidophilic bacteria. The combination of a high rate of Fe(III) replenishment with the relatively high solubility of Fe(III) at low pH can lead to a greater overall pyrite oxidation than at neutral pH, given the same oxygen availability. Iron sulfides may also be oxidised by NO₃⁻ under anaerobic conditions, however, this rate is often assumed to be low.

The overall reaction all the way to Fe(OH)_{3(s)} (or goethite) is then as was given in Eq 3.1, with four moles of H produced per mol of pyrite oxidised. Pyrite-bearing soils with neutral pH are referred to as potential acid sulfate soils (PASS); once oxidation begins and sufficient "actual" acidity is produced to lower pH, the material is referred to as an actual acid sulfate soil (AASS). Under certain conditions,

minerals such as jarosite may precipitate initially, and later hydrolyse with associated acidity release, e.g.:



In acid base accounting, this reaction contributes to the retained acidity (RA). Other mineral phases that may delay the release of acidity after pyrite oxidation include schwertmannite ($Fe_2O_2.55(SO_4)_{0.45}.2H_2O$):



Acidity neutralisation (Figure 3.1, Process 3 and 4)

Acid neutralising processes are summarised as:

- buffering by dissolved carbonate species, e.g.



- dissolution of carbonate minerals, such as calcite or aragonite, e.g.



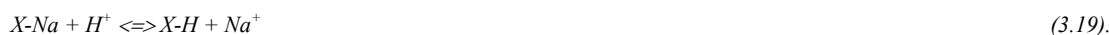
- dissolution of aluminosilicate minerals, e.g. :



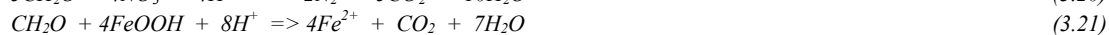
- dissolution of hydroxide minerals such as gibbsite:



- cation exchange reactions, e.g. on clays:



Under anoxic conditions, microbial reduction of NO_3^- , $Fe(III)$ and SO_4 also consumes acidity, according to:



In these reactions, NO_3^- is lost as N_2 and is not reversible, but exposure of $Fe(II)$ and HS^- to oxygen will result in re-oxidation. However, under continued anoxic conditions, with sufficient levels of $Fe(II)$ and sulfide (and non acidic pH values), iron sulfide minerals will precipitate out of solution, possibly in the form of amorphous iron sulfide minerals, which are an important component in so-called "monosulfidic black oozes" (MBOs):



Under suitable conditions, MBOs may eventually convert to FeS_2 . If conditions remain anoxic, the acidity released in the original oxidation reaction (Eq.3.1) has in effect been re-sequestered. Note that the rates of microbially mediated reactions (Eq 3.20-3.22), and associated alkalinity generation, may be inhibited at low pH. This is an important consideration in defining the acidity consumption pathways in the model.

Alkalinity, or the capacity of a solution to resist a reduction in pH into an acidic conditions, is in natural waters often equivalent to the carbonate alkalinity. This is defined as the amount of acid required to titrate all carbonate and bicarbonate ions in solution to $H_2CO_{3(aq)}$ (or $CO_2 + H_2O$, cf. Eq 3.14 and 3.15), which occurs at a pH below 5. For waters with a highly basic pH, the contribution of hydroxyl ions may also contribute significant alkalinity. For natural waters with pH in the range of ~6-10, the dominant ion contributing to carbonate alkalinity is HCO_3^- . The concentration of dissolved inorganic carbon (DIC) will thus typically reflect the majority of the total available alkalinity in the water column, on a 1:1 molar basis. For pH values above this range, considering DIC alone will underestimate the contribution of carbonate and hydroxyl ions to alkalinity.

Solubility controls

As concentrations of chemical species in solution increase, for example as a result of mineral weathering or evapo-concentration, concentrations may exceed solubility thresholds for a number

of common secondary minerals. In particular, aqueous concentrations of Fe(III), Al, and sulfate are often affected by precipitation of hydroxide, hydroxysulfate, or sulfate minerals, such as ferric hydroxide ($\text{Fe}(\text{OH})_3$), microcrystalline gibbsite ($\text{Al}(\text{OH})_3$), schwertmannite ($\text{Fe}_2\text{O}_2.55(\text{SO}_4)_{0.45}.2\text{H}_2\text{O}$), gypsum ($\text{CaSO}_4.2\text{H}_2\text{O}$), or at low pH, K- or Na- jarosite (e.g., $\text{KFe}_3(\text{SO}_4)_2(\text{OH})_6$) or alunite ($\text{KAl}_3(\text{SO}_4)_2(\text{OH})_6$).

Solubility equilibria can affect and be affected by pH, for example in the case of ferric and aluminium hydroxides (Eq. 3.9 and 3.18). If more H^+ is added to solution, any $\text{Fe}(\text{OH})_3$ present will dissolve (i.e., the reaction 3.9 will move to the left until the balance between H^+ and Fe^{3+} in solution equilibrates (or until the mineral is consumed). Conversely, if alkalinity is added, Fe^{3+} will precipitate (i.e., the reaction will move to the right). If Al and/or Fe(III) are present in solution in sufficient quantities, dissolution/precipitation reactions of their hydroxides occur sufficiently quickly to buffer pH. This is commonly observed to occur at around pH 5 to pH 3. Similarly, precipitation/dissolution of carbonate minerals, such as calcite (Eq 3.16), can also affect and be affected by solution pH.

Control of aqueous concentrations by solubility equilibria can be investigated by calculating the saturation indices for the various minerals. These calculations require analysis of all major ions in solution, the ionic strength and solution pH. Based on thermodynamic equilibrium, aqueous speciation calculations can be performed with readily available software such as MINTeq or PHREEQC. It is also possible to specify solubility equilibrium control of aqueous concentrations in CAEDYM (see Section 4.1).

Note that Fe(II) is rarely limited by solubility control (unless high pH, or high carbonate concentrations), and thus under anoxic conditions can be highly mobile even at neutral pH. However, upon exposure to oxygen, Fe(II) is relatively quickly oxidised to Fe(III) (Eq. 3.7), which may lead to both oxygen depletion and generation of H^+ due to $\text{Fe}(\text{OH})_3$ precipitation (Eq. 3.9).

Interactions between the soil and the water body

The processes described above will take place in the exposed soil around the lake, and only affect soil quality unless transport mechanisms mobilise the acidity and deliver to the standing waters. The three main mechanisms that may mobilise the soil acidity are:

- rainfall induced vertical percolation of acidity from the unsaturated zone and subsequent lateral transport (e.g., baseflow or interflow);
- surface ponding following excess rainfall and surface runoff;
- inundation of acidified soil by raised water levels (either from lake filling or periodic seiches) and subsequent diffusive transport across the sediment-water interface.

In the short term, the water quality (including pH) after an influx of acidity will depend upon the composition of the lake water, that is, the available alkalinity in the water column (\approx DIC concentration, see above) will constitute the capacity of the lake to buffer addition of H^+ (e.g., Eq. 3.14), as well as additional H^+ produced from the relatively fast precipitation reactions of Al and Fe.

Over longer periods of time and depending on environmental conditions, such as pH, temperature, oxygen, salinity, and the availability of organic matter, slower processes in the surface water sediments such as SO_4 reduction (e.g. Eq. 3.20-3.22) may generate alkalinity and contribute to acidity neutralisation.

Physical processes (e.g., stratification dynamics, circulation patterns, dilution and mixing) and biological processes, (e.g., carbon and nutrient cycling through phytoplankton-zooplankton-bacteria) will also mediate how the acidity loading to the surface water will ultimately manifest.

3.4 Review of models and modelling approaches for simulation of acid sulfate soils

Various models were reviewed for their suitability of use in the current project. There are numerous codes for simulating the physical and chemical processes in the vadose or unsaturated zone (see Ravi and Williams, 1998; Simunek and Bradford, 2008). The available codes tend to all share a common theoretical basis for dealing with the wetting and draining of water in the unsaturated zone and associated reactions and solute transport, although they do have a number of differences. The common basis is therefore presented separately upfront, after which the specific details of a range of models that could potentially be used for acid sulfate soil geochemistry are described below.

Theoretical basis for unsaturated zone model framework

For exposed lake sediment/soil, Richard's equation may be used to represent the vertical movement of water through the unsaturated region. In 1D, it is defined as:

$$\frac{\partial \theta}{\partial t} = \frac{\partial}{\partial z} \left(K(\psi) \left(\frac{\partial \psi}{\partial z} + 1 \right) \right) \quad (3.24)$$

where K , the hydraulic conductivity, is a function of ψ , the pressure head; z is the elevation above a vertical datum, θ is the volumetric water content, and t is time. The vertical soil moisture profile then is solved numerically using a layered grid and an implicit finite difference method (e.g., Thomas algorithm). The top boundary condition is the rainfall and evaporation and at the bottom the solution is constrained by the presence of the water table, or it could set to be free draining. Several well-known codes are used to solve Richard's equation, and the above approach is able to be extended and solved in 3D.

The water flow solution is often coupled with a solute dynamics model to simulate the movement and transformations of chemical solutes within the water, for example:

$$\frac{\partial C_j}{\partial t} = \frac{\partial}{\partial z} \left(\theta D^w \frac{\partial C_j}{\partial z} \right) - \underbrace{v C_j}_{\text{advection}} + \underbrace{R_j}_{\text{reactions}} \quad (3.25)$$

Table 3.1: Summary of important processes to be considered within the acid sulfate soil modelling framework and methods required to generate the necessary data required for model parameterisation.

Processes (cf. Figure 3.1) and factors upon which they depend	Methods to quantify these processes
1. Rate of oxygen diffusion a) soil properties – porosity, macropores (cracking) b) water content c) rate of consumption by pyrite oxidation (see 2) d) rate of consumption by other processes, e.g. organic matter mineralisation	Characterisation: - soil physical properties - pyrite and organic matter content - porespace O ₂ and CO ₂ profiles (see e.g. Cook et al., 2004) Kinetic experiments to determine rate of pyrite oxidation (see below) and organic matter mineralisation (compare with literature rates).
2. Rate of pyrite oxidation a) intrinsic pyrite oxidation rate constant b) oxygen availability (see 1) c) bulk pyrite content and reactive surface area d) pH	Kinetic experiments to determine intrinsic pyrite oxidation rate constant (compare with literature rates used in the model). Sediment characterisation: -pyrite content and surface area -porewater pH -rate of oxygen diffusion (see above)
3. Neutralisation/pH buffering due to mineral reactions a) Mineral content (e.g. carbonate minerals, hydroxide minerals, clays) and reactive surface area, including the effect of armouring (coating of surfaces)	Sediment characterisation-identify minerals, reactive surface area Kinetic experiments to identify how much is available and rate of release; Also, if buffering is due to dissolution of Al and Fe hydroxides, what are the resulting concentrations of metals (toxicity of Al; release of other sorbed Me)
4. Neutralisation due to redox reactions of NO₃, Fe(III) and SO₄ with organic matter a) presence of O ₂ (neutralisation requires anoxia) b) presence of organic matter c) pH	Kinetic experiments to determine rates under conditions likely to exist in the lake (compare with literature rates used in the model). Sediment characterisation to determine in situ conditions, and therefore potential for these reactions to occur.
5. Acidity storage – precipitation as minerals a) porewater pH and availability of other species, e.g. Ca ²⁺ , K ⁺ b) redox conditions (e.g. presence of O ₂ , OM)	Sediment characterisation (solid and aqueous phase)
6. Transport of acidity into the lake by advection a) Water balance: rainfall, evaporation, saturation of soil storage capacity, regional groundwater gradients/flow b) Soil properties, e.g., hydraulic conductivity, porosity	Field study – detailed water balance and related physical properties of the sediments (e.g. Rassam and Cook, 2002)
7. Transport of acidity into the lake by diffusion upon rewetting a) existing acidity (including whether solid or aqueous phase) b) soil properties	Characterisation; Laboratory studies Field mesocosms, benthic chambers on re-wetted areas?

where C_j is the concentration of the j^{th} solute, D^w is the dispersivity, q is the vertical volume flux and R is the net sum of any reactions that are occurring and producing or consuming solute C . This may also be extended for multiple reacting components and the equations are linked through the R terms.

The dynamics of acid sulphate soils are predominantly controlled by the availability of oxygen, which is mainly determined by the rate of downward transport and by consumption processes within the soil matrix. A vertical diffusion-reaction equation can therefore be defined:

$$\frac{\partial(\varphi_a C_a(z))}{\partial t} = \frac{\partial}{\partial z} D_a(\varphi_a) \left(\frac{\partial C_a(z)}{\partial z} \right) - R_{OMox} - R_{FeS_2Ox} \quad (3.26)$$

where $C_a(z)$ is the concentration of oxygen in air-filled pores (m^3 per unit volume of soil), D_a is the diffusion coefficient of oxygen in air-filled pores ($\text{m}^2 \text{ day}^{-1}$), φ_a is the air-filled porosity, R_{OMox} is the volumetric consumption rate of oxygen by organic material, and R_{FeS_2Ox} is the consumption rate due to pyrite oxidation (day^{-1}).

The diffusion term is not straightforward since macropores may exist and provide preferential paths for oxygen diffusion. Blunden and Indraratna (2001) and Bronswijk and Groenenberg (1996) describe approaches for approximating the diffusion rate, by assuming steady state profiles. The solution is calculated assuming diffusion ~ consumption, and consumption is calculated in the soil matrix and macropore regions explicitly. Within the soil it is based on the amount of pyrite and the size of the particles, the organic matter content, and the temperature.

Once the pyrite is oxidized a known amount of H^+ , Fe^{3+} and SO_4^{2-} is liberated and each is subject to the solute transport equation (2) above. Before entering the lake, these materials may be subject to both kinetic and equilibrium chemical reactions, and these must be considered in the modelling approach as source/sink terms, indicated by R in equation 3.25. If these solutes reach the water table, they will be subject to the saturated flow conditions simulated by a groundwater flow model. Note that each model tends to configure simulated solutes differently and the reaction processes are also model-specific; these are discussed specifically below. An important consideration that is common across the model platforms is the separation between equilibrium dynamics (such as aqueous speciation and mineral precipitation and dissolution) and the kinetically controlled reaction rates. This complicates the solution of Eq 3.25, since the term ' R ' may not be simply accounted for and included in the numerical solution scheme that is adopted. To account for these dynamics the codes sometimes employ a reaction 'splitting' procedure, sometimes described as the non-iterative sequential coupling method (SNIA). This method has been queried by some authors who describe the mass balance errors may occur using this procedure (e.g., see Steefel and MacQuarrie, 1996, Mayer, 1999, cited in Jacques and Simunek, 2005). However, this issue can be minimised through selection of appropriate time steps, and, as pointed out in Jacques and Simunek (2005), "we believe that uncertainty in the assumed processes and its parameters likely will contribute much more to uncertainty in the model simulations than possible (limited) numerical errors caused by the coupling procedure". In simple terms, the method essentially serves to split a numerical timestep, Δt , into two components and solves the transport components of the equation system on the time step, and the kinetic and equilibration reactions on the $1/2^{\text{th}}$ timestep, without any iterative adjustments, despite the transport and reaction components being non-linearly dependent on each other.

Upon rewetting of a previously exposed sediment column that has been undergoing reaction, the soil will become saturated and solutes within the vadose zone will become mobile. At the sediment-water interface, a diffusive flux into the overlying water will occur due to a significant concentration gradient between the soil and water. Fick's Law may be applied to predict the flux, J , by numerically approximating the vertical gradients of solutes at the sediment-water interface, assuming that diffusivity within the soil is the limiting step:

$$J_j = D_s^w \left. \frac{dC_j}{dz} \right|_{z=0} \quad (3.27)$$

where D_s^w is the diffusivity at the sediment-water interface.

HP1

The code HP1 (HYDRUS1D-PHREEQC) was obtained "by coupling the HYDRUS-1D one-dimensional variably-saturated water flow and solute transport model with the PHREEQC geochemical code. The HP1 code incorporates modules simulating (1) transient water flow in variably-saturated media, (2) transport of multiple components, and (3) mixed equilibrium/kinetic geochemical reactions" (Jacques and Simunek, 2005). The model therefore allows for coupled estimation of water content and the major biogeochemical transformations. Specific highlighted features include:

- One-dimensional transient water flow for different boundary conditions including atmospheric conditions (precipitation, evaporation, transpiration)
- Root water uptake as a sink for water
- Root growth
- One-dimensional transient convective and conductive heat transport for time-variable temperatures at the soil surface
- One-dimensional advective, dispersive and diffusive transport of multiple solutes
- Effect of temperature on transport parameters, thermodynamic constants, and rate parameters
- Different functional forms for the soil hydraulic properties, including hysteresis
- Physical non-equilibrium solute transport
- Physical and chemical spatial heterogeneity
- Equilibrium aqueous speciation reactions and kinetically controlled aqueous reactions such as radioactive decay
- Multi-site cation exchange related to type and amount of minerals present
- Equilibrium and kinetic dissolution/precipitation of primary and secondary minerals
- User-defined kinetic reactions
- Simultaneous presence of different reactions (sequential and parallel kinetic reactions, equilibrium and kinetic reactions, homogeneous and heterogeneous reactions, biogeochemical reactions)

There are, however, other non-operational components of the model that include

- surface complexation, solid solutions, and redox reactions;
- diffusion and advection of components in the gas phase are not considered
- the model does not account for changes in the volume of minerals and corresponding changes in porosity, hydraulic properties, and solute transport parameters.

The model HYDRUS solves the 1D Richards equation as described in Eq. 3.24, but includes two major changes. First the model allows for the domain reference dimension to be non-vertical and allows for a sloping or horizontal domain through definition of the slope angle, and secondly the model includes a water sink term, $S(h)$, to account for the amount of water extracted from the soil by roots. The water content and the unsaturated hydraulic conductivity are nonlinear functions of the pressure head. Three analytical models are available in HYDRUS-1D to describe these soil hydraulic properties: Brooks and Corey (1966); van Genuchten (1980); and Vogel and Cislerova (1988). The flow and transport equations are solved numerically using Galerkin-type linear finite element schemes.

The model allows for various boundary configuration methods, both at the top and bottom of the domain. When precipitation, and evaporation (or evapo-transpiration) are specified, the water flux across this boundary depends dynamically on the soil moisture conditions. If the potential rainfall is larger than the infiltration capacity, excess water on the soil surface is either assumed to be immediately removed by surface runoff processes, or is permitted to build up and pond on the soil surface. At the bottom of the soil profile, the following boundary conditions can be implemented (Jacques and Simunek, 2005): (i) a seepage face boundary condition that assumes a zero-flux when the bottom of the soil profile is unsaturated and a zero pressure head when it is saturated; (ii) a tile drain boundary condition that approximates flow to horizontal subsurface drains using selected analytical solutions; and (iii) a deep drainage boundary condition that uses a functional relationship that relates the water table depth with the deep recharge from the soil profile.

HYDRUS has the advantage of solving the 1D heat transport equation, and allows the user to set a prescribed temperature condition at the soil surface. Solute transport is dealt with as above (Eq. 3.25) and includes advection and dispersion, however HYDRUS also has the specific ability to simulate extraction based on plant use. Additionally, the model accounts for physical non-equilibrium solute transport processes by parameterising a two region separation of the flow by dividing into a 'flowing' (mobile) and 'stagnant' (immobile) region. Dispersion in the model is also linked to the temperature model.

Reaction terms in the solute equation, R , are dealt with entirely by PHREEQC. As described generically above, the method of coupling HYDRUS-1D and PHREEQC, uses the non-iterative sequential coupling method (SNIA). Given that simulation of acid sulfate soils involves multi-component reactive transport, the solution first considers the physical part (coupled in space, uncoupled over the components) by solving Eq. 3.25 without the reaction term, and then the chemical part is solved uncoupled in space, (i.e., no transport) but coupled over the components by simultaneously solving the equilibrium and kinetic geochemical reactions (Figure 3.2).

Practically, the model is developed by coupling the Fortran routines of HYDRUS-1D and the C functions of PHREEQC. There are some minor modifications to each model to enable the coupling, and several additional functions that manage the interactions between the two models. To run the model, it requires exactly the same input files as for the single HYDRUS-1D codes and PHREEQC codes, and an additional HP1 specific file that is required to configure the transportable master species. The main HYDRUS-1D and PHREEQC input files may also be configured using the associated interfaces available on the web.

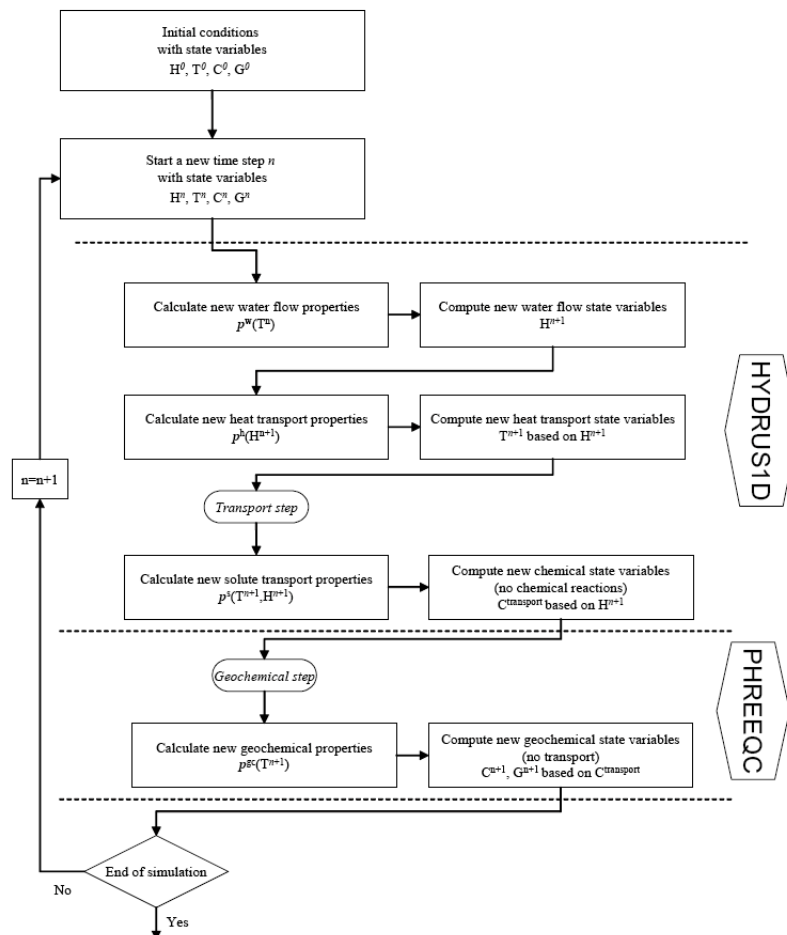


Figure 3.2: Schematic of the sequential modelling approach used by HP1 (taken from Jacques and Simunek, 2005). Symbols: n the n th time step, H variables related to water flow (pressure heads, fluxes), T variables concerning heat transport (temperature), C variables dealing with components and species in the system, G variables concerning the solid phase (mineralogical composition, exchange site, surface site, reactive surfaces), p^w vector of parameters needed to solve the water flow equation, p^h vector of parameters needed to solve the heat transport equation, p^s vector of parameters needed to solve the solute transport equation, p^g vector of parameters needed to solve the geochemical reactions.

LEACHM

The LEACHM model system (Hutson, 2003) is a set of separate models that share a common numerical solution scheme to simulate the vertical flow of water and chemicals. These include (Hutson and Wagenet, 1992): LEACHN (for N & P), LEACHP (pesticide dynamics), LEACHC (inorganic ions) and LEACHB (microbial population dynamics), which all share a common utility library and water flow routine.

The LEACHM model domain is a uniform thickness, vertically-resolved grid. As outlined in the generic sections above the model solves the 1D Richard's equation, and includes a sink term for water loss by plant uptake, which may vary with depth and time. The Thomas algorithm is used to numerically solve the equation by adopting a Crank-Nicholson numerical differencing approach. The upper boundary condition is able to account for ponded or non-ponded infiltration, evaporation or a zero

flux. Similar to HYDRUS-1D described above, the lower boundary condition may be set to represent a fixed depth water table, a free-draining profile, zero flux or a lysimeter tank.

The LEACHM system includes a separate heat balance, and similar to HYDRUS-1D, applies a sine curve function to describe the diel varying upper boundary condition. Solute transport is similar to Eq. 3.25, although in LEACHM no splitting of the physical and chemical dynamics occurs and the full advection-dispersion-reaction equation for solutes is discretized using an upstream differencing method and solved with the Thomas algorithm. For the pesticide module, the model also includes ability to simulate gas phase diffusion and advection, and adopts an 'effective' diffusion coefficient that is used within Eq. 3.25. Partitioning between soil and water is also accounted for within this module.

The inorganic chemistry module is separated from the nutrient dynamics and pesticide modules. The chemistry is based around neutral-alkaline equilibrium processes, and uses an iterative solution to solve the aqueous speciation reactions. Precipitation/dissolution is accounted for in the solution, but this is only for calcite and gypsum. Simulatable components are fixed as Ca Mg, Na, K, DIC and SO₄, and no metals are included. Redox process relating to Fe, S, Mn etc. are not simulated, and dynamics of N and P related species are not accounted for in the speciation. Pyrite and oxygen dynamics are also not included.

The modules are written in Fortran 77 and each model LEACHC, LEACHN and LEACHP are compiled as separate models. Inputs are provided using structured format ASCII files.

UZF & MODFLOW

UZF is the 1-Dimensional Unsaturated Zone Flow component of the popular MODFLOW groundwater model. It is unique since it adopts a kinematic wave approximation to Richards' equation that is solved by the method of characteristics to simulate vertical unsaturated flow (Niswonger et al., 2006). The approach assumes that unsaturated flow occurs in response to gravity potential gradients only and ignores negative potential gradients; the approach further assumes uniform hydraulic properties in the unsaturated zone for each vertical column of model cells. The Brooks-Corey function is used to define the relation between unsaturated hydraulic conductivity and water content. Variables required include initial and saturated water contents, saturated vertical hydraulic conductivity, and an exponent in the Brooks-Corey function. Residual water content is calculated internally on the basis of the difference between saturated water content and specific yield. The method of characteristics solution for unsaturated flow precludes the need to develop a structured grid of the unsaturated zone for numerical stability and simplifies handling of the moving boundary defined by the interface between the water table and unsaturated zone (Smith, 1983).

The module currently includes no capacity to solve for either solute transport or heat dynamics, and no geochemical dynamics are included. However, coupling of PHREEQC to UZF is underway (H. Prommer, pers. comm.). The model is written in Fortran 90 and links directly as a module within MODFLOW.

ACID3D

ACID3D includes unsaturated zone flow in addition to the 3D groundwater dynamics. Blunden and Indraratna (2001) initially presented the model, which is conceptually similar to the SMASS model described next) in the unsaturated zone, and links with FEMWATER for the 3D simulation of the groundwater dynamics. The models are coupled statically such that the flow field is solved for by FEMWATER and then the output is fed into the ACID3D specific equations for simulation of oxygen diffusion and pyrite oxidation.

SMASS

The Simulation Model for Acid Sulfate Soils (SMASS) was developed by Bronswijk and Groenenberg (1993) and has been applied to various ASS situations (e.g., van Wijk et al., 1993). The model is particularly designed to capture the vertical dynamics of pyrite oxidation and acidity generation and attenuation. In addition to vertical water content prediction, it is able to simulate solute transport, atmospheric ingress of oxygen and some chemical speciation dynamics.

The model solves Richard's equation as in Eq 3.24 and in the other models, and also accounts for water uptake by roots. The upper boundary condition may be defined as precipitation or evaporation, and the bottom boundary condition may be defined as the groundwater level, pressure head or allowed free drainage flux. It is solved implicitly using the Thomas algorithm. A standard solute transport model is also used like Eq 3.25.

The SMASS model has a detailed sub-model for oxygen diffusion and consumption. The model adopts Eq 3.26, and includes a diffusion model that accounts for the typical macropore/matrix structure within an acid sulfate soil. It adopts a unique method for calculating oxygen consumption and includes a constant rate due to organic matter mineralisation, and calculates a rate of pyrite

oxidation according to the pyrite content, oxygen content and density/diameter of the pyrite crystals. Oxygen penetration is then based on the thickness of the aerobic zone in the soil matrix component, and within the macropore component it is based on diffusivity, which is calculated as a function of tortuosity and air content (Figure 3.3).

The geochemical sub-model includes some limited redox reactions and chemical speciation and cation exchange dynamics. The redox reactions include oxidation of pyrite (described above) and reduction of Fe (which may be split into reducible and non-reducible fractions). Weathering/dissolution of jurbanite ($\text{Al}(\text{OH})\text{SO}_4$) is considered and cation exchange dynamics are also accounted for. Aqueous speciation and precipitation are also included and the combined set of equations are solved using a Newton-Raphson technique.

The model is run at an hourly time-step but the pyrite oxidation, oxygen diffusion and geochemical dynamics are solved daily, and hence split from physical flow solution (Figure 3.4).

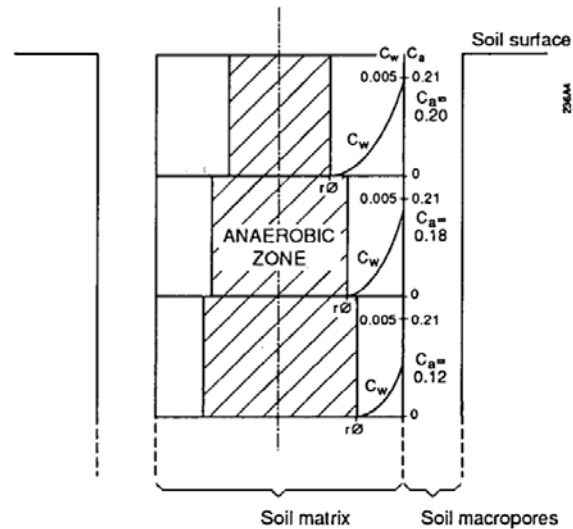


Figure 3.3: Example of a simulated two dimensional steady-state oxygen concentration profile in a structured acid sulphate soil; C_w = oxygen concentration in water ($\text{kg O}_2 \text{ m}^{-3}$ water), C_a = concentration of oxygen in air-filled macropores ($\text{m}^3 \text{ O}_2 \text{ m}^{-3}$ air), $r\phi$ = thickness of the anaerobic zone (m) (taken from Bronswijk and Groenenberg, 2004).

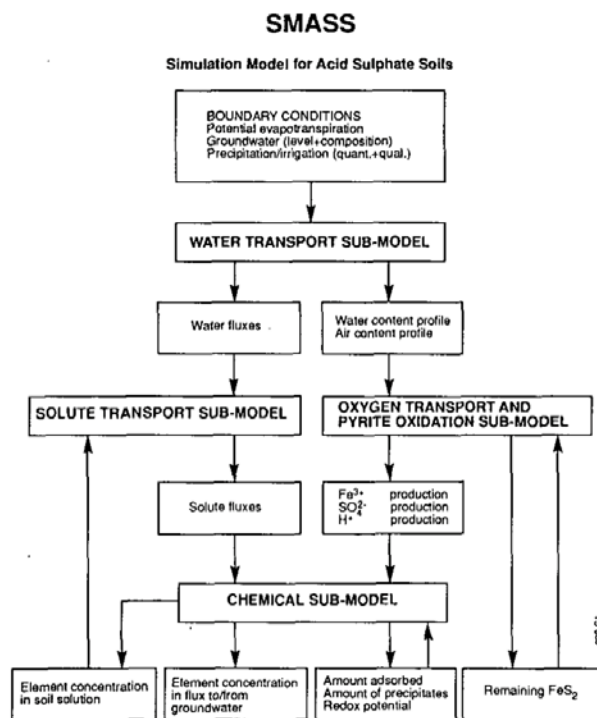


Figure 3.4: Overview of the operation of the SMASS model (taken from Bronswijk and Groenenberg, 1993).

CAEDYM geochemical & diagenetic model

The Computational Aquatic Ecosystem Dynamics Model (CAEDYM) is a general water quality model described in detail in Hipsey and Hamilton (2008) that has been extended to include geochemical dynamics and sediment-water interaction. The model is not designed for simulation of acid sulfate soils, however the model contains numerous abilities of relevant to the dynamics of acid sulfate soils that are reviewed here.

Aqueous speciation and solubility equilibrium control is simulated by including Ca, Mg, Na, K, Fe(II), Fe(III), Mn(II), Mn(IV), SiO₂, Cl, DIC, SO₄, PO₄, NO₃, NH₄, calcite, MnO₂, Fe(OH)₃ and Al(OH)₃ as components and solving the associated mass-action expressions according to the numerical method of Barrodale and Roberts (1980), as discussed originally in Parkhurst and Appelo (1999) and in the CAEDYM documentation (Hipsey and Hamilton, 2008). The mass-action constants used for speciation are generally taken from the WATEQ4F thermodynamic database (Nordstrom et al., 1990), although custom values may be easily configured. For a given total number of moles of each element in each computational cell, CAEDYM solves for the activity of each aqueous species, ionic strength and pH. For initialisation, the scheme can be adapted to solve for the charge balance by fixing the initial pH. The initial charge balance is stored for each computational cell, and as the model begins advancing in time, the scheme switches to solve for pH by assuming that the charge balance is conserved. The charge balance variable is subject to advection and mixing as all other state variables and must provided as a boundary condition.

The CAEDYM dynamic diagenesis model was originally based on the 1D 'Carbon and Nutrient Diagenesis' (CANDI) model (Boudreau, 1996), and its subsequent revisions (Luff et al., 2000; Luff and Moll, 2004), and designed for the simulation of aquatic sediments. The model is based on a 1D approximation of the sediment and pore-water dynamics. Each active sediment 'cell' in CAEDYM is discretized into a user definable number of layers (Figure 3.5) that start at thicknesses of <1mm at the sediment-water interface and increase exponentially down to a pre-defined sediment depth. Facility also exists within the model to use sediment 'zones' that are identical to the above description but are not necessarily coincident with the grid-structure of the water column domain (as shown in Figure 3.5). This way sediment-zones may be defined for the domain, and depending on the nature of the grid, the water cells above the sediment will be averaged for the purposes of the interfacial fluxes, allowing for more efficient simulations.

As the model has previously only been applied to saturated sediments, the model does not solve the Richard's equation like the above described codes, but does solve an advection-dispersion-reaction equation for particulate and dissolved components, with boundary conditions that always assume a ponded water surface and saturated conditions within the soil matrix. The diffusion terms parameterise bioturbation and irrigation effects of aquatic macroinvertebrates, and also allows for different rates of advection/sedimentation for both particulates and solutes:

$$\frac{\partial \phi C_j}{\partial t} = \frac{\partial}{\partial z} \left(\phi D^w \frac{\partial C_j}{\partial z} \right) - \phi \frac{\partial u C_j}{\partial z} + \omega(z) \left[\frac{C_j}{1} - \frac{C_j}{4} \right] \pm R_j \quad (3.28)$$

dispersion
advection
surface irrigation
reactions

$$\frac{\partial \phi_s C_p}{\partial t} = \frac{\partial}{\partial z} \left(\phi D_B(z) \frac{\partial C_p}{\partial z} \right) - \phi_s \frac{\partial v C_p}{\partial z} \pm R_j \quad (3.29)$$

bioturbation
burial
reactions

where C_j is the j^{th} solute, ϕ is the soil porosity, $\phi_s = 1 - \phi$, D^w is the dispersion coefficient, u is the water velocity, and v is the particulate sedimentation rate. ω is the irrigation rate, and may also be used to described cracking or a zone of homogenisation, and D_B is the bioturbation coefficient, which decreases with increasing z .

The model considers four main sets of reactions: those related to OM decomposition, the primary redox reactions, the secondary reactions, and the adsorption and equilibrium reactions. Note that the CAEDYM implementation described here has diverged significantly from the original CANDI code, and the main differences pertain to the treatment of organic matter, and the simulation of the geochemical conditions known to influence the diagenetic equations. Some of the secondary redox reactions are also modified. However, the core organic matter breakdown equations (and their numerical solution) remain similar as the original descriptions presented in Boudreau (1996), and to other similar codes such as those presented by Luff et al. (2001), Wang and Van Capellan (1996), and Meysman et al. (2003).

Like HP1, the approach adopts a splitting procedure to separate physical and chemical dynamics, but like LEACHM it includes the kinetic reactions in the main solute transport solution, and sequentially simulates (or 'splits') the geochemical equilibrium dynamics. Therefore in the first part of the time-step the transport and kinetic reactions are solved using the VODE solution scheme (Brown et al., 1989). Following this the updated solution is passed to the geochemistry module described above, which

then supplies necessary information on geochemical configuration, mineral solubility, pH, and aqueous speciation, following a similar solution technique as PHREEQC does for non-kinetic processes. The configuration of the equilibrium model applies to both the water column cells and each of the sediment layers.

The organic matter groups configurable within the main nutrient cycles (DOM_L , DOM_R , POM_L and POM_R) are mapped identically into the sediment. That is, labile and refractory forms of particulates settling into the sediment will then form the fuel to drive the diagenesis reactions through the pathways described above. Sedimented material is added to the top layer of the sediment model. The one difference between the sediment and water column OM groups is that sediment includes a third 'Very Refractory' (VR) particulate organic matter form, which can be used as a relatively inert OM fraction, as is often seen deep in sediments. The kinetically controlled reactions are comprehensive and include the reactions for organic matter breakdown and eventual oxidation, the re-oxidation of various by-products and the dynamics of the metal sulfide precipitation. FeS and FeS₂ formation under anoxia is included as a kinetic process but it is mediated by the solubility product calculated by the geochemical solver, and subsequent oxidation by available oxidants (including NO₃) is also parameterised using second-order rate dynamics.

The model includes various functions for the surface particulate boundary condition. The user may select dynamic prediction of the particulate fluxes based on the particle deposition rate from the water column as predicted by CAEDYM. Alternatively the model may use assumed surface concentrations (i.e., flux is implied), and the model will retain the initial surface value at the sediment-water interface. A third option is similar to the first (flux BC), but with the flux rates constant, and not dynamically determined by CAEDYM. The boundary condition for dissolved components is set to the value in the bottom water above the sediment. Fluxes of dissolved species between the sediment and water column are calculated dynamically according to the concentration gradient of the particular solute near the sediment-water interface according to Fick's Law (Eq 3.27 above). At the bottom boundary, the user may switch between either a known concentration or zero-gradient BC. The former will assume the initial sediment pore-water concentration is the value at the bottom and this will be held constant over the course of the simulation.

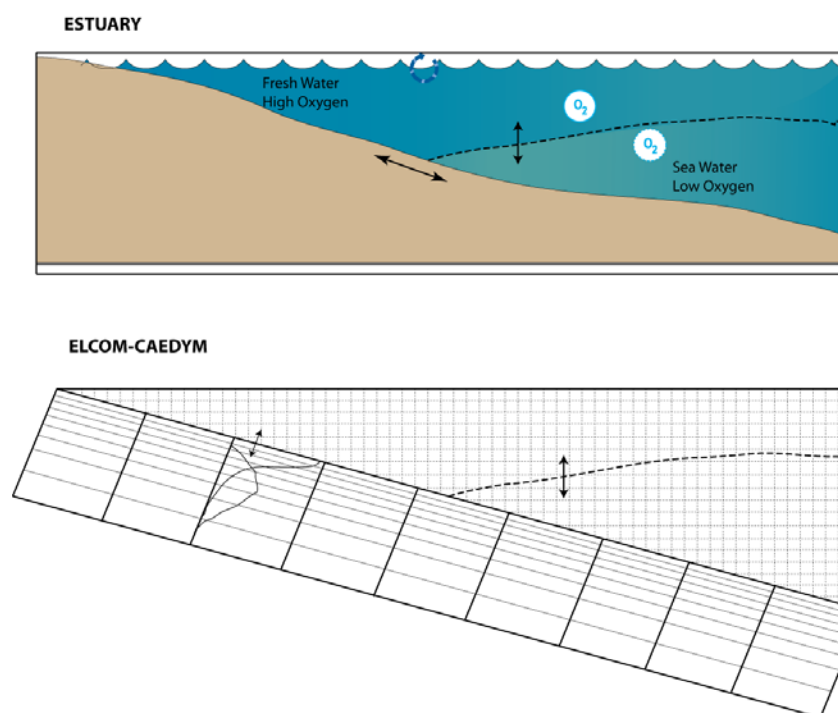


Figure 3.5: Conceptual view of ELCOM-CAEDYM simulation run to include the dynamic diagenesis model (taken from Hipsey and Hamilton, 2008).

Due to concerns being raised regarding the exposure of acid sulfate soils, the University of Western Australia (UWA) undertook a prognostic (2008 through to 2010) modelling assessment of potential acid loading to the Lower Lakes for a variety of scenarios on behalf of the South Australian Environment Protection Authority (Hipsey and Salmon, 2008). This work included modification to the

existing ELCOM-CAEDYM hydrodynamics and water quality model to include acid generation and loading from exposed ASS. Two acid loading models were originally developed and coupled to CAEDYM:

- *Simple empirical model:* based on simplified, relationships between acidity loading and exposed surface area that were known a priori. The model included the buffering of pH by dissolved carbonate in the water body, but no buffering through the dissolution of carbonate minerals (pH 7-8) or the dissolution of Fe and Al hydroxides (pH 2-5; also resulting in the release of these metals). The model also included no generation of alkalinity by in situ redox processes; and
- *Dynamic ASS model:* this was the natural extension of the above approach and was extended to include pyrite oxidation rates (the simple model assumed immediate release of acid following exposure) and a variety of mechanisms for transport of acidity from sediments into the water body. The dynamic model included: spatial variation in acidity potential, rate limitations on the oxidation process and dynamic loading based on simple horizontal flow and rewetting estimates. The dynamic model includes three main components, the Potential Acid Sulfate Soil (PASS – including the full load of potential acid which may or may not be eventually oxidised) the Actual Acid Sulfate Soil (AASS – including the components of PASS that are oxidised and available for transport as moles of H^+ from the sediment) and Acidity Flux, comprising the rate of transfer of acidity from the sediment to the surface water boundary. The acidity flux incorporates components of groundwater level fluctuations, rainfall induced leaching and mobilisation due to re-wetting. Fluxes due to baseflow and rainfall only occur if a given model cell is dry and these components are tracked downslope in the model domain until they reach the nearest surface water, or alternatively enter a ‘pit’ in the modelled terrain (in which case they are made available for future rewetting). Rewetting flux includes an immediate impact from flushing of moles of acid from the pore water, and ongoing diffusion through the soil matrix during periods of inundation.

The dynamics conceptual model of acid generation and transport into the water body, as implemented in the modified CAEDYM code is as shown in Figure 3.6. Note that while the model split each cell into a saturated and unsaturated zone, the model did not explicitly simulate vertical processes by solving the Richard’s equation and adopted for simplistic lateral flow assumptions.

Pyrite oxidation rates were obtained from the literature and experimental data from field investigations. The model was found to be sensitive to parameters characterising the following:

- rate of pyrite oxidation;
- potential acidity of the exposed sediment; and
- diffusion of acidity from the sediment following rewetting.

The results of the modelling undertaken indicated that pH values would fall well below accepted guideline levels for aquatic ecosystems, and the resultant mobilisation of heavy metals, were likely to result. However, the report highlights a significant amount of uncertainty with many of the model parameterisations and parameters adopted to represent processes governing acid generation and transport into the surface water.

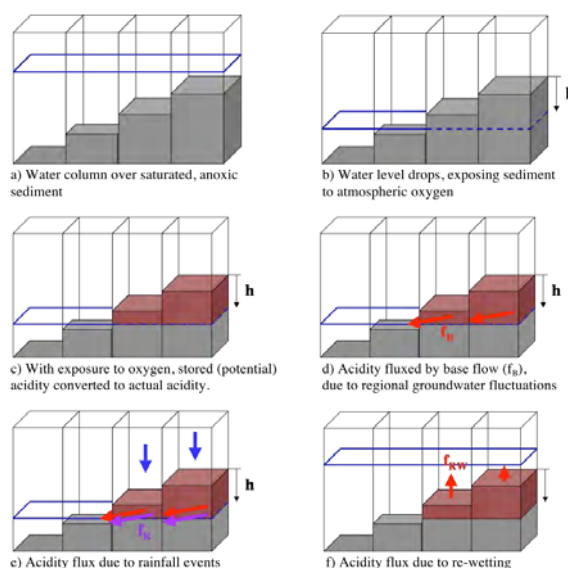


Figure 3.6: Conceptual ASS model of acid generation and transport (taken from Hipsey and Salmon, 2008).

4 Model description

In the context of the present application, there is no clear code of those reviewed above that can be applied directly. The HP1 model is widely used and robust, and includes capacity to simulate much of the required complexity, however it is computationally intensive should it need to be applied at fine spatial resolution, and doesn't explicitly deal with oxygen diffusion, POM decay or allow for a detailed model of pyrite oxidation. The SMASS model is fairly complete for this study, however a considerable effort would be required to dynamically link the model to a 3D model of surface water dynamics. CAEDYM includes the most complete set of geochemical reactions, and already includes solute transport connected to the surface waters, however there is currently no facility for exposed cells to drain and become unsaturated, and for atmospheric oxygen diffusion to drive the pyrite oxidation process.

Given the long scenario run-times required for this study, serious consideration must also be given to manage long simulation run-times. Therefore a direct coupling with HP1, although feasible, would create unmanageable run-times when applied on a spatially resolved lake grid that reflects the heterogeneity observed during soils surveys. Similarly, the Richard's equations solvers are all computationally intensive when applied across 1000's of lake sediment cells. The MODFLOW UZF package is an attractive alternative since it is a simplification of the complete Richard's equation and has been designed for coupling with the 3D, horizontally explicit, model equations. In its present form however, the UZF module allows for no solute transport or unsaturated zone geochemical reactions (Prommer pers. comm.), such as are required for the acid sulfate soil analysis.

After consideration of the above advantages and disadvantages, and bearing in mind time constraints associated with the project, the approach adopted was to develop a soil geochemical and hydrology model that can be coupled with the 3D ELCOM-CAEDYM lake model (described in Section 4.1) and that has already been applied to the Lower Lakes (Hipsey et al., 2009). The module is developed as a stand alone module with hydrological and geochemical algorithms (Section 4.2) that are relatively simple to those described above, and dynamically coupled to the surface water dynamics. Capacity to include a more sophisticated Richard's equation solution to resolve the moisture profiles at higher resolution has been allowed for in the module design, but is not presented here.

The model developed allows for simulation of soil dynamics and surface water processes through a dynamic coupling. The model provides for spatial heterogeneity in soil properties, draining and flooding of exposed acid sulfate soil material, and hydrological and geochemical interaction with the surface water dynamics. The surface water model is able to simulate hydrodynamics and biogeochemical processes and can be used to explore future scenarios of lake drawdown or stabilisation with freshwater or seawater via configuration of relevant inflow boundary conditions. While the soil hydrological model is more simplistic than some of those presented above, the adopted approach does provide for key dynamics while not requiring significant input parameters, accounts for spatial heterogeneity, and is able to simulate for multi-annual to decadal time-frames, which would not be possible otherwise.

4.1 Model platform

The lake model platform ELCOM-CAEDYM, used for this investigation, is a coupled hydrodynamic-biogeochemical model developed at the Centre for Water Research, University of Western Australia (<http://www.cwr.uwa.edu.au>). ELCOM (Estuary, Lake and Coastal Ocean Model) is a three-dimensional hydrodynamics model used for predicting the velocity, temperature and salinity distribution, including stratification, in natural water bodies subjected to external environmental forcing such as wind stress, inflows, surface heating or cooling. The model has been validated with field measurements across a range of sites in the coastal ocean, large lakes, reservoirs, estuaries and coastal lagoons, including in the Lower Murray River below Lock 1 (Hipsey et al., 2009).

ELCOM solves the unsteady Reynolds-averaged Navier-Stokes (RANS) equations using a semi-implicit method similar to the momentum solution in the TRIM code with the addition of quadratic Euler-Lagrange discretisation, scalar (e.g. temperature) transport using a conservative flux-limited approach, and elimination of vertical diffusion terms in the governing equations. ELCOM does not assume a relationship between the vertical Reynolds stress terms and the resolved shear, but instead applies a mixing model to directly compute the vertical turbulent transport. Molecular diffusion in the vertical direction is neglected as turbulent transport and numerical diffusion are generally dominant.

The free-surface evolution is governed by vertical integration of the continuity equation for incompressible flow in the water column applied to the kinematic boundary condition.

Heat exchange through the water's surface is described by standard bulk transfer models found in the literature. The energy transfer across the free surface is separated into non-penetrative components of long-wave radiation, sensible heat transfer, and evaporative heat loss, complemented by penetrative shortwave radiation. Non-penetrative effects are introduced as sources of temperature in the surface-mixed layer, whereas penetrative effects are introduced as source terms in one or more grid layers on the basis of an exponential decay and an extinction coefficient (Beer's law). The bulk-transfer equations are corrected for non-neutral atmospheric stability within the internal boundary layer over the water surface (based on Monin-Obukhov similarity), and spatially variable meteorological conditions can be included.

The fundamental numerical scheme is adapted from the TRIM approach of Casulli and Cheng (1992) with modifications for accuracy, scalar conservation, numerical diffusion, and implementation of a mixed-layer turbulence closure. The solution grid uses rectangular Cartesian cells with varying Δx and Δy (horizontal) and vertical Δz spacing. The grid stencil is the Arakawa C-grid: velocities are defined on cell faces with the free-surface height and scalar concentrations on cell centres. The free-surface height in each column of grid cells moves vertically through grid layers as required by the free-surface evolution equation. Replacement of the standard vertical turbulent diffusion equation with a mixed-layer model eliminates the tri-diagonal matrix inversion for each horizontal velocity component and transported scalar required for each grid water column in the original TRIM scheme. This provides computational efficiency and allows sharper gradients to be maintained with coarse grid resolution.

ELCOM couples with the Computational Aquatic Ecosystem Dynamics Model (CAEDYM) to simulate the transport and fate of the numerous biogeochemical parameters. CAEDYM optionally models inorganic particles, oxygen, organic and inorganic nutrients (C, N, P and Si), multiple phytoplankton and other biological groups. CAEDYM includes a geochemistry module similar to that is able to solve for kinetic and equilibrium dynamics of geochemical components, as described in Section 3.4. The module allows the user to input inorganic components of interest (e.g. ions, metals) and account for any pure phases (i.e. minerals, gases), and the model will solve speciation of the complete system based on a thermodynamic equilibrium. Optional kinetic processes are also configured such as microbially mediated redox transformations. The geochemical components are subject to transport and mixing by ELCOM, like all CAEDYM variables, and they are influenced by biology, such that processes such as photosynthesis, nutrient uptake and organic matter mineralisation will dynamically affect the aqueous speciation and pH. In addition, static and dynamic sediment diagenesis models have been included within CAEDYM, which allow for prediction of oxygen, nutrient and metals fluxes at the sediment water-interface. Atmospheric and sediment transfers of relevant geochemical components are also configurable. The geochemical model has been tested from mine lakes impacted by acid mine drainage (AMD; Oldham et al., 2009) to pH neutral waters (both fresh and saline; Read et al., in prep).

4.2 *Acid sulfate soil model and parameterisation*

Overview and assumptions

In field environments, it is well known that the pyrite oxidation process is rate limited and dependent on numerous factors such as the chemical kinetics, biotic factors, and in particular, the rate of oxygen diffusion into the soil profile (see Section 3.3). Once sulfuric material is generated and acidity is liberated into pore-waters, the loading of the leachate into the surface waters is not immediate and depends on suitable loading mechanisms, such as flushing of the soil profile in response to rainfall events or diffusive fluxes from oxidised sediment into the standing water upon re-wetting of the sediment. As a result of the above two factors, and since the water level is not static, in order to predict the dynamics and the testing of alternate water level management scenarios the model must allow for these potentially important controls on acidity generation and transport in order to estimate the loading fluxes and ultimate state of the lake.

The model presented here is designed to allow for these important process dynamics. Conceptually, the model is outlined in Figure 4.1 and includes three main components:

- 1) the Potential Acidity, χ , which is the 'reservoir' of acidity in any given sediment volume (also referred to in this report as PASS);
- 2) the Available Acidity, ϕ , which is the moles of acidity available at any given time within a soil/sediment unit (also referred to in this report as actual acidity, or AASS, and subdivided into

unsaturated zone UZAASS and saturated zone SZAASS), and subject to neutralisation and transport processes;

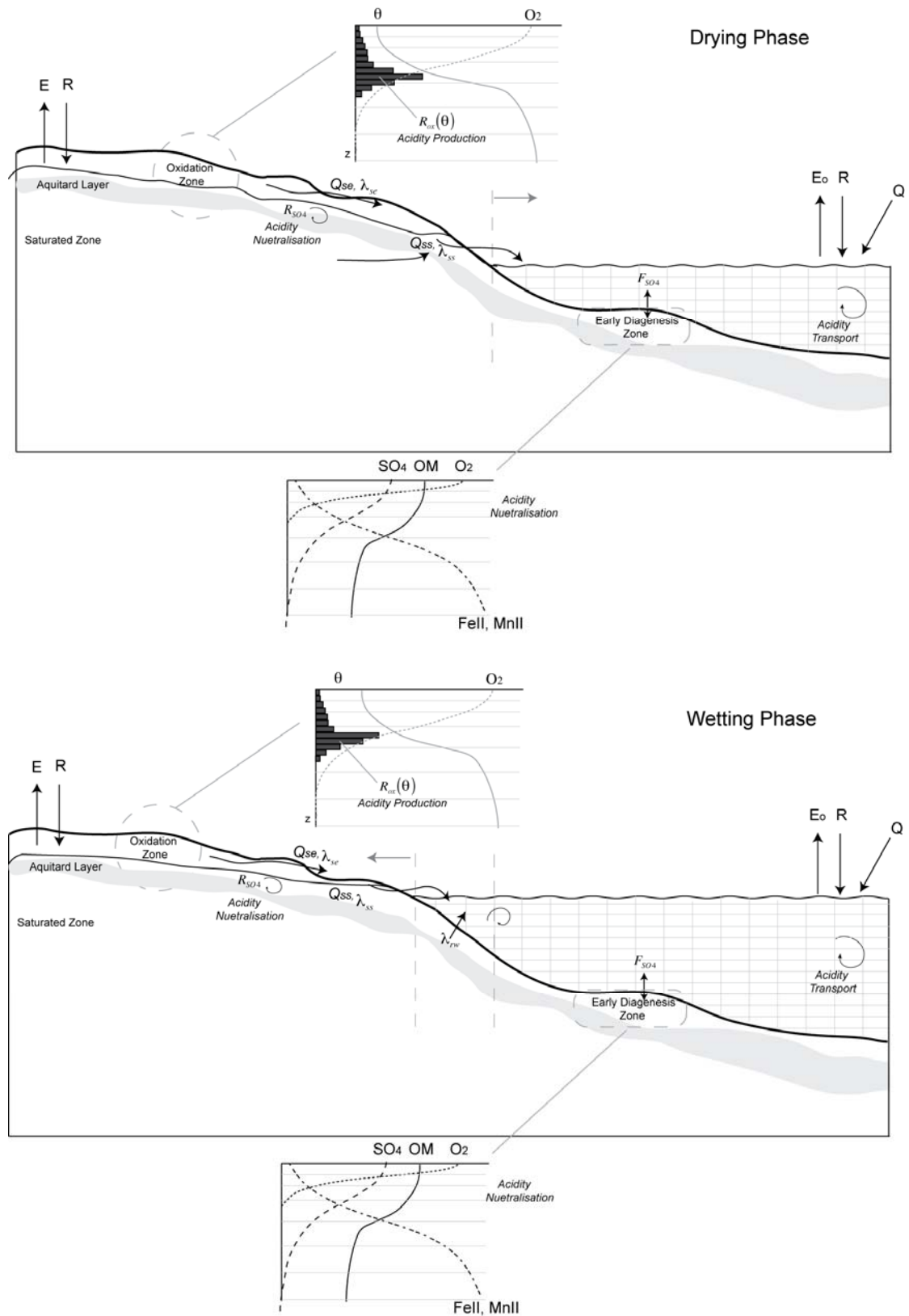


Figure 4.1: Conceptual model of acid generation and transport processes for the drying phase (top) and the wetting phase (bottom). Notation: E = evaporation; R = rainfall; Q = general inflows coming to the lake; SO_4 = dissolved sulfate concentration; OM = organic matter; F_{ell} = dissolved iron; $MnII$ = dissolved manganese; θ = soil moisture; O_2 = oxygen concentration; Q_{se} = saturation excess flow; Q_{ss} = seepage flow; R_{SO_4} = acidity consumption via SO_4 reduction; R_{ox} = pyrite oxidation; F_{SO_4} = acidity consumption by SO_4 reduction in lake sediments; λ_{rv} = flux of acidity from acidified sediment following rewetting.

3) the Acidity Flux, λ , which is the rate of transfer of the acidity from the reservoir within the soil to the surface water and this is based in the soil hydrological model or prescribed diffusive flux rates if a cell becomes inundated.

These terms are described in detail in the following sub-sections.

Key Model Assumptions:

- Alkalinity generation in the sediment and soil through SO_4 reduction only occurs in the Saturated Zone (SZ) and in the submerged lake sediments
- ANC consumes acidity based on a kinetic rate (i.e. not immediately consumed)
- Acidity fraction that is mobile is assumed to be constant and not sensitive to pH
- Soil textural properties are assumed constant with depth
- Soil PASS and ANC profiles below 20cm are averages from each lake for each soil type
- Seepage is routed to the water on a daily basis, not each time-step
- Negative seepage (i.e., 'backflow' from lake into the soil) does not occur
- pH and temperature dependence are not currently included in the PASS oxidation rate

Soil hydrology

The key factor in determining the generation and mobilisation of acidity is the soil hydrology since these dynamics control the amount of oxygen that can penetrate into the soil, and the amount of lateral flow that may be able to transport the acidity to the lake. The soil hydrology model implemented here is based on a conceptual 2-layer storage-capacitance model able to resolve the unsaturated zone thickness and moisture content, and the saturated zone thickness and seepage flux (Figure 4.2).

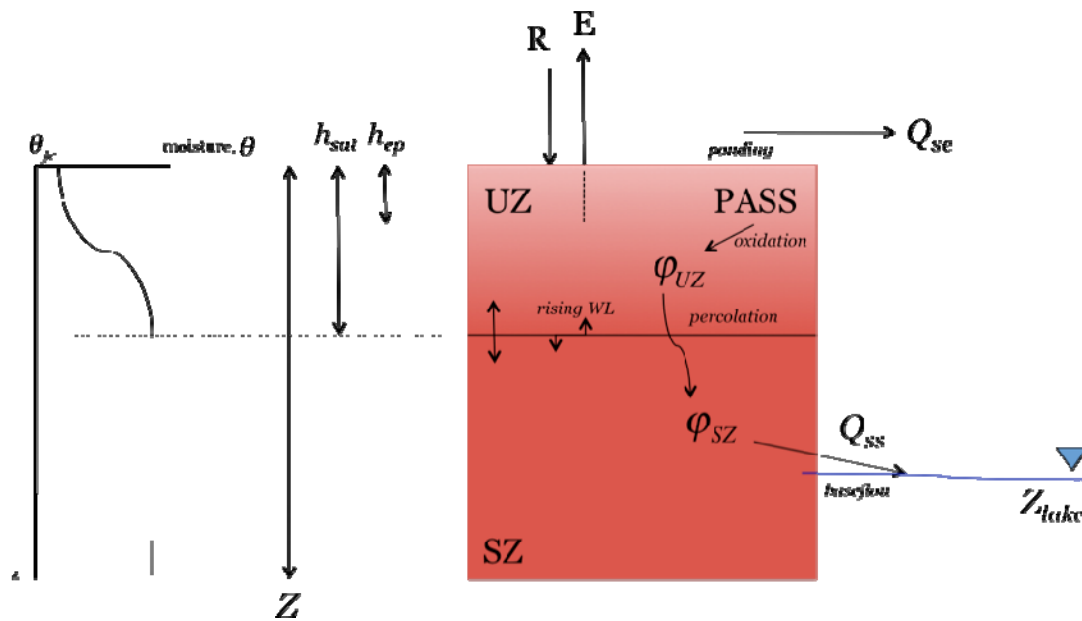


Figure 4.2: Soil unit hydro-geochemical model. Notation: E = evaporation; R = rainfall; UZ = unsaturated zone; SZ = saturated zone; h_{sut} = depth of unsaturated zone, h_{ep} = depth of influence of evaporation; Z_{lake} = lake water level; Q_{se} = saturation excess flow; Q_{ss} = seepage flow; PASS = potential acid sulfate soil material (χ); θ = soil moisture; θ_{fc} = soil field capacity; ϕ_{UZ} = unsaturated zone available acidity (UZAASS); ϕ_{SZ} = saturated zone available acidity (SZAASS).

The model is conceptually similar to Famer et al. (2003) but modified for the present situation given the different context (i.e. lake bed hydrology rather than a typical hillslope application). Within the present application the soil hydrology is resolved in each of the exposed sediment (i.e., 'soil') cells. In this model, the soil column is driven at the surface by daily rainfall and evaporation fluxes. Saturation and infiltration excess water is considered to 'pond' or contribute to fine-scale through-flow

processes above the water table and is routed to the closest lake cell based on the local topographic relief. Vertical percolation of water that infiltrates is assumed to occur within the daily timestep, leaving the surface soil at field capacity. Excess water (that is, water above field capacity) is added to the saturated zone store whose vertical dimension will change in response to this infiltration amount, and also evaporation and lateral flow (seepage) processes. The processes of evaporation, infiltration and seepage are all dependent on the soil texture and the model allows for input of different soil types (e.g., coarse sand, s , medium sand, m , and fine/clay material, f), which must be defined for each cell of the model grid.

For each computational soil unit (i.e., the i^{th} soil cell) the maximum possible storage, S , is defined as:

$$S_i = Z_i \phi_i \quad (4.1)$$

where ϕ is the soil porosity and depends on the soil type according to $\phi_i \in (\phi_s, \phi_m, \phi_f)$, and Z is the soil depth calculated based on the local bathymetry in the i^{th} cell and a global reference depth, set by the user. The water budget equation for the entire soil column is defined as:

$$\frac{dS_i}{dt} = R - E_i - (Q_{ss_i} - Q_{se_i}) / A_i \quad (4.2)$$

where R is rainfall, E_i is the cell-specific bare-soil evaporative flux, both in units of m day^{-1} , Q_{ss} is the saturated zone lateral flow amount, and Q_{se} is the surface lateral flow generated by saturation excess runoff, in units of $\text{m}^3 \text{ day}^{-1}$, normalised by area, A , in units of m^2 . The total store of water in each soil column is comprised of saturated and unsaturated regions, such that:

$$S_i = S_{sat_i} + S_{us_i} \quad (4.3)$$

The water balance for each region is defined as:

$$\frac{dS_{us_i}}{dt} = (R - Q_{se_i} / A_i) - E_{us_i} - I_i \quad \text{and} \quad \frac{dS_{sat_i}}{dt} = I_i - E_{sat_i} - Q_{ss_i} / A_i \quad (4.4)$$

where I_i is the infiltration amount percolating from the unsaturated profile to the saturated region (m day^{-1}). Evaporation is only able to remove water from the top h_{ep} (m) (calculated as $Z_{ep_i} = Z_i - h_{ep}$), and this is set to be specific to the soil textural properties. The total evaporation is calculated according to:

$$E_i = \begin{cases} \alpha_{ep} E_p \left(\frac{S_{us_i}}{S_{\max_i} - S_{sat_i}} \right) & \text{for } S_{sat_i} \leq Z_{ep_i} \phi_i \\ \alpha_{ep} E_p \left(\frac{S_{us_i} + (S_{sat_i} - Z_{ep_i} \phi_i)}{S_{\max_i} - Z_{ep_i} \phi_i} \right) & \text{for } S_{sat_i} > Z_{ep_i} \phi_i \end{cases} \quad (4.5)$$

where α_{ep} is an adjustment factor scaling total soil evaporation to potential evapo-transpiration (E_p), $Z_{ep_i} \phi_i$ and $h_{sat} = Z_i - S_{sat_i} / \phi_i$ is the phreatic depth (i.e., depth from the soil surface to the water table). The evaporation specifically from the saturated zone component of the soil cell is:

$$E_{sat_i} = \begin{cases} 0 & \text{for } S_{sat_i} \leq Z_{ep_i} \phi_i \\ E_i \frac{S_{sat_i} - Z_{ep_i} \phi_i}{S_{us_i} + (S_{sat_i} - Z_{ep_i} \phi_i)} & \text{for } S_{sat_i} > Z_{ep_i} \phi_i \end{cases} \quad (4.6)$$

and E_{us} is then calculated as $E - E_{sat}$.

Infiltration from the unsaturated to the saturated sub-store is defined in this model as the amount of water in the unsaturated zone above field capacity, θ_{fc} . The excess water is calculated after losses from evaporation and surface runoff, such that $S_{us_i}^* = S_{us_i}^{t-1} + (R^t - Q_{se_i}^t) - E_{us_i}^t$, and then infiltration, I_i , is calculated from this intermediate estimate:

$$I_i^t = k \left[S_{us_i}^* - (S_{\max_i} - S_{sat_i}^t) \frac{\theta_{fc}}{\phi_i} \right] \quad (4.7)$$

where θ_{fc} is the soil field capacity. The remaining moisture content is θ , and the moisture by weight is approximated as:

$$\psi_i = \frac{\theta_i \rho_w}{\theta_i \rho_w + (1 - \phi_i) \rho_s} \quad (4.8)$$

where ρ_s is the soil bulk density. While the model described above is a two layer model, with a depth integrated value for the unsaturated zone moisture, a vertical moisture distribution function is imposed on the unsaturated region that accounts for the characteristic moisture profile that would likely exist in soils. This is required since, as described below, the vertical pyrite content is largely variable and the oxidation rate is highly sensitive to soil moisture; a simple lumping over the entire depth of the unsaturated zone would not give an accurate integration. The full solution of the Richards equation, while appropriate, is not computationally possible at the desired time step and given the numerous cells that would require its solution. Instead the model assumes the unsaturated soil profile consists of three zones that are parameterised using a piecewise function (Figure 4.3): the capillary rise zone (near saturation), transition region (moisture grades down from near saturation to field capacity), and the surface zone (field capacity). The vertical dimension of each zone is based on the soil texture, which is estimated by the air-entry head for the various soil types used in the model. For example, a clayey soil has higher capillary rise zone than for a sandy soil. The function works up from the water table, so if the soil surface is lower than the height of the capillary rise or transition zone, then no top zone would be present at that time and the zones would be fractionally defined.

Suction is also considered in the model, albeit simply. If the evaporative demand removes water from the unsaturated zone, and there is insufficient unsaturated water to meet that required by imposing the moisture distribution described above, the water is raised from the saturated zone to maintain mass conservation.

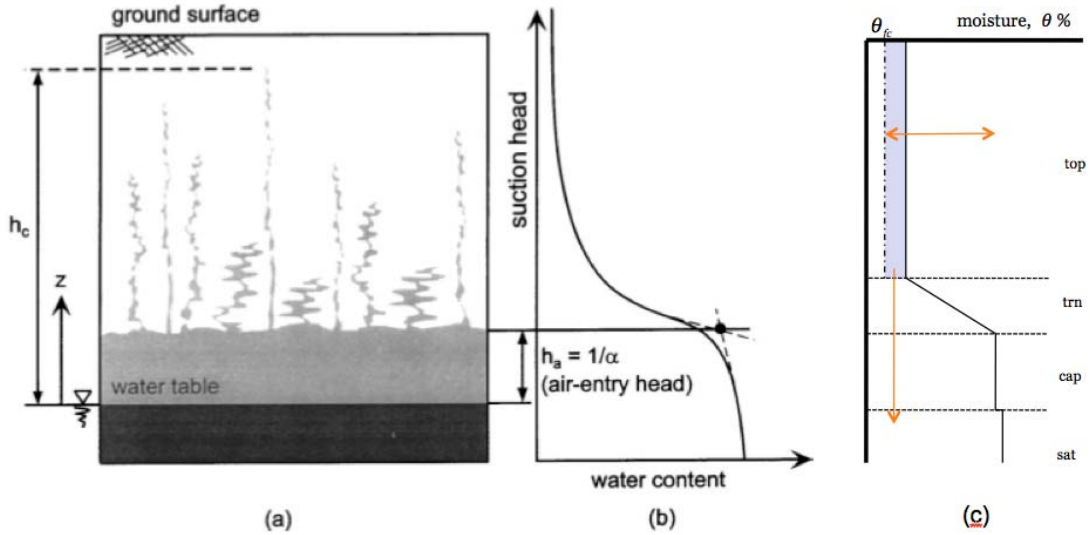


Figure 4.3: Conceptual basis (a & b) of vertical moisture profile (taken from Lu and Likos, 1994), and outline of vertical moisture profile model implementation (c) that is used to resolved vertical moisture dynamics in the soil hydrology model.

The surface runoff is calculated as the surface infiltration excess, and is equal to

$$Q_{se_i} = \begin{cases} 0 & \text{for } R \leq I_{se_i} \\ R - I_{se_i} & \text{for } R > I_{se_i} \end{cases} \quad (4.9)$$

The seepage, Q_{ss} , is parameterised based on a storage-capacitance approach that assumes:

$$Q_{ss_i} = \begin{cases} 0 & \text{for } \phi_i S_{sat_i} \leq (\overline{Z}_{lake} + \varepsilon) \\ \alpha_{ss} \left[\frac{\phi_i S_{sat_i} - (\overline{Z}_{lake} + \varepsilon)}{\phi_i S_{max_i} - (\overline{Z}_{lake} + \varepsilon)} \right]^{\beta_{ss}} & \text{for } \phi_i S_{sat_i} > (\overline{Z}_{lake} + \varepsilon) \end{cases} \quad (4.10)$$

where α_{ss} is the maximum seepage rate as a fraction of the storage (assumed to be when the soil store is fully saturated), β_{ss} is an exponent that determines the shape of the seepage rate response to

reduced water stores and \overline{Z}_{lake} is the basin average water level (m AHD) of the standing water in the lake at time t , where the lake average is used to smooth over high frequency variations in water level due to surface waves. The factor ε is defined as a small depth (~5-10 cm) that can be configured by the user to prevent seepage occurring under low head conditions where it is considered friction would prevent flows towards the lake. The lateral flow processes are assumed to be immediately routed to the surface waterbody over the course of the day. This simple routing assumption may over-estimate the rate at which acidity is delivered to the water column. Equation 4.10 is developed has a conceptual basis and was created as a meta-model from high resolution numerical simulations conducted with a representative lake-shore cross section using HYDRUS-2D, discussed separately in Section 4.3

Acidity generation

The potential acidity for the depth of the unsaturated zone, h_{sat} (m) of a given sediment unit, i , is defined as:

$$\chi(h_{sat})_i = \int_{h_{sat}} \kappa_i \rho_s A_i dh_{sat} \quad (4.11)$$

where χ is the potential acidity for the sediment unit at location i (mol H⁺), κ is the total acid generation potential per unit sediment mass (mol H⁺ kg⁻¹), which varies as a function of depth, ρ_s is the bulk density (kg m⁻³), and A is the area of the sediment unit i (m²). The depth of oxidised sediment, h_{sat} , is related to the surface water level of the lake and the local groundwater dynamics as outlined by the soil hydrological model described above.

Once the potential acidity is exposed to oxygen, the rate of conversion to actual acidity, φ , is predicted using a first-order reaction constant that is based on the unsaturated zone moisture content:

$$\frac{d\chi_i}{dt} = \underbrace{\frac{dh_{sat}}{dt} \kappa(h)_i}_{\text{increase in potentially reactable sulfides due to water level decline}} - \underbrace{R_{ox}(\theta)}_{\text{oxidation of sulfidic material}} \chi_i \quad (4.12)$$

where the rate of pyrite oxidation, R_{ox} (day⁻¹), is strongly dependent upon a number of factors, including the availability of oxygen. Note that the acidity generated here is considered to be the sum of both the available and retained components (TAA and RA in Eq 3.4, respectively). In the literature on the geochemistry of mineral weathering, there are numerous studies of pyrite oxidation rates with careful control of experimental conditions and characterisation of the materials used. In such experiments, the mineral weathering rate is generally normalised to the mineral surface area present; if the experiment is performed over a sufficiently long period of time for there to be a significant decrease in mineral surface area, the weathering rate is often corrected for this. With this kind of experimental control, it is possible to reproduce mineral weathering rates (in different experiments with the same conditions) to within, say, an order of magnitude. In contrast, a brief survey of the literature to obtain typical rates of pyrite oxidation in ASS samples (or pyritic marine or estuarine sediments) indicated that experimental conditions are often uncontrolled and unmonitored, in particular with regards to oxygen availability, pyrite grain size and specific surface area. The resulting apparent oxidation rates of acid sulfate soils (or pyritic marine sediments) vary by over three orders of magnitude (Table 4.1 and Figure 4.3). The model here assumes a typical first order reaction rate based on the amount of sulfide present.

Oxidation rates of pyrite in acid sulfate soils are generally much higher than pyrite oxidation in waste dumps from mining operations, due to a much higher specific surface area (Wiersma and Rimstidt, 1984), and may furthermore be higher than pyrite found in coal deposits (Borma et al., 2003). The highest rates in Table 4.1 were observed in experiments where oxygenated conditions were maintained.

Fully oxygenated conditions are highly unlikely to be the case in the lower lake sediments, and the rate of pyrite oxidation is likely limited by oxygen diffusion into the sediments. The rate of oxygen diffusion is a function of the porosity of the sediment, the water content of the porespace, the presence of macropores (e.g., cracks), etc. Furthermore, aerobic organic matter mineralisation occurring in the exposed sediments will also consume oxygen, and therefore potentially also competing for oxygen and decrease the rate of pyrite oxidation (e.g., Borma et al., 2003; Cook et al., 2004; Bronswijk et al., 1993; Vegas-Vilarrubia et al., 2008). Recent experimental work conducted by Earth Systems (2010) on Lower Lakes sediments enabled development of a relationship between

oxygen consumption due to pyrite oxidation and the soil moisture (see also Table 5.2). This relationship was parameterised within the model by linking the unsaturated zone moisture content estimate (from the above described soil hydrology model) with the oxidation rate. The oxidation rate is given as:

$$R_{ox}(\psi_i) = f_{Ox} k_{PyrOx}(\psi(t)) \chi \quad (4.13)$$

where f_{Ox} is a adjustment parameter that can be used to test the sensitivity of the oxidation rate in the model, or used to account for potential oxygen diffusion limitation. The oxidation rate function is parameterised for sand and clay material as:

$$k_{PyrOx}(\psi(t)) = \begin{cases} -9.7011\psi^3 + 2.1949\psi^2 + 0.0025\psi + 0.0006 & \text{SAND} \\ -0.0142\psi + 0.0068 & \text{CLAY : } 0.225 < \psi < 0.48 \\ 0.0142\psi & \text{CLAY : } 0 < \psi < 0.225 \end{cases} \quad (4.14)$$

Table 4.1: Overview of literature pyrite oxidation rates

Reference	Approximate rate (mol FeS ₂ mol FeS ₂ ⁻¹ s ⁻¹) [day ⁻¹]	Comments
Ward et al. (2004a)	~1x10 ⁻⁷ [~0.009]	ASS: Not fully oxic, (gauze bag)
Ward et al. (2004b)	~2 x10 ⁻⁸ [~0.002]	ASS: Not fully oxygenated, light clay, 40 um thick plastic bag.
Borma et al. (2003)	1 x10 ⁻⁹ -2.8 x10 ⁻⁸ [0.00009 – 0.0024]	Sediments: “crumbled” samples, layer <1cm.
Rigby et al. (2006)	~2 x10 ⁻⁷ [~0.018]	ASS: Assumptions (data not given): 25L volume liquid in reactor, density fines 1.5 kg/L. Oxygen limitation in at least one of the experiments.
Di Nanno et al. (2007)	~1 x10 ⁻⁶ [~0.086]	Sediments: With nutrients and microbial inoculation. Oxygen concentrations not measured, and samples high in organic matter (possible alternative oxygen sink)
Morse (1991)	Initial: (0.4-2) x10 ⁻⁶ ; [~0.086] Later: (1-8) x10 ⁻⁸ [~0.003]	Marine sediments: Initial (<10d) / later rate , oxic (but no details), oxidation in seawater. Initial rate due to v. fine particles (<0.3 um)

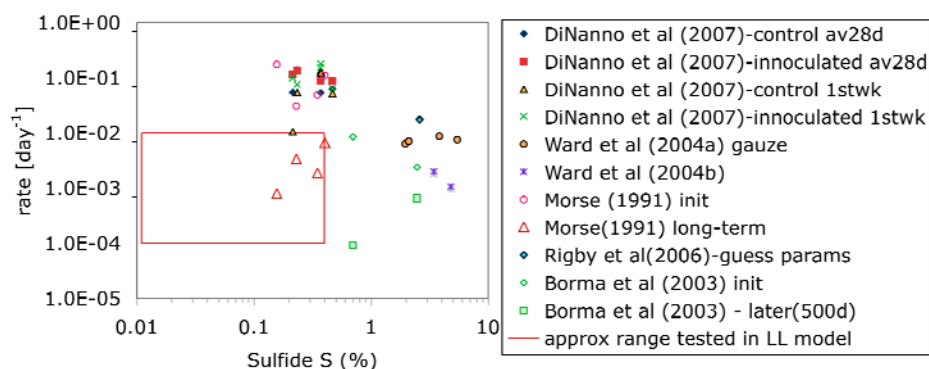


Figure 4.3: Range of pyrite oxidation rates from literature laboratory weathering experiments on acid sulfate soils and sediments (see Table 4.1 for details), vs. the sulfide content of the material. Red box indicated approximate range originally tested in Hipsey and Salmon (2008) Lower Lakes acid sulfate soil model.

Since the oxidation process is rate limited, and the lake water level (and h), changes with time, the available acidity within the soil column varies in each computational cell dynamically. Additionally, there are time varying acidity fluxes and sinks. The unsteady balance equation for the available acidity in the unsaturated zone is therefore summarised:

$$\frac{d\phi_{UZ_i}}{dt} = R_{ox}(\psi_i) - R_{neut}(ANC_i) - \lambda_I - \lambda_{rw} - \lambda_{se} - \lambda_{wt} \quad (4.15)$$

where λ_I is the rate of acidity mobilisation from the unsaturated zone to the saturated zone in response to percolation of rainfall, λ_{rw} is the flux of acidity to the water column following inundation (ie. rewetting), λ_{se} is the acidity mobilised from the unsaturated soil profile once rainfall ponding occurs, and λ_{wt} is the acidity flux from the unsaturated to the saturated zone due to a rising water table. All fluxes are in units of mol H⁺ day⁻¹. The neutralisation function is defined as a first order acidity consumption rate:

$$R_{neut}(ANC_i) = \begin{cases} -k_{ANC}ANC & \text{if } \phi_{UZ} > 0 \\ 0 & \text{if } \phi_{UZ} \leq 0 \end{cases} \quad (4.16)$$

where k_{ANC} is the daily fraction of ANC that can be consumed. Acidity percolating down from the unsaturated zone will enter the saturated zone and may become consumed, or transported via seepage to the lake:

$$\frac{d\phi_{SZ_i}}{dt} = \lambda_I + \lambda_{wt} - \lambda_{ss} - R_{SO4}\phi_{SZ_i} \quad (4.17)$$

where λ_{ss} is the acidity that is mobilised by the seepage term Q_{ss} . In addition to the transfer of acidity between compartments within the model, R_{SO4} is also specified to consume available acidity in response to activity by sulfate reducing bacteria and may be prescribed by the user.

Fluxes

Once generated, acidity can flux from any sediment/soil unit due to a combination of the factors described earlier, and they are primarily driven by the hydrological fluxes predicted by the soil hydrology model. The soil cells are connected to CAEDYM by fluxes due to seepage, overland flow and diffusion following reinundation. The first two only occur if the cell is dry and the flux due to re-wetting only occurs when the cell becomes inundated after a period of exposure to the atmosphere (see Figure 4.1 above)

Leaching/Seepage from exposed sediments:

The functions are limited to ensure that flux rate does not exceed the available acidity store. The percolation of acidity down the soil profile is calculated as a function of the infiltration rate compared to the unsaturated zone depth:

$$\lambda_I = f_{mob} \left(\frac{I}{h_{sat}} \right)^\eta \phi_{UZ_i} \quad (4.18)$$

where η controls the non-linearity of this response. Similarly, overland flow is calculated assuming that the excess water is able to mobilise a fraction of acidity by again comparing to the unsaturated zone depth:

$$\lambda_{se} = f_{mob} \left(\frac{Q_{se}}{h_{sat}} \right) \phi_{UZ_i} \quad (4.19)$$

where f_{mob} is the mobilisation fraction parameter to account for the immobile (particulate) acidity components being unavailable for transport. The transfer of acidity due to a rising water table is calculated linearly based on the fraction of unsaturated zone that is removed from one time step to the next:

$$\lambda_{wt} = \begin{cases} 0 & \text{for } h_{sat}^t \leq h_{sat}^{t-1} \\ \frac{(h_{sat}^t - h_{sat}^{t-1})}{h_{sat}^t} \phi_{UZ_i} & \text{for } h_{sat}^t > h_{sat}^{t-1} \end{cases} \quad (4.20)$$

The baseflow flux is calculated by estimating the fraction of the acidity that is mobilised from the ratio of the flow to the saturated zone depth:

$$\lambda_{ss} = f_{mob} \left(\frac{Q_{ss}}{\min(\phi S_{sat}, 0.5)} \right) \phi_{SZ_i} \quad (4.21)$$

where acidity is assumed to be contained in the top 0.5 m from the phreatic surface.

Diffusive transport from re-wetted sediments

The rate of solute diffusion through water was found from literature sources (Boudreau, 1997; Schnoor, 1996) to be approximately 10^{-4} (m^2s^{-1}), although this is dependent on salinity. For fluxes of substances in the re-wetted sediment back to the water column, the rate of diffusion would be lower than through water due to the tortuosity of the diffusion pathway through the sediment, and Schnoor (1996) indicates the diffusion rates through compacted sediment could be an order of magnitude lower than the molecular rate. Field observations (e.g., Fitzpatrick et al., 2008) have indicated that the sediments vary from fine clay materials to coarse sand. However, particularly clay-rich sediments often develop macro-pore structures (cracking) as a result of drying, which would enhance diffusion, as would turbulent fluid motions in the lake, particularly in this shallow, energetic system.

The mobilisation flux in this model is designed so that when the cell is re-wet it is calculated on a per cell basis depending on the underlying soil type. It accounts for two distinct mechanisms; the first is flushing of porewater at the sediment-water interface of a newly re-wetted cell (only applicable during first day following re-wetting). The fast release of available acidity from lower lake sediments when diffusion was not a limiting factor was clearly indicated in short-term (24h) remobilisation experiments performed by Simpson et al. (2008), the laboratory columns of Sullivan et al. (2009), and the mesocosm experiments of Hicks et al. (2009), as well as the fast response of pH after rainfall in Currency Creek in 2009 (cf. Section 6.3). The second mechanism is the ongoing diffusive flux from the deeper sediment, should the cell continue to be inundated. The diffusive flux of any dissolved species is calculated from an approximation to Fickian diffusion algorithm, but due to the available field data, here we prescribe an empirical flux rate algorithm that reflects the observations:

$$\lambda_{rwi} = \begin{cases} (F_{1st_i} + k_{1st_i} [S_i/35]) A_i & \text{if } t_{rw} > 0 \text{ and } t_{rw} < 1 \\ (F_{difi} + k_{difi} [S_i/35]) A_i & \text{if } t_{rw} > 1 \text{ and } t_{rw} < 90 \\ -F_{SO4_i} A_i \frac{[SO_{4_i}]}{K_{SO4} + [SO_{4_i}]} & \text{if } t_{rw} > t_{so4} \end{cases} \quad (4.22)$$

where F_{1st_i} and F_{difi} are the first pulse and subsequently lowered rate of acidity diffusion, respectively, following rewetting of exposed (and potentially acidified) soil. The parameters k_{1st_i} and k_{difi} mediate the flux rate in response to salinity, S (psu), of the overlying water as was observed in Hicks et al. (2009). F_{SO4_i} is the alkalinity flux rate (negative sign implies acidity consumption) due to SO_4 reduction in the organic matter rich sediment of the lake ($mol\ H^+ \text{ consumed } m^{-2} \text{ day}^{-1}$), A is the area of the sediment cell and the net flux is related to the sulfate concentration in the overlying water. In Eq 4.22 the piecewise function is evaluated based on the time a cell has been rewet, t_{rw} , using an internal time-counter for each cell based on the inundation history. If the time of rewetting is greater the t_{so4} , then the cell is considered to no longer contribute to the acidity flux, and it will return to being an alkalinity producing sediment cell.

The model equations above are numerically solved using explicit finite difference (Euler's method) and the fluxes are routed to CAEDYM at the same frequency as the ELCOM-CAEDYM time step.

4.3 2D lake cross section HYDRUS model

The response of surficial groundwater in the exposed bed of the River Murray Lower Lakes to water level changes and climatic forcing is of critical interest since it is an important control in determining the load of acidity to the lake system following oxidation of pyritic sediments. The present analysis was motivated to better quantify the delivery of groundwater to the lake under various environmental conditions, given our present understanding of the lake-bed geology. In particular, the aims are to a) present typical seepage rates to the lakes under different water levels, and b) to develop a non-dimensional scaling relationship to relate seepage to soil capacity that can be applied within other models and analyses.

Model Approach:

In order to simulate the seepage flow rate into the lake(s) from the surrounding exposed lake bed material, the numerical model HYDRUS 2-D was used to resolve the water movement through the two-dimensional variably saturated media. The model is based on a finite volume solution of the two-dimensional Richard's equation and includes facility to apply an atmospheric boundary over the exposed lake bed (including rainfall and evaporation), a seepage face, and a constant lake level boundary.

Due to data availability the model is based on a conceptual cross-section of the Western shore of Lake Albert, however, given spatial mapping that has been undertaken to date (Fitzpatrick et al., 2010), the configuration of the model that is presented below is considered to be applicable to much of the sandy shores flanking the lake system. The basis for the conceptual model is a sandy wedge above a relatively impermeable clay layer separating the surficial exposed lake sediment from the deeper groundwater formations, such as the regional bridgewater formation (Figure 4.4).

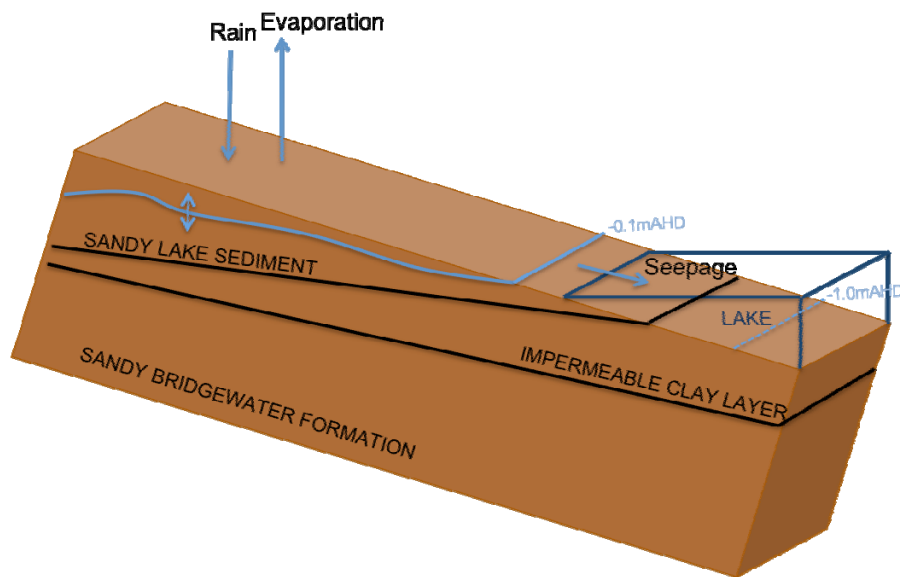


Figure 4.4: Schematic diagram outlining hydro-geological setting of lake shore zone on which the numerical domain was configured.

The model configuration was run under environmental conditions measured near the site for 2009, and was validated against a limited period of available soil moisture and water level data. Subsequently, the model is used to explore the seepage response to a lowering of the lake level, as is forecast to occur in 2010-2011, and to determine the sensitivity of the seepage estimates to the hydraulic properties of the sand. Finally, the results were analysed to develop a simple, non-dimensional seepage equation.

In the simulation, the domain was considered as a two-dimensional cross-section (1 km long and 5m deep, see Figure 4.5). A variably sized mesh was used, with generally finer resolution near the surface.

At the surface, the boundary conditions are divided into three regions including a constant head portion, representing the standing water region occupied by the lake, and a small seepage face, which is considered to be under atmospheric forcing when the seepage is inactive. The remaining reach is specified to be under free atmospheric conditions (i.e. subject to rainfall and evaporation). In the bottom of the cross section area the boundary was assumed to be deep drainage (very low flow rate over the total 1000m) and in the lateral boundary it was considered as having a no flux boundary (Figure 4.5).

Two lake levels were tested (relative to the zero level datum): -0.1 and -1m AHD (Figure 4.5). The boundary conditions assumed were 378 and 200m under constant head (representing the lake bottom), 42 and 47m of seepage face, and 580 and 753m under free atmospheric forcing (subject to rainfall and evaporation), for -0.1 and -1m respectively.

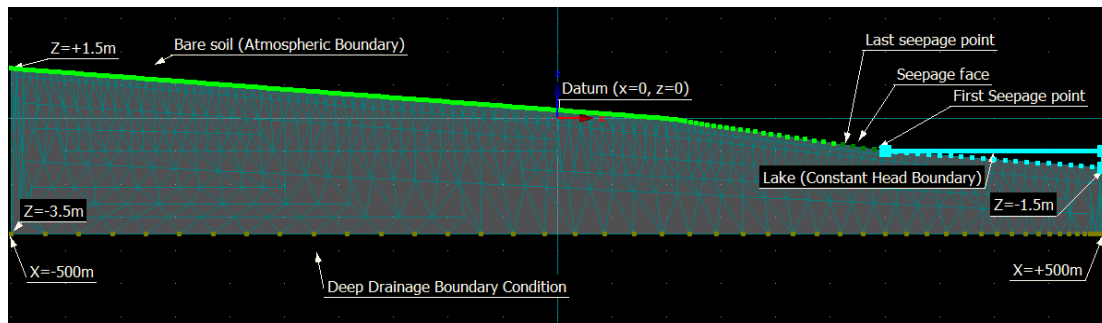


Figure 4.5: Boundary conditions (lake level at -1m).

The domain is considered to have variable soil types and is configured qualitatively based on core data collected by Earth Systems along different transects around the lakes, as summarised in the schematic depiction in Figure 4.4. The first soil layer (between 1 and 1.5 m deep) is comprised of loamy sand (saturated conductivity $K_s = 1.0 \text{ m day}^{-1}$; dark blue in Figure 4.6), the second layer is a clay (0.5 to 2 m deep), with a characteristic saturated conductivity $K_s = 0.001 \text{ m day}^{-1}$ (light blue) and the third layer is a very conductive sand ($K_s = 5.0 \text{ m day}^{-1}$; green). For the initial condition for calibration and simulation, the water table depth was set at 30cm from the soil surface.

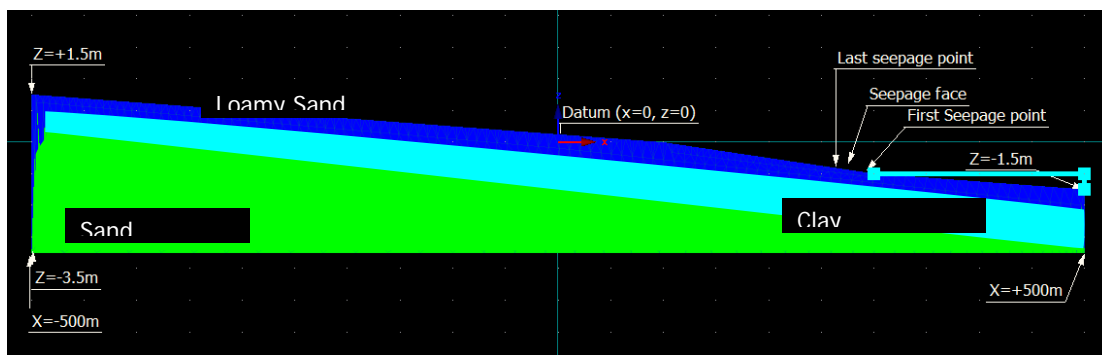


Figure 4.6: Soil material distribution throughout the cross section area.

Validation

The field data used for model calibration comprises three weeks of observed pressure head and moisture content data sampled from the Campbell Park site in Lake Albert, collected by Earth Systems during August 2009. The samples of moisture content were taken at 10, 20 and 30cm below the soil surface. The observation nodes used to calibrate the model are shown in the Figure 4.7 (10, 20, 30 cm deep and at about 350 m from the seepage face for soil moisture and 2.1, 2.6 and 3.0 m below the initial water table level for pressure head). The lake level used in the calibration was -0.1 m, which was typical of Lake Albert water level during the validation period. Given the idealised domain, the purpose of the validation is to characterise the general trends in unsaturated zone moisture content and changes in the water table elevation.

The model simulation was forced with daily rainfall and evaporation data from the SA MDB NRM board Narrung weather station. The model was configured to output moisture content (MC) for points at 10, 20 and 30 cm deep (see Figure 4) and the output was compared to field data as shown in Figure 4.8. The discrepancy in moisture content at 10 and 20 cm between model and field data can be related to an over-estimation in the maximum water content by the loamy sand, taken as constant in the simulation, and also due to overly coarse near-surface resolution of the computational mesh. The results for pressure head are presented in Figure 4.9.

Seepage Rate

The head difference (water table height relative to the lake level) and seepage rates, Q_{ss} , were calculated by the model for the period of 250 days in 2009 (Figure 4.10) in order to explore the range of conditions experienced in winter and summer. Assuming a 1m wide cross-section, rates of

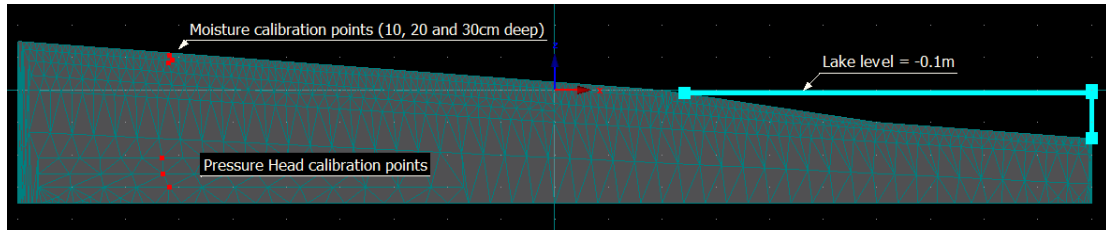


Figure 4.7: Location of moisture content and pressure head calibration points in the domain (red dots).

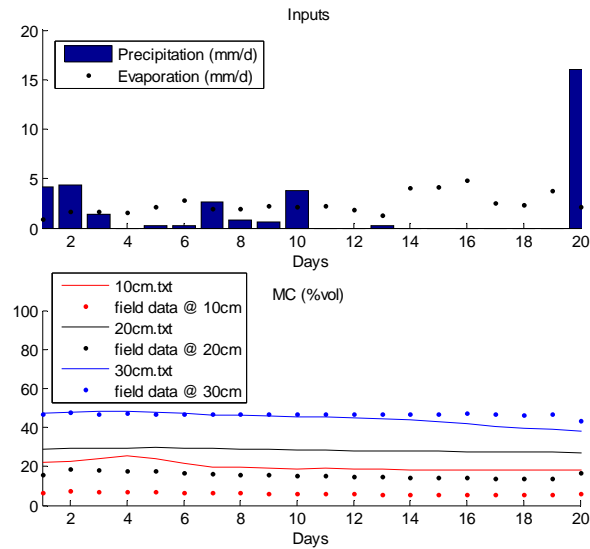


Figure 4.8: Field data and predicted moisture content (% volume).

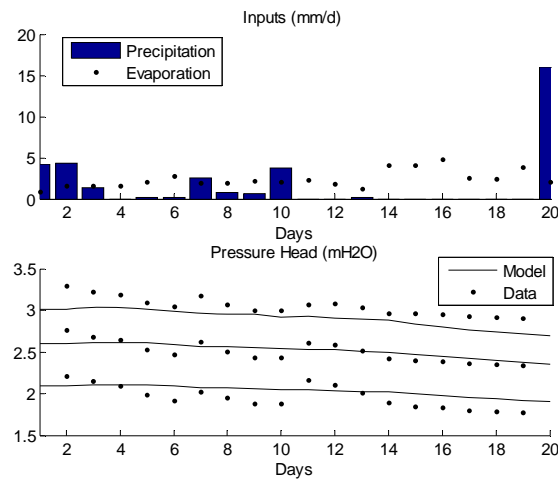


Figure 4.9: Field data and predicted soil pressure head. In the model, the observation points were located at 3, 2.1 and 2.6m below the initial water table.

between $0.0 \text{ m}^3 \text{ day}^{-1}$ (from the end of summer prior to the autumn rains) and $0.04 \text{ m}^3 \text{ day}^{-1}$ (during the winter peak) were simulated with the lake at -0.1 mAHD . By reducing the lake level to -1.0 mAHD , the peak seepage increased by 50% to $0.06 \text{ m}^3 \text{ day}^{-1}$. Note that these rates are applicable for sandy regions around the lake margin and so care must be taken to scale this value up to lake total seepage. In particular, clay regions that have been previously discussed should be excluded from the analysis.

For the purposes of cross-checking, from first principles using Darcy's Law, flow rate can be calculated according to:

$$Q_{ss} = A_x * K_s * \Delta H/L \quad (4.23)$$

where:

Q_{ss} = Seepage flow rate ($m^3 \text{ day}^{-1}$)

A_x = Cross sectional area of flow discharge (i.e., seepage face)

ΔH = the difference in pressure head between the upstream and downstream reach of the lake shore (m)

L = the length of the exposed shore (m)

When the lake is at -0.1 m AHD, if we assume a K_s of 1.0 m day^{-1} and a seepage area of 32.9 m^2 , length of 580 m and a head difference of 0.55 m , then we estimate $Q \sim 0.03 \text{ m}^3 \text{ day}^{-1}$, which is similar to the predictions by the model in simulations with similar pressure heads.

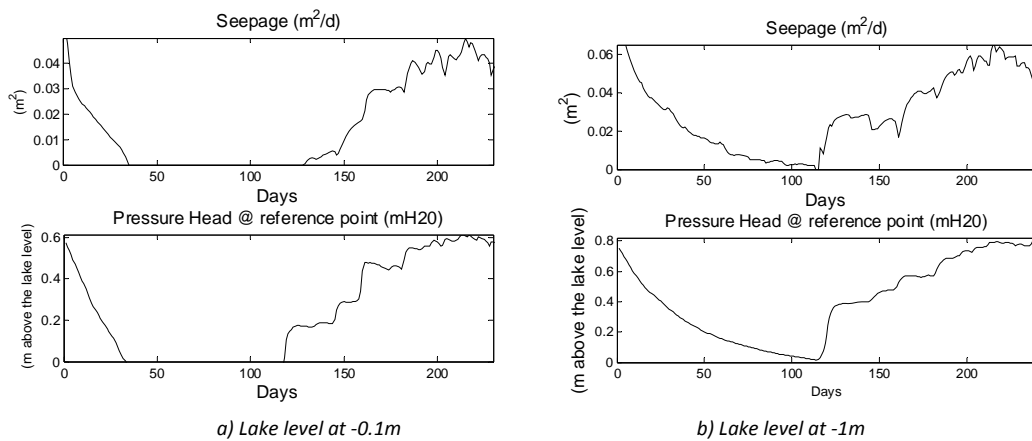


Figure 4.10: Seepage flow ($m^2 \text{ day}^{-1}$) and pressure head (m) calculated for the period between January 1st (day 0) and September 2009 (day 250). The rate is $m^3 \text{ day}^{-1}$ if a 1m width cross-section is assumed.

In order to relate the pressure head at a single point within the recharge area to the seepage flow rate into the lake, a reference point was defined that was located 200 and 335 m away from the seepage face when the level was set at -0.1m and -1m, respectively (Figure 4.11). The results show an almost linear relationship between seepage flow and water table height above the lake surface. For the -0.1 m AHD simulation, there is a cut-off at ~ 0.25 of the height between the soil surface and the lake, however for the -1.0 m AHD simulation the soil drains linearly down to a pressure head difference of 0m. The near-linear relationship reflects the linear dependence in pressure head in Darcy's Law, and indicates that Darcy's Law is a reasonable approximation in this case.

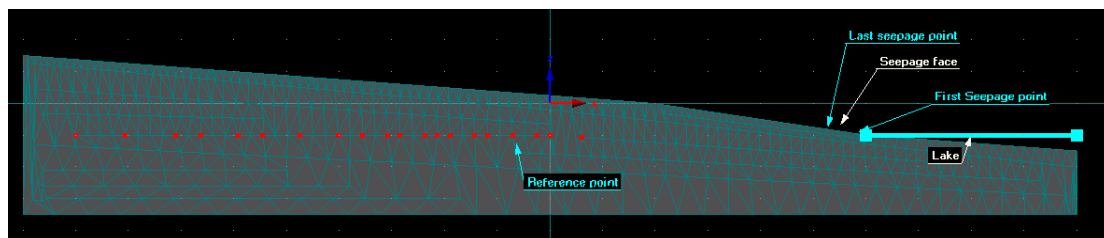


Figure 4.11: Reference point for pressure head when lake level is constant and equal to -1m.

Seepage relationship to soil water storage

Here we aim to develop a non-dimensional seepage relationship between the soil water store and the seepage rate for application in our models, and to explore the sensitivity of the relationship to the hydraulic conductivity of the surface sandy material. The model is based on a non-linear power law relationship that is often used in storage-capacitance hydrological models, and takes the form:

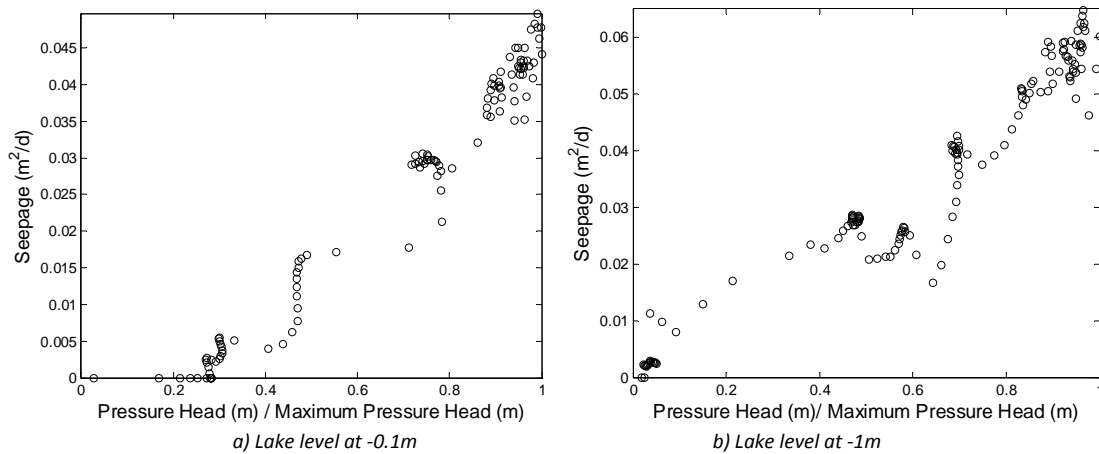


Figure 4.12: Relationship between seepage flow ($\text{m}^2 \text{ day}^{-1}$) and pressure head (m) taken from a single point calculated for the period between January 1st (day 0) and September 2009 (day 250). The rate is $\text{m}^3 \text{ day}^{-1}$ if a 1m width cross-section is assumed.

$$Q^* = \alpha (S/S_{max})^\beta \quad (4.24)$$

where Q^* is the non-dimensional seepage 'fraction' (day^{-1}) related to Q_{ss} according to $Q^* = Q_{ss}/A$, S is the storage and S_{max} is the maximum storage possible between the soil surface and the lake level (not the clay layer), both in metres. The maximum storage capacity is defined as the effective storage area above the lake level, defined previously as Z_{lake} , which takes in account the soil porosity. Seepage area is not considered storage area. In the figures, the pressure head is divided by the maximum pressure head to give us a percentage of storage (S/S_{max}). Therefore, a value of one represents a fully saturated soil column to the soil surface. The relationship between seepage fraction and storage capacity for a lake level equal to -0.10 mAHD and for a lake level equal to -1 mAHD is shown in Figure 4.12.

The relationships for lake level at -0.1 and -1 m are slightly different due to the fact that, in the lower lake level case, the volume of storage is also comprised of a layer of clay, which does not occur in the same proportion when the lake is in a higher level. The slope of the relationship is always higher when just sand is present in the storage volume.

To explore the sensitivity of the relationship the simulations were repeated by adjusting the sand saturated hydraulic conductivity (K_s). Values of $K_s = 0.5$ and 1.5 m day^{-1} were used for both lake levels. The relationships between seepage fraction and storage capacity for each case are presented in Figure 4.14 and 4.15. As expected, the same volume of soil become more "efficient" in generating seepage flow when the pressure head or saturated hydraulic conductivity was increased, and the reverse is true when its value is decreased. The cutoff figure for the seepage equation (Eq 4.21) used as the parameter ϵ in equation 4.10 was derived from these plots and was estimated to be 0.1 m. A summary of parameters and simulations is shown in Table 4.2.

Table 4.2: Summary of seepage rates and flow parameters for different model configurations

Level	K_s	Max Q	α	β
-0.1	0.5		0.0002129	1.2680
-1.0	0.5		0.0001542	2.7190
-0.1	1.0	0.049	0.0003225	1.6047
-1.0	1.0	0.065	0.0002498	1.2589
-0.1	1.5		0.000665	1.5178
-1.0	1.5		0.000376	1.1313

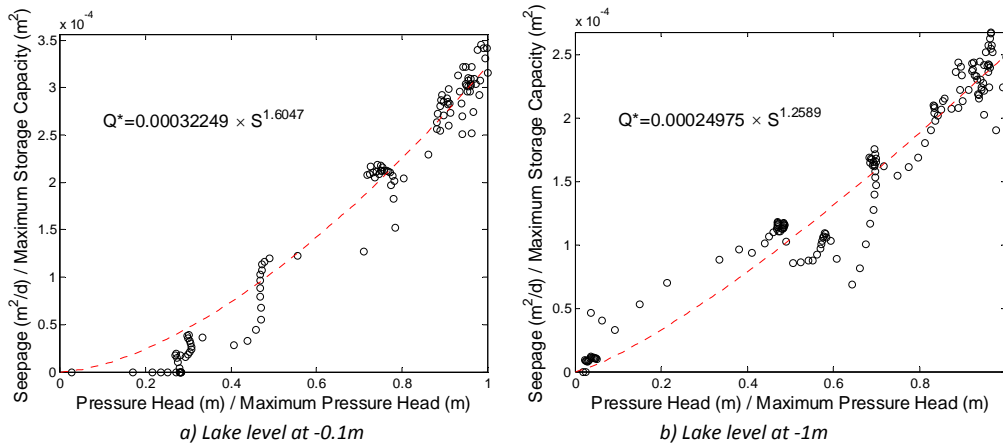


Figure 4.13: Relationship between seepage fraction (day⁻¹) and non-dimensional storage capacity of the sand above the clay lens for points taken in the period between January 1st (day 0) and September 2009 (day 250), assuming $K_s = 1.0 \text{ m day}^{-1}$.

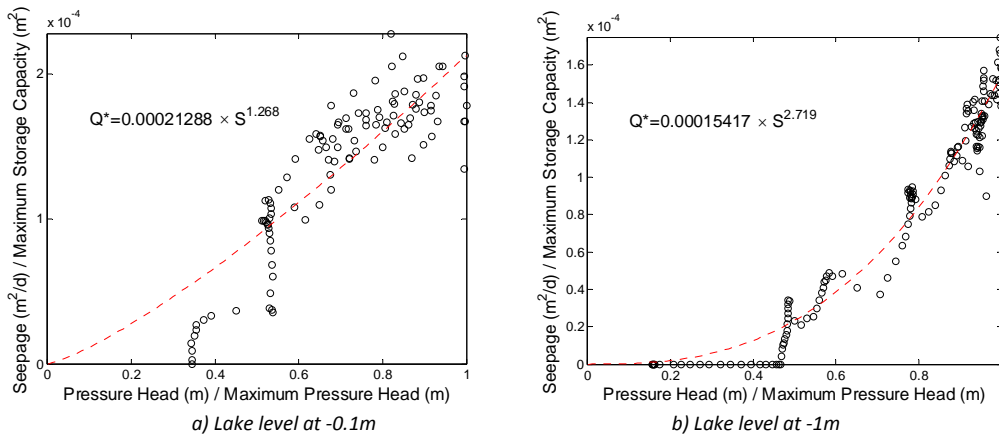


Figure 4.14: Relationship between seepage fraction (day⁻¹) and non-dimensional storage capacity of the sand above the clay lense for points taken in the period between January 1st (day 0) and September 2009 (day 250), assuming $K_s = 0.5 \text{ m day}^{-1}$.

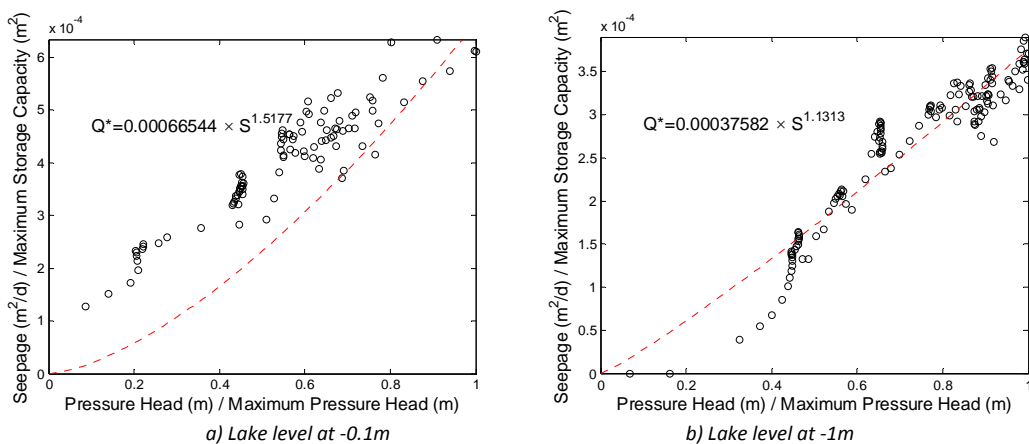


Figure 4.15: Relationship between seepage fraction (day⁻¹) and non-dimensional storage capacity of the sand above the clay lense for points taken in the period between January 1st (day 0) and September 2009 (day 250), assuming $K_s = 1.5 \text{ m day}^{-1}$.

5 Model setup and application to the Lower Lakes

5.1 Model configuration and simulated variables

Due to disconnections constructed between regions of the lakes (e.g., within Narrung Narrows and the Clayton regulator), three model domains have been configured for the study, including:

- Lake Albert
- Lake Alexandrina (pre and post construction of the Clayton Regulator);
- Currency/Finniss domain from Clayton to Goolwa Barrage

These domains are described in more detail in the following sub-sections, however all share many common aspects that are discussed generally next.

For all simulations, the biogeochemical model was configured to simulate the variables outlined in Table 5.1, and their interactions are shown schematically in Figure 5.1. The model includes the general CAEDYM nutrient and phytoplankton variables as described also in Hipsey et al. (2009). In addition, the geochemical module was configured to simulate the major ions, iron, manganese and aluminium, and pH. To test the importance of solubility control two simulations were run in Lake Albert to compare the role of simulating pure (i.e., solid) phase minerals including $\text{Fe}(\text{OH})_3$, MnO_2 , $\text{Al}(\text{OH})_3$ and CaCO_3 (calcite) – these are denoted 'nPP' and 'yPP' for no inclusion and inclusion of these components respectively (see Section 5.2).

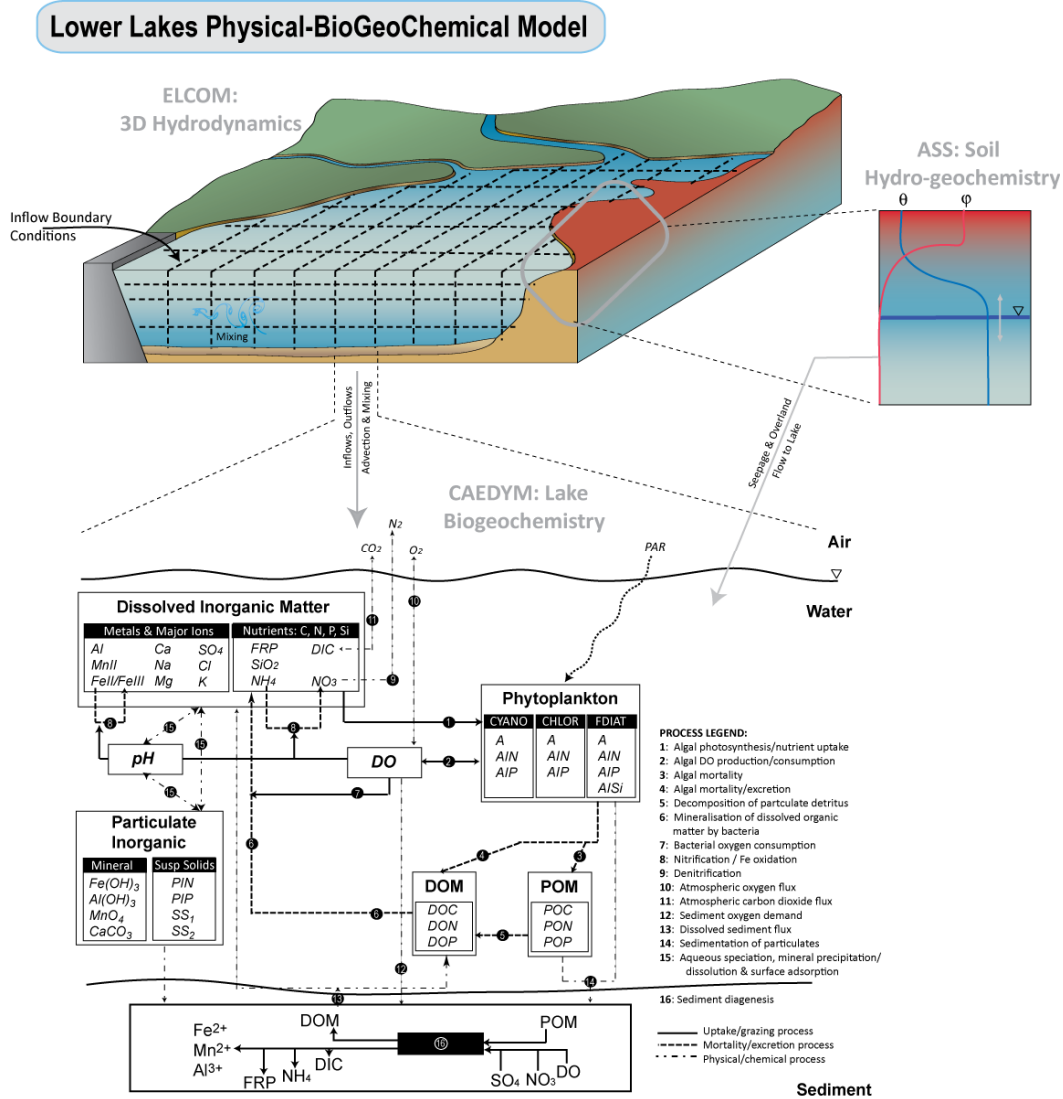


Figure 5.1: Conceptual outline of the coupled hydrodynamics-biogeochemical-acid sulfate soil model as configured to the Lower Lakes simulations.

In all the domains the submerged sediment was simulated using the static CAEDYM diagenesis model (i.e., using empirical flux coefficients mediated by temperature and oxygen). Nutrient and oxygen flux rates were specified as in the Lower Murray HydroModel study (Hipsey et al., 2009), and the alkalinity flux was specified as described from literature and the other commissioned Lower Lakes acid sulfate soil research studies, summarised in Table 5.2.

The exposed soil within the domain was simulated using the acid sulfate soil module, described in detail in the Section 4.2. This module supports definition of multiple soil types across the domain; we defined three soil classifications: coarse sand, medium sands and clays. Note that as exposed soil becomes submerged in a simulation, it takes on the general characteristics that are assumed by the static diagenesis model after it has been inundated for t_{so4} days. The acid sulfate soil module was configured to simulate the processes outlined in Section 4.2 including the various acidity generation, neutralisation and transport mechanisms, with parameter values and justifications outlined in Table 5.2. Many of the parameters are based on direct field data collected as part of the related acid sulfate soil research projects, and readers are also referred to those publications for more detailed accounts.

Table 5.1: Simulated variable list and descriptions.

Variable	Units	Common Name	Process Description
Physico-Chemical Variables			
T	°C	Temperature	Temperature supplied by hydrodynamic driver.
S	psu	Salinity	
EC	$\mu\text{S cm}^{-1}$	Electrical conductivity	
I	$\text{mE m}^{-2} \text{s}^{-1}$	Shortwave light intensity	Incident light, I_0 , is attenuated as a function of depth
η_{PAR}	m^{-1}	PAR extinction coefficient	
SS₁	g m^{-3}	Inorganic suspended solids - small	Settling, resuspension
SS₂	g m^{-3}	Inorganic suspended solids – large	Settling, resuspension
CT	NTU	Turbidity	Derived from SS1+SS2 using empirical eq:
DO	g DO m^{-3}	Dissolved oxygen	Algal production/respiration, organic decomposition, nitrification, surface exchange, sediment oxygen demand
DOC	g C m^{-3}	Dissolved organic carbon	Mineralization, settling, algal mortality/excretion
POC	g C m^{-3}	Particulate organic carbon	Mineralization, settling, algal mortality/excretion
FRP	g P m^{-3}	Filterable reactive phosphorus	Algal uptake, organic mineralization, sediment flux
DOP	g P m^{-3}	Dissolved organic phosphorus	Mineralization, settling, algal mortality/excretion
POP	g P m^{-3}	Particulate organic phosphorus	Mineralization, settling, algal mortality/excretion
TP	g P m^{-3}	Total Phosphorus	Sum of all P state variables
NH₄⁺	g N m^{-3}	Ammonium	Algal uptake, nitrification, organic mineralization, sediment flux
NO₃⁻	g N m^{-3}	Nitrate	Algal uptake, nitrification, denitrification, sediment flux
DON	g N m^{-3}	Dissolved organic nitrogen	Mineralization, settling, algal mortality/excretion
PON	g N m^{-3}	Particulate organic nitrogen	Mineralization, settling, algal mortality/excretion
TN	g N m^{-3}	Total Nitrogen	Sum of all N state variables
RSi	g Si m^{-3}	Reactive Silica	Algal uptake, sediment flux
Biological Variables			
a		Phytoplankton group index, a={D,G,B}	
N_A		Number of simulated phytoplankton	
A_D	g chla m^{-3}	Diatoms	Growth, respiration, mortality, excretion, settling, resuspension
A_G	g chla m^{-3}	Greens	Growth, respiration, mortality, excretion, settling, resuspension
A_B	g chla m^{-3}	Blue-Greens	Growth, respiration, mortality, excretion, settling, resuspension
IP_D	g P m^{-3}	Diatom Internal Phosphorus store	Growth, mortality, excretion, settling, resuspension
IP_G	g P m^{-3}	Greens Internal Phosphorus store	Growth, mortality, excretion, settling, resuspension
IP_B	g P m^{-3}	Blue-Greens Internal Phosphorus store	Growth, mortality, excretion, settling, resuspension
IN_D	g N m^{-3}	Diatoms Internal Nitrogen store	Growth, mortality, excretion, settling, resuspension
IN_G	g N m^{-3}	Greens Internal Nitrogen store	Growth, mortality, excretion, settling, resuspension
IN_B	g N m^{-3}	Blue-Greens Internal Nitrogen store	Growth, mortality, excretion, settling, resuspension
ISi_D	g Si m^{-3}	Diatoms Internal Silica store	Growth, mortality, excretion, settling, resuspension

Table 5.1 (continued)

Variable	Units	Common Name	Process Description
Lake Geochemical Variables			
DIC	g C m ⁻³	Dissolved inorganic carbon	Algal uptake, organic mineralization, sediment flux
pCO ₂	atm	Partial pressure of CO ₂	Calculated as a function of DIC from Henry's Law
SO ₄	g SO ₄ m ⁻³	Dissolved Sulfate	
FeII	g Fe m ⁻³	Dissolved Ferrous Iron	
FeIII	g Fe m ⁻³	Dissolved Ferric Iron	
Fe(OH) _{3(s)}	mol L ⁻¹	Iron Hydroxide	
Na	g Na m ⁻³	Dissolved Sodium	
Cl	g Cl m ⁻³	Dissolved Chloride	
Ca	g Ca m ⁻³	Dissolved Calcium	
Calcite	mol L ⁻¹	Calcite	
K	g K m ⁻³	Dissolved Potassium	
Mg	g Mg m ⁻³	Dissolved Magnesium	
MnII	g Mn m ⁻³	Dissolved Manganese (II)	
MnO _{2(s)}	mol L ⁻¹		
Al	g Al m ⁻³		
Al(OH) _{3(s)}	mol L ⁻¹		
pH	-	pH	
CHGBAL	meq	Charge Imbalance	Assumes electroneutrality
Soil Hydro-geochemical Model			
SUBSTRATE	-	Soil type: Clay/Sand etc	
SOILST	m	S_i : Soil water storage	Rainfall, evaporation, runoff, baseflow
PHREATIC	m	h_{sai} : Depth of Phreatic Surface	Evaporation, infiltration and percolation
UZMOIST	%w	ψ : Unsaturated Zone Moisture	Evaporation, infiltration and percolation
PASS	mol	χ : Potential Acid Sulfate Soil Material	Exposure and subsequent oxidation
ANC	mol	Acid Neutralising Capacity	Acidity consumption
UZAASS	mol	ϕ_{UZ} : Unsaturated Zone Available Acidity	Oxidation, percolation and consumption losses
SZAASS	mol	ϕ_{SZ} : Saturated Zone Available Acidity	Percolation, baseflow and consumption losses

(* denotes model state variable derived from available field data – see text for details)

Table 5.2: Overview of acid sulfate soil model parameters and justifications

Parameter	Units	lower	mean	upper	Comments/References
REWETTING PARAMETERS					
Freshwater acidity flux 1 st day following soil inundation – SAND, F_{1st}	mol H ⁺ m ⁻² day ⁻¹	0.050	0.138	0.150	<u>Hicks et al. (2009)</u> : 0.138 mol H ⁺ m ⁻² day ⁻¹ acidity flux during first ¼ of a day following inundation of mesocosm at Pt Sturt (min 0.129; max 0.147). EC =1.48 dS/m. <u>Sullivan et al. (2009)</u> : Study of the 15 sites (including the Point Sturt South site) over the first 4 days of inundation with freshwater the first pulse mean acidity was 0.016 mol H ⁺ m ⁻² day ⁻¹ (min -0.015 ; max 0.044 mol H ⁺ m ⁻² day ⁻¹). For this period the acidity flux was 0.027 mol H ⁺ m ⁻² day for the Pt Sturt site also examined by Hicks et al. (2009) and is comparable given that our 4 days inundation period is 16 times longer than their ¼ of a day measurement period.
Freshwater acidity flux 1 st day following soil inundation – CLAY, F_{1st}	mol H ⁺ m ⁻² day ⁻¹	0.159	0.161	0.163	<u>Hicks et al. (2009)</u> : 0.161 mol H ⁺ m ⁻² day ⁻¹ acidity flux during first ¼ of a day following inundation of mesocosm at Boggy Crk (min 0.159; max 0.163). EC =2.18 dS/m.
Acidity Flux after prolonged soil inundation (day 2-90) – SAND, F_{dif}	mol H ⁺ m ⁻² day ⁻¹	0.002	0.007	0.010	<u>Sullivan et al. (2009)</u> : -ve fluxes measured in lab for 13 sandy cores from Lower Lakes, implies 0.0 acidity flux (it was a positive alkalinity flux if we take into account sulfate reduction) <u>Hicks et al. (2009)</u> : ~0.010 mol H ⁺ m ⁻² day ⁻¹ acidity flux during first ¼ of a day following inundation of mesocosm at Pt Sturt, corrected for evaporation and seepage. EC=0.81 dS/m day 5 to 2.2 dS/m day 85. 5–12 days: 0.011 (min 0.010; max 0.012) 5–85 days: 0.007 (min 0.006; max 0.008)
Acidity Flux after prolonged soil inundation (day 2-90) – CLAY, F_{dif}	mol H ⁺ m ⁻² day ⁻¹	0.006	0.010	0.012	<u>Hicks et al. (2009)</u> : ~ 0.010 mol H ⁺ m ⁻² day ⁻¹ acidity flux following initial inundation of mesocosm at Boggy Crk, corrected for evaporation and seepage. EC= 1.2 dS/m day 7 to 4.0 dS/m day 87. 7–14 days: 0.006 (min 0.006; max 0.006) 7–87 days: 0.010 (min 0.010; max 0.010)
RW dependence on salinity – SAND, k_{dif}	(mol H ⁺ m ⁻² day ⁻¹) 35psu ⁻¹	0.001	0.006	0.011	<u>Sullivan et al. (2009)</u> : 0.011 mol H ⁺ m ⁻² day ⁻¹ increase in acidity flux per unit psu increase in salinity averaged from 13 sediment columns from the Lower Lakes <u>Hicks et al. (2009)</u> : 0.0011 mol H ⁺ m ⁻² day ⁻¹ increase in acidity flux per unit psu increase in salinity from mesocosms at Pt Sturt, based on comparison of fresh water flux rates (above) and seawater inundated experiments (EC=56.1 dS/m day 5 to 59.7 day 85): 5–12 days: 0.012 (min 0.009; max 0.015) 5–85 days: 0.007 (min 0.007; max 0.007)
RW dependence on Salinity – CLAY, k_{dif}	(mol H ⁺ m ⁻² day ⁻¹) 35psu ⁻¹	0.026	0.033	0.040	<u>Hicks et al. (2009)</u> : 0.033 mol H ⁺ m ⁻² day ⁻¹ increase in acidity flux with increase in salinity from mesocosms at Pt Sturt, based on comparison of fresh water flux rates (above) and seawater inundated experiments (day 7 EC=53.8 dS/m to 56.8 day 63): 7–14 days: 0.034 (min 0.027; max 0.041) 7–63 days: 0.014 (min 0.013; max 0.014)

PYRITE OXIDATION PARAMETERS					
Max Oxidation Rate – SAND, $R_{Ox}(\theta)$	day ⁻¹	0.008	0.018	0.08	<p><u>Ward et al. (2004a)</u>: 0.0086 day⁻¹ ASS. Not fully oxic, (gauze bag). Fully oxic examples were also provided in these papers.</p> <p><u>Borma et al. (2003)</u>: 0.0001 – 0.0024 day⁻¹, sediments, “crumbled” samples, layer <1cm.</p> <p><u>Di Nanno et al. (2007)</u>: 0.086 day⁻¹, sediments, with nutrients and microbial inoculation. Oxygen concentrations not measured, and samples high in organic matter.</p> <p><u>Morse (1991)</u>: 0.086 & 0.0017 day⁻¹, marine sediments, initial (<10d) & later rate, oxic (but no details), oxidation in seawater. Initial rate due to v. fine particles (<0.3 um).</p> <p><u>Hollings et al. (2001)</u>: Laboratory measurement of oxidation rate via data-logged O₂ sensor fitted inside test chamber (O₂ consumption assumed to be entirely attributable to sulfide oxidation).</p> <p><u>Earth Systems (2010)</u>: 1.8 wt% FeS₂ day⁻¹, estimated by oxygen consumption rate in soil with varying moisture.</p>
Max Oxidation Rate – CLAY, $R_{Ox}(\theta)$	day ⁻¹		0.006		<p><u>Ward et al. (2004b)</u>: 0.0017 day⁻¹ ASS. Not fully oxygenated, light clay, 40 um thick plastic bag Fully oxic examples were also provided in these papers.</p> <p><u>Rigby et al. (2006)</u>: 0.017 day⁻¹, Oxygen limitation in at least one of the experiments</p> <p><u>Earth Systems (2010)</u>: 0.6 wt% FeS₂ day⁻¹, estimated by oxygen consumption rate in soil with varying moisture.</p>
Ox dependence on Moisture – SAND, $R_{Ox}(\theta)$	-		<i>poly-nomial</i>		<p><u>Earth Systems (2010)</u>: change in oxygen consumption rate in sand per fractional decrease in % moisture generated the following relationship: $y = -9.7011x^3 + 2.1949x^2 + 0.0025x + 0.0006$ (R² = 0.8409, n=8), where y = wt% FeS₂ day⁻¹ and x = gravimetric moisture content (wt%). Above x=23% y=0.</p> <p><u>Hollings et al. (2001)</u>: similar relationship between moisture and oxidation rate as Taylor for waste rock piles</p>
Ox dependence on Moisture – CLAY, $R_{Ox}(\theta)$	-		<i>poly-nomial</i>		<p><u>Earth Systems (2010)</u>: change in oxygen consumption rate in sand per fractional decrease in % moisture generated the following relationship: $y = -0.0142x + 0.0068$ (R² = 0.4022, n=5) where y = wt% FeS₂ day⁻¹ and x = gravimetric moisture content (wt%). Above x=48% y=0. Below 23% y = 0.0142x is assumed.</p>
FeS ₂ :H ⁺ stoichiometry	-	3	4	4	<p>Related to completeness of pyrite oxidation reaction (4 implies complete oxidation; less implies acidity storage in intermediate minerals such as jarosite, etc.). Almost complete oxidation is modelled as phases such as schwertmanite indicate 7/8 of the acidity has already been generated and released from this secondary assemblage, and jarosite only permits temporary storage and cannot buffer acidity. Also, montmorillonite can buffer acidity, but rates will be very slow.</p>

SOIL ACIDITY NEUTRALISATION & ALKALINITY PRODUCTION					
Acid Neutralising Capacity (ANC) rate coefficient, $R_{neut}(ANC)$	day ⁻¹	0	2.74 x10 ⁻⁴	5.48 x10 ⁻⁴	Assumes ANC is not immediately available and follows a first order kinetic consumption rate. Mean number provided is equivalent to 10 wt% of available ANC consumed per year. The upper limit is based on experience from Currency Creek – i.e. no more than 20 wt % per year could have been used during this event based on mass balance calculations.
Saturated Zone soil acidity consumption rate, R_{SO4}	day ⁻¹	0	0.005	0.02	Sullivan et al. (2009)
Mobilisable acid fraction, f_{mob}	-	0.4	0.5	0.75	Estimated based on indicative porewater solution analysis using PHREEQC
LAKE SEDIMENT ALKALINITY PRODUCTION					
Max alkalinity production (eg. SO ₄ reduction) @ 20C of inundated sediment, F_{SO4}	mol H ⁺ m ⁻² day ⁻¹	0.002	0.005	0.008	<u>Koschorreck & Tittel (2007)</u> : Eutrophic lake ~6.85 mmol H ⁺ m ⁻² day ⁻¹ ; oligotrophic lake ~1.06 mmol H ⁺ m ⁻² day ⁻¹ <u>Sullivan et al. (2009)</u> : ~ -5.0 mmol H ⁺ m ⁻² day ⁻¹ noted in sand cores inundated for 35 days with fresh water implying net alkalinity generation due to process such as SO ₄ reduction.
Half-saturation constant for effect of SO ₄ limitation on sediment alkalinity production, K_{SO4}	mM		1.60		<u>Boudreau & Westrich (1984)</u> : Marine sediments reported to have K _{SO4} of ~ 1.6mM
SOIL HYDROLOGICAL PARAMETERS					
<i>SAND</i> average depth to clay layer, $Z_{c,s}$	m		1.50		<u>Earth Systems (2010)</u> : Albert = 1.1m max and Alexandrina = ~ 2.0m max. Also data in <u>Hicks et al. (2009)</u> Also data in <u>Fitzpatrick et al. (2008)</u>
<i>CLAY</i> nominal depth, Z_f	m		1.50		Assumed
Porosity – <i>SAND</i> , ϕ_s	-		0.42		<u>Earth Systems (2010)</u> : 0.40 - 0.48 <u>Hicks et al. (2009)</u> : 0.422 – surficial sediment (0-20cm) at Pt Sturt (medium sand)
Porosity – <i>CLAY</i> , ϕ_f	-		0.60		<u>Hicks et al. (2009)</u> : 0.49-0.67 – surficial sediment (0-20cm) at Boggy Creek (sandy clay)
Evaporation extinction depth – <i>SAND</i> , h_{ep}	m	0.30	0.40	0.55	<u>Cook and Rassam (2002)</u> : Numerical estimate of depth where evaporation is uninhibited from the free value (H _a) as 0.3-0.55m for sandy loam dependent on evaporation intensity. Here a slightly higher value is assumed since evaporation continues below H _a , just at a reduced rate.
Evaporation extinction depth – <i>CLAY</i> , h_{ep}	m	0.15	0.2	0.3	<u>Cook and Rassam (2002)</u> : Numerical estimate of depth where evaporation is uninhibited from the free value (H _a) as 0.1-0.35m for clay dependent on evaporation intensity. Here a slightly higher value is assumed since evaporation continues below H _a , just at a reduced rate.

Field capacity – SAND, θ_{fc}	v%		0.15		15% volumetric water content typical field capacity for sands after 1 day free drainage
Field capacity – CLAY, θ_{fc}	v%		0.40		40% volumetric water content typical field capacity for clays after 1 day free drainage
Baseflow a coefficient – SAND, α_{ss}	day ⁻¹		0.005		0.5% of full soil storage above lake level discharged per day (reduced as a function of S_b/S_{max} using B parameter) <u>Farmer et al (2003)</u> : Used values of 0.03 – 0.003 for similar capacitance model approach <u>Section 4.3</u> : 0.003 day ⁻¹ based on HYDRUS-2D cross-sectional numerical model output analysis
Baseflow a coefficient – CLAY, α_{ss}	day ⁻¹		5.00x10 ⁻⁴		Assumed to be very low for poorly conductive clays
Baseflow B coefficient – SAND, β_{ss}	-	1.0	2.0	3.0	<u>Farmer et al (2003)</u> : Recession curve analysis of ~30 catchments reported to give typical value of 2.0. <u>Section 4.3</u> : ~1.0 based on HYDRUS-2D cross-sectional numerical model output analysis (Figure 4.8)
Baseflow B coefficient – CLAY, β_{ss}	-		3.0		Assumed, as above.
Head threshold, ϵ	m		0.1		Head difference between soil groundwater and lake level that must be exceeded before flow occurs ~0.1 based on HYDRUS-2D cross-sectional numerical model output analysis (Figure 4.8)
Bulk density – SAND, ρ_s	kg m ⁻³		1530	1750	<u>Hicks et al. (2009)</u> : 1.53 t m ⁻³ – surficial sediment (0-20cm) at Pt Sturt (medium sand)
Bulk density – SAND, ρ_s	kg m ⁻³		1230	1600	<u>Hicks et al. (2009)</u> : 0.88-1.35 t m ⁻³ – surficial sediment (0-20cm) at Boggy Creek (sandy clay)

5.2 Application to Lake Albert

Bathymetric information from Lake Albert was supplied by the South Australian Department of Environment and Natural Resources, and interpolated onto a 200m square grid (Figure 5.2). Some manual smoothing of coarsely resolved regions was conducted to improve flow continuity. A vertical grid resolution was set at 0.4m, and based on typical Courant-Freidrich-Lowry (CFL) numerical stability limitations, a time-step of 600 seconds was adopted.

In addition to wind and inflow forcing, the model was configured to simulate the surface thermodynamics, and the correction for non-neutral atmospheric boundary layers was also applied. Meteorological data was used from a variety of sources. The 15-minute data from the Narrung weather station (located in the north-west of the domain) was used for rain, relative humidity, air-temperature, and wind speed and direction. After initial trial simulations, it was noted that the evaporative fluxes were under-predicted. Wind data from Pelican Point (south of the domain; Figure 5.3-5.4) was then trialled and found to give a better prediction. Therefore, for wind forcing purposes, the domain was split into two wind-regions, one covering the Narrung Narrows, using wind data from the Narrung weather station, and one covering the remainder of the lake that used the Pelican Pt wind station data. The drag coefficient was set to $1.4 \times 10^{-3} \text{ Nm}^{-2}$ after preliminary simulations showed this gave the best prediction of surface water temperature and evaporation rate (not shown). Solar radiation data was obtained from Hindmarsh Valley (61 km West of the site), and long-wave radiation was estimated from available net-radiation data also collected at this site by subtracting the shortwave component (Figure 5.5). The extinction coefficient is dynamically calculated by CAEDYM, but found to be critical in capturing the evaporation rate and subsequent water balance of the site. In CAEDYM, the photosynthetically active component (PAR) was set to 45% and had an

extinction value generally $>2\text{m}^{-1}$, and the remainder of the shortwave bandwidth was configured to be even more highly attenuated ($>3\text{m}^{-1}$).

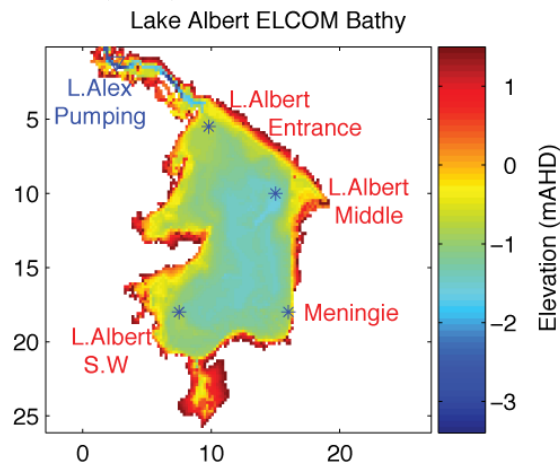


Figure 5.2: Lake Albert ELCOM bathymetry, pixel size is the grid resolution of 200x200m.

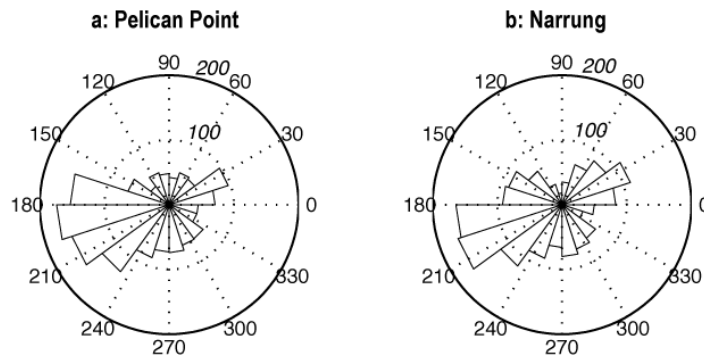


Figure 5.3: Comparison of wind direction data between weather stations located at a) Pelican Point (south of Lake Albert) and b) Narrung (north-west of Lake Albert).

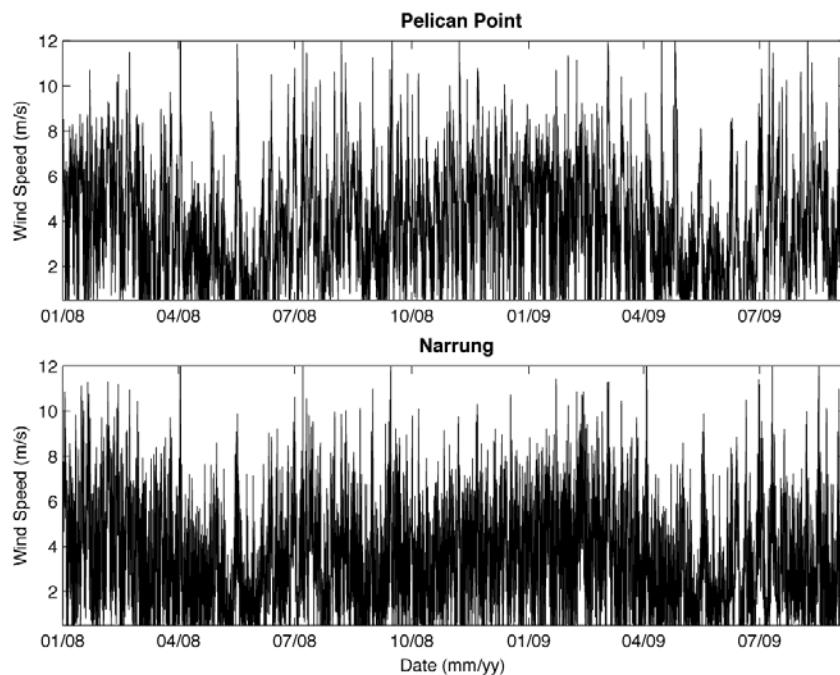


Figure 5.4: Comparison of wind speed data between weather stations located at a) Pelican Point (south of Lake Albert) and b) Narrung (north-west of Lake Albert). Mean values for the two wind stations were 3.91 and 3.43 m/s respectively over the time period Jun 2008 – Sept 2009.

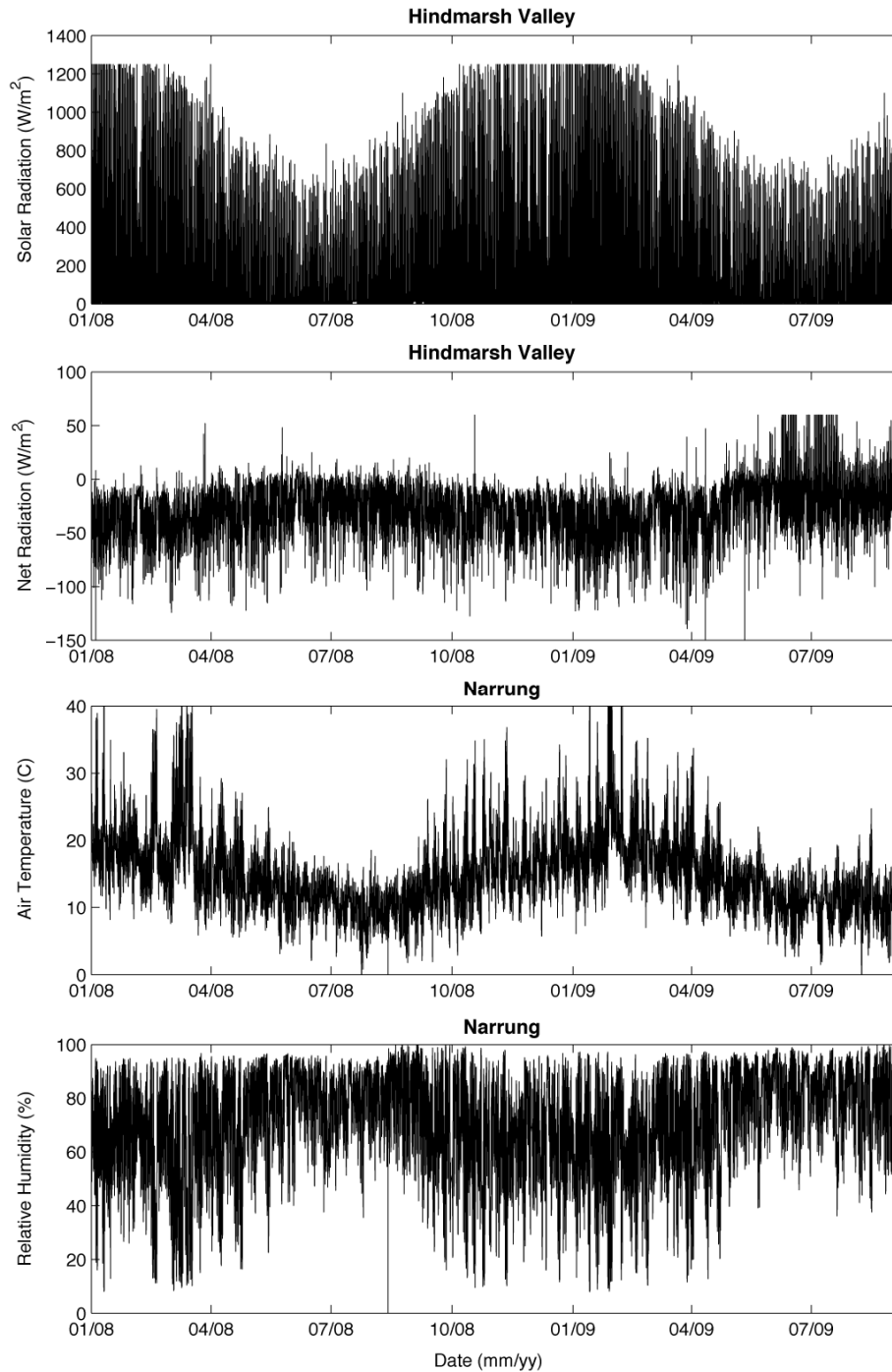
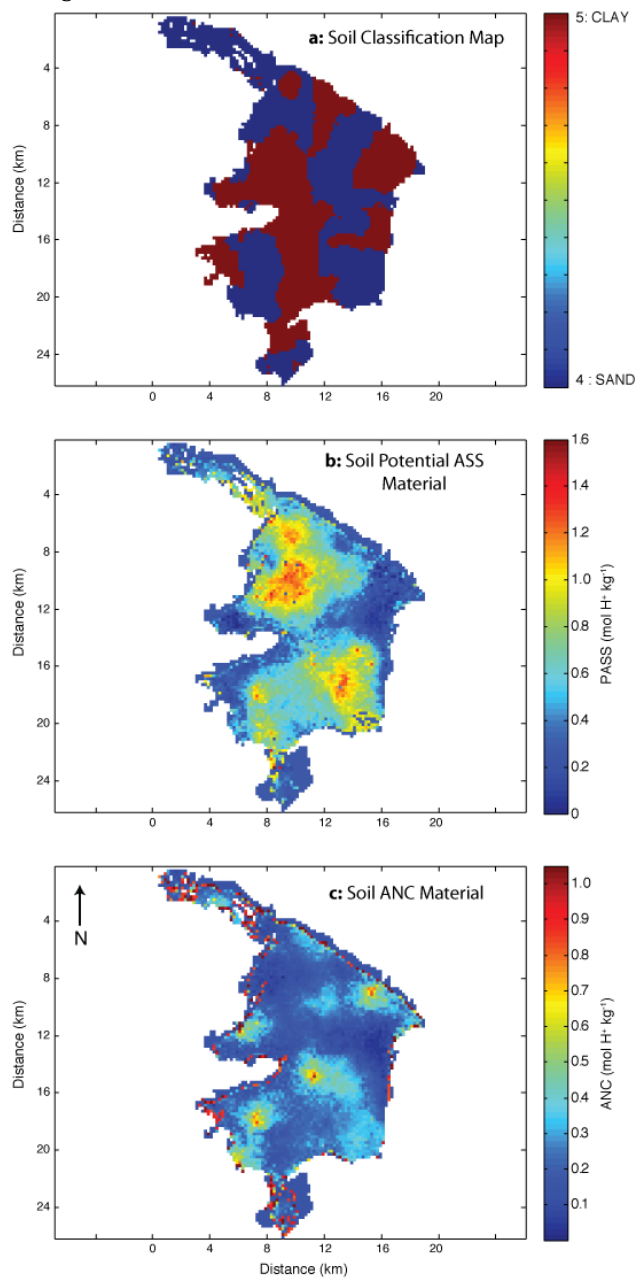


Figure 5.5: Solar radiation and net radiation data from Hindmarsh Valley (top panels) and air temperature and relative humidity from the SA MDB NRM Narrung weather station from January 2008 – September 2009.

The soil characteristics defined for the acid sulfate soil model are shown in Figure 5.6. The lake-bed was configured to have areas of 'sandy' and 'clayey' material as outlined in Figure 5.6a, and these distributions are based on interpolation of soil survey data reported in Fitzpatrick et al. (2010) onto the ELCOM 200×200m grid.

The simulation was configured to begin at midnight on 1 Jun 2008. Initial values for the lake were estimated from available water level, temperature, salinity (DFW) and water quality data (EPA)

collected at that time from the central station, and assumed to be horizontally and vertically homogenous.



Initial values of soil properties were input at each grid cell for PASS (Figure 5.6b) and ANC (Figure 5.6c), again by interpolating mapping data from Fitzpatrick et al. (2010) onto the ELCOM 200x200m numerical domain. Vertical profiles of ANC and PASS below the top 20cm were specified based on Figure 5.7.

Pumping of water into Lake Albert by the Narrung pumping project was input to the model as a time-series of daily pumping rates (Figure 5.8). Actual flow data was used to Jan 2010, and beyond this various pumping rates were used to test the future lake response to acid sulfate soils at different stabilisation levels (-0.5, -0.75 and -1.0m AHD). This was configured to enter the domain at the station indicated in Figure 5.2, and assumed to have the attributes of Lake Alexandrina water. For temperature and salinity, these were obtained by examining the seasonal trends from the station Alex Middle, and monthly data was linearly interpolated for use at the boundary condition. For water quality data, constant values were assumed based on available monitoring data from the closest site. For 2010-2013 data, 2009 data was repeated for each year.

Figure 5.6: Comparison of model soil classification map

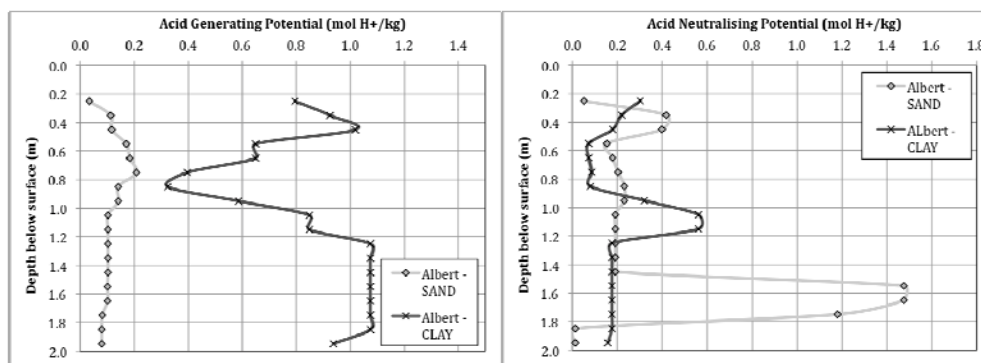


Figure 5.7: Vertical profiles of acid generating potential (AGP, left) and acid neutralising capacity (ANC, right) estimated from available core information from Lake Albert. Data compiled by Earth Systems (2010).

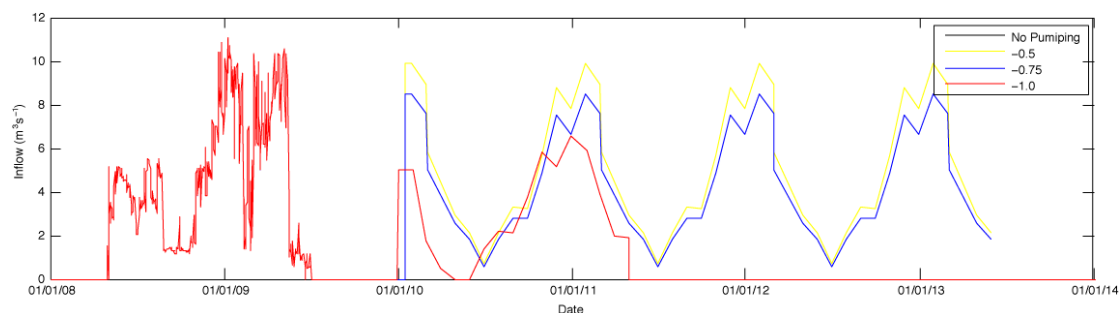


Figure 5.8: Time-series of pumping rate between Lake Alexandrina and Lake Albert, conducted at Narrung.

5.3 Application to Lake Alexandrina

Bathymetric information for Lake Alexandrina was supplied by DENR, and interpolated onto a variable width grid to accommodate areas where high and coarse resolution were required, ranging from 200m in the morphologically complex regions such as near the River Murray inflow, and Goolwa to Tauwichee Barrage, and the gradually increasing to 500 m in the centre regions of the main body of Lake Alexandrina (Figure 5.9). Some manual smoothing of coarsely resolved regions was conducted to improve flow continuity. A vertical grid resolution was set at 0.5 in the top 3 m, and then increased gradually to 1 m in the deep regions. Based on numerical stability limitations a time-step of 600 seconds was adopted and this maintained the CFL condition < 0.7 .

Due to the mix of hindcast and forecast scenarios to be run and the implementation of the Clayton regulator and the potential implementation of the Wellington Weir at Pomanda, it was necessary to develop three modifications of the base grid. The main grid included the complete Lake Alexandrina domain from the River Murray to Goolwa, including the Currency and Finniss tributaries, but with Lake Albert removed (Figure 5.9, top). This domain was used for hindcast simulations that were used to validate the model against observed water quality from Jan 2008 – Sep 2009. The second grid was based on that described above, but with the region from the Clayton regulator to the Goolwa Barrage truncated (Figure 5.9b). This domain was used to simulate the near-term forecast simulations from Oct 2009. A third domain (Figure 5.9c) was also required that was identical to this but with a boundary condition for seawater entrance configured at Tauwichee Barrage, and an optional weir in place across from Pomanda Island configured to overtop at 0.1m AHD.

All three grids were configured to have a River Murray inflow boundary condition, and an outflow boundary condition for pumping to Lake Albert at locations shown in Figure 5.9. The grids truncated at Clayton also had a boundary condition configured to pump water from the main body of Lake Alexandrina to the Clayton region. The grid that includes the Currency/Finniss region also has flow boundary conditions for the tributaries and a small leakage component specified at the Goolwa Barrage. The third grid, used for the seawater inundation simulations, has a flow boundary condition specified at the deepest point across the Tauwichee barrage.

The lake-bed was configured to have areas of sand and clay as outlined in Figure 5.9d, based on the CSIRO mapping data (Fitzpatrick et al., 2010). The validation simulations were configured to begin at midnight on 15 Jan 2008, and initial values for the lake were estimated from available water level, temperature, salinity (DFW) and water quality data (EPA) collected at that time from various stations, across the site. Initial values of soil properties were input at each grid cell for PASS (Figure 5.9e) and ANC (Figure 5.9f). Vertical profiles of ANC and PASS below the top 20cm were specified based on Figure 5.10. During Sept 2009 the model was stopped and the results were transferred from the AA ELCOM domain to initialise the ANC ELCOM domain for Oct 2009-2013 simulations. Note: The transfer of soil data from the 2008 AA sim to the forecast ANC sim was not possible and so the SUBSTRATE, PASS and ANC data were used to initialise both the AA and ANC domain.

Flow data used as input or output to/from the model consisted of a time-series of daily flow rates from the River Murray at Wellington and pumping rates for the Narrung pumping project (Figure 5.11). For the simulations with the Currency/Finniss region included, flow values for Currency and Finniss rivers were also specified as shown in Figure 5.11b. For the other domains, the specified pumping rate at the Clayton regulator was used (Figure 5.11c).

In addition to wind and inflow forcing, the model was configured to simulate the surface thermodynamics, and the correction for non-neutral atmospheric boundary layers was also applied. Meteorological data was used from a variety of sources. The 15-minute data from the Narrung weather station (located in the south-east quarter of the domain) was used for rain, relative humidity,

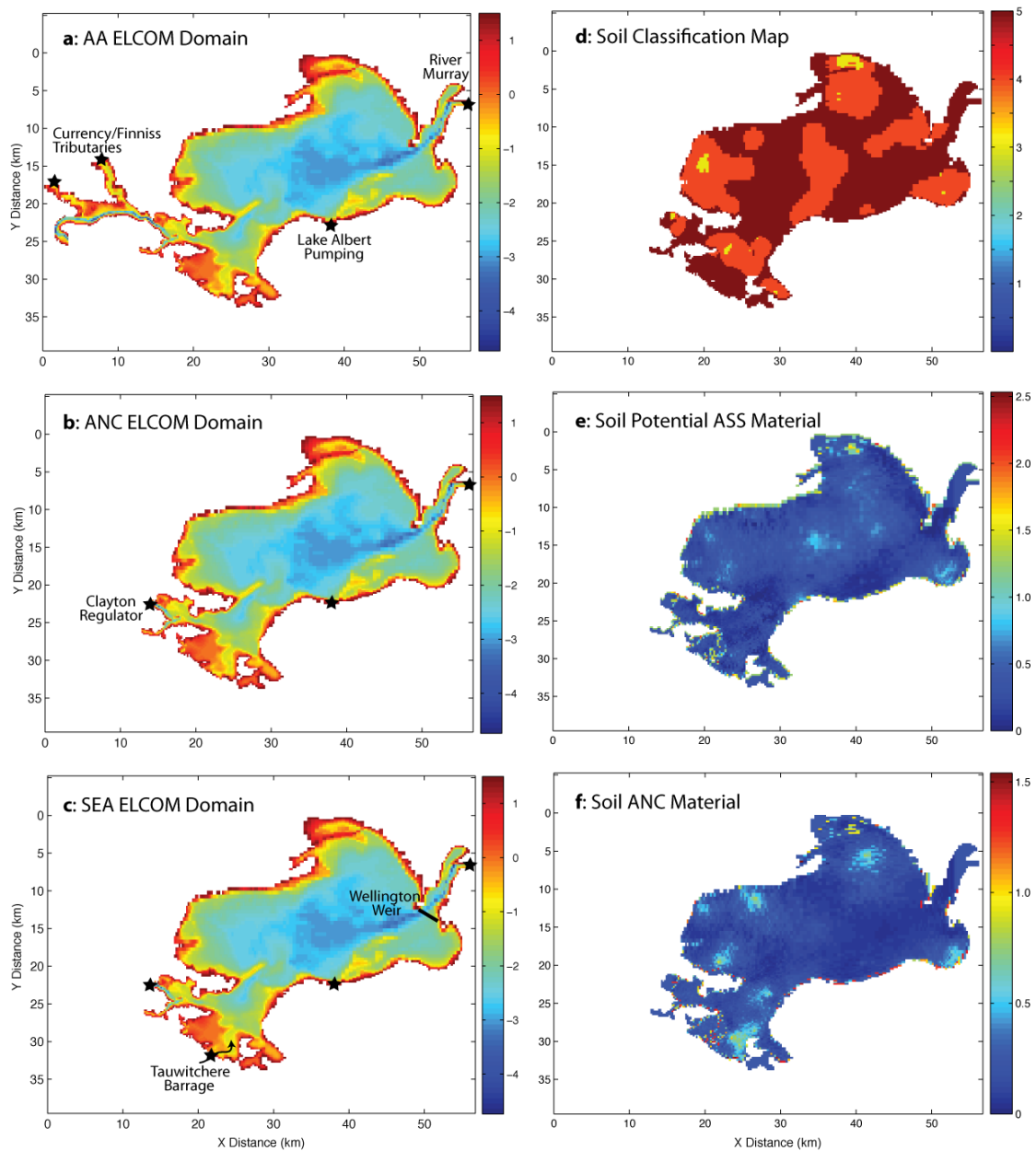


Figure 5.9: ELCOM bathymetric grids configured (a-c) and soil property specifications (d-f).

air-temperature, and wind speed and direction. The domain was split into two wind-regions, one west of the Clayton regulator that used data from the Currency Crk meteorological station (see Section 5.4) and one for the remainder of the lake that used Narrung weather data. In line with the Lake Albert validation, the drag coefficient was set to $1.4 \times 10^{-3} \text{ Nm}^{-2}$. Solar radiation data was obtained from Hindmarsh Valley (47 km west of the site), and long-wave radiation was estimated from available net-radiation data also collected at this site (Figure 5.5) by subtracting the shortwave component. The extinction coefficient is dynamically calculated by CAEDYM, but found to be critical in capturing the evaporation rate and subsequent water balance of the site. In CAEDYM the photosynthetically active component (PAR) was set to 45% and had an extinction value generally $>2\text{m}^{-1}$, and the remainder of the shortwave bandwidth was configured to be even more highly attenuated ($>3\text{m}^{-1}$).

Various flow scenarios were also tested in the model to explore the sensitivity of the lake to acidification under different freshwater or seawater flow regimes. These included various freshwater and seawater alternatives. The freshwater simulations were made by switching to a 1850GL SA Border flow allocation at different times, with the changes specified as occurring at different times within the simulations (Figure 5.11a). Exact volumes were provided from DFW based on BIGMOD predictions entering at Wellington.

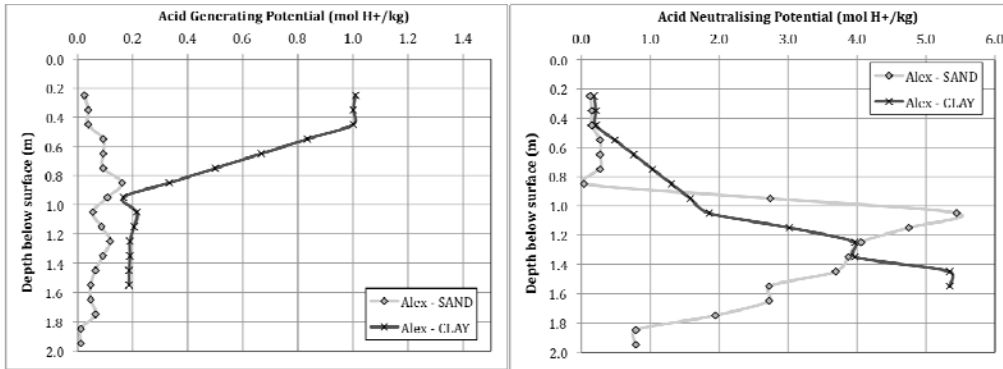


Figure 5.10: Vertical profiles of acid generating potential (AGP, left) and acid neutralising capacity (ANC, right) estimated from averaging available soil core information from Lake Alexandrina. Data compiled by Earth Systems (2010).

The seawater entrance scenario was configured with seawater pumping occurring over the summer (Figure 5.11d) and intended to maintain the lake at around -1.0m AHD (+/-0.25m).

For each of the flow boundaries into the model domain, water quality properties (temperature, salinity, oxygen, nutrients and geochemical properties) were specified as a function of time. For the River Murray, data from the Murray Bridge and Tailem Bend offtakes were used. For the Currency and Finniss tributaries data was available for salinity and assumed values similar to the lake centre were used for water quality attributes. For seawater, a salinity time series was available for 2008; this was used to provide the salinity boundary value and repeated year-to-year for the forecast scenarios. Geochemical properties of the seawater were assumed to be typical seawater concentrations, however due to periods of evapo-concentration in the Coorong water, the major ions were scaled in concentration based on the salinity relative to 35 g L⁻¹. Charge imbalance, as required for accurate pH determination, was recalculated following the scaling of the major ion concentrations.

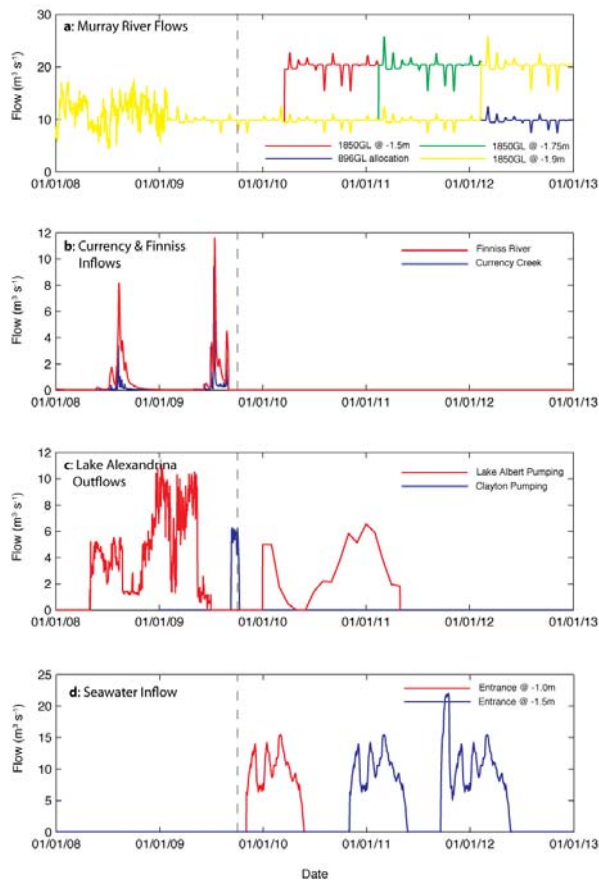


Figure 5.11: Inflow and outflow boundary condition time-series used in the Lake Alexandrina hindcast (before dashed grey line) and forecast (after dashed grey line) simulations.

5.4 Application to Currency Creek and Finnis River region

Bathymetric information for the Currency Creek and Finnis River high-resolution sub-domain was supplied by DENR and interpolated onto a constant width grid of 100m in the area from Goolwa to Clayton (Figure 5.12). Some manual smoothing of coarsely resolved regions was conducted to improve flow continuity. A variable vertical grid resolution was used to better resolve the shallow areas, the resolution was set at 0.2m for the top 1.6m and then gradually increased to a maximum of 0.5m at the bottom of the domain. Based on numerical stability limitations a time-step of 200 seconds was adopted and this ensured the Courant-Friedrich-Lowry (CFL) condition remained <0.7 .

The model has several boundary forcing locations configured (Figure 5.12):

- Open boundary forcing at connection to main lake;
- Finnis River inflow;
- Currency Creek inflow;
- Goolwa barrage saline seepage.

On the eastern most edge of the domain (approximately 1km east of Clayton), the model is configured to have an open boundary and the height is specified based on water level data. The physico-chemical, geochemical and biological water attributes are specified from the AA domain (see Figure 5.9a) validation simulation conducted over the same period, thereby nesting this high-resolution sub-domain within this larger simulation. River boundary conditions were specified upstream of the Finnis River and Currency Creek tributaries. Flow data for these are as plotted previously (Figure 5.11b). The water quality attributes of the rivers and open edge are plotted in Figure 5.13 for key variables (other unmeasured or not important variables were set to default values or zero, respectively).

In addition to wind and inflow forcing, the model was configured to simulate the surface thermodynamics, and the correction for non-neutral atmospheric boundary layers was also applied. Meteorological data was used from a variety of sources. The 15-minute data from the Currency Creek weather station was used for rain, relative humidity, air-temperature, and wind speed and direction (Figure 5.14). Solar radiation data was obtained from Hindmarsh Valley (located approximately 20 km west of the site), and long-wave radiation was estimated from available net-radiation data also collected at this site (Figure 5.5) by subtracting the shortwave component. The extinction coefficient is dynamically calculated by CAEDYM, but found to be critical in capturing the evaporation rate and subsequent water balance of the site (refer to description for Lake Albert validation). In CAEDYM the photosynthetically active component (PAR) was set to 45% and had an extinction value generally $>2\text{m}^{-1}$, and the remainder of the shortwave bandwidth was configured to be even more highly attenuated ($>3\text{m}^{-1}$) as was the case in Lake Albert.

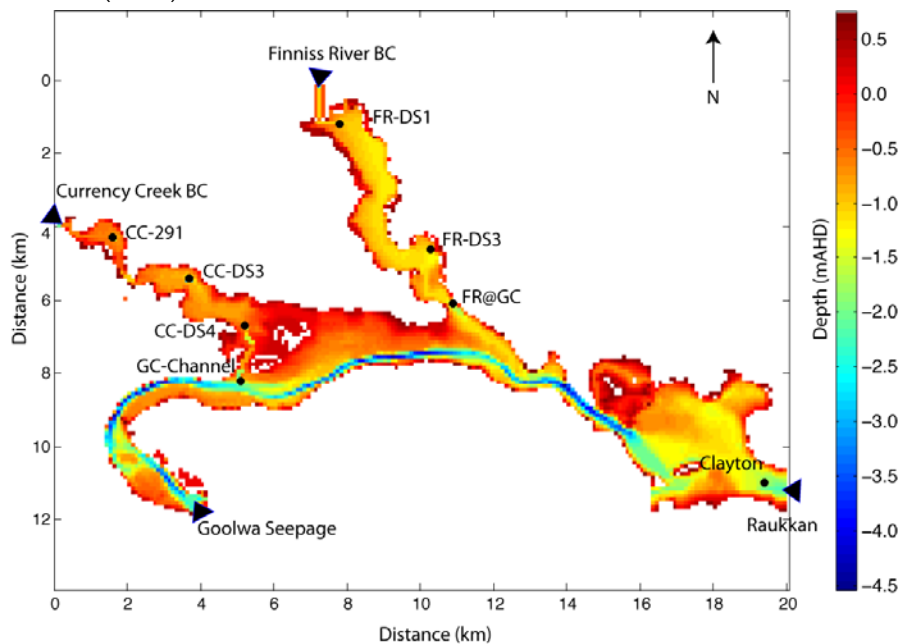


Figure 5.12: Model bathymetry for high-resolution (100 × 100m) Currency Creek and Finnis River domain, showing the boundary forcing locations, the open boundary connection point with the main Lake Alexandrina domain, and the sampling locations (●) used to validate the model.

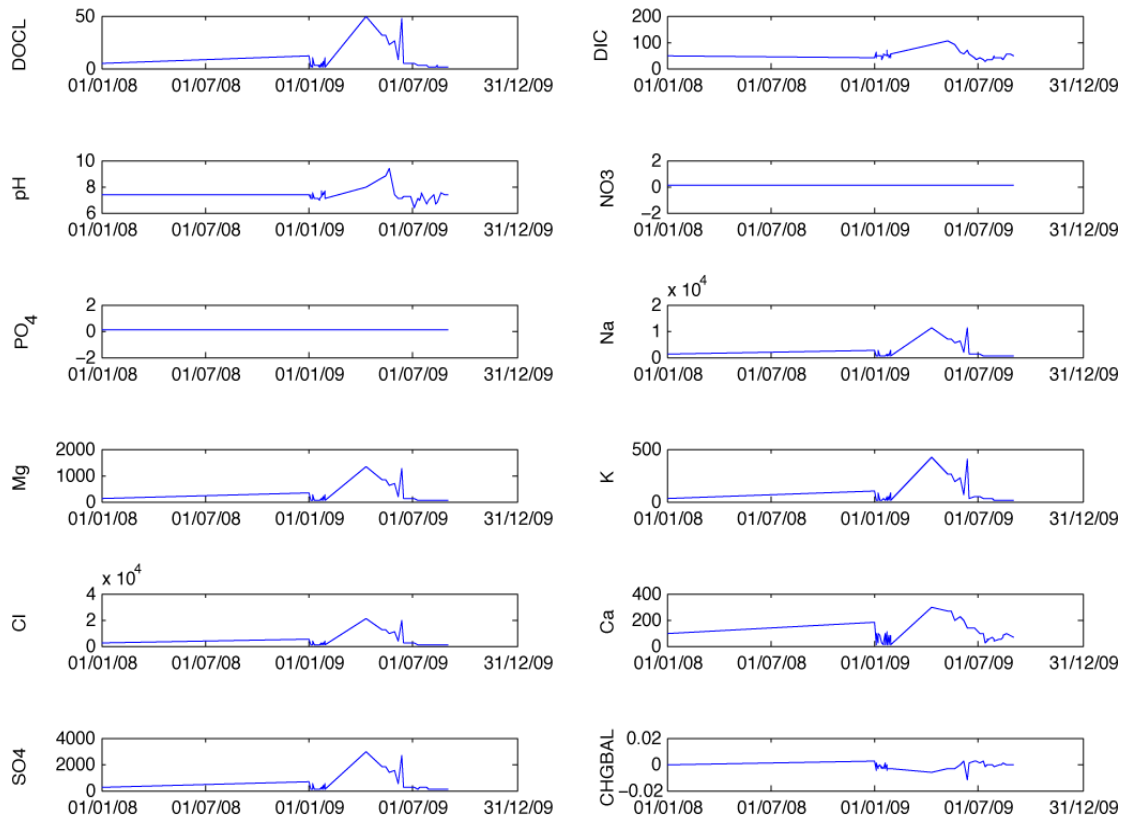


Figure 5.13a: Time-series water quality attributes used for the Finniss River boundary condition.
 Note a lack of data prior to Jan 2009 and constant values used for 2008.

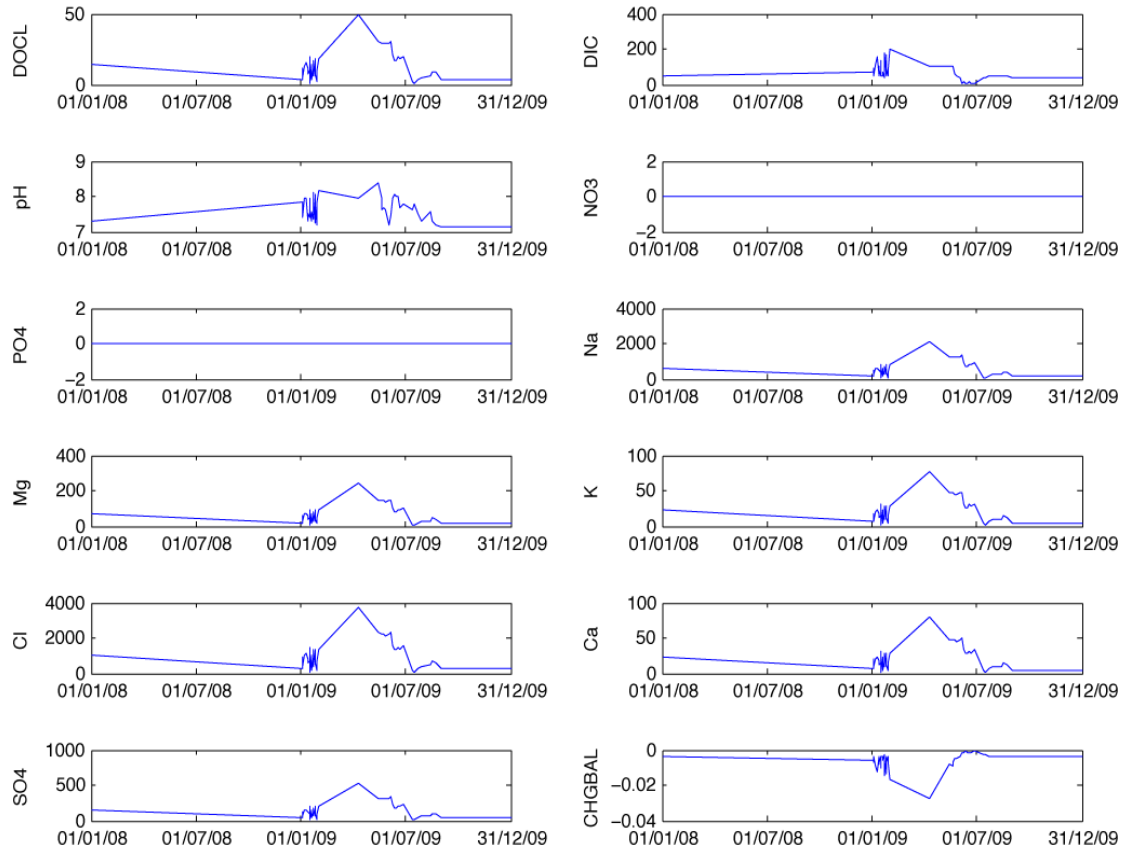


Figure 5.13b: Time-series of water quality attributes used for the Currency Creek boundary condition.
 Note a lack of data prior to Jan 2009 and constant values used for 2008.

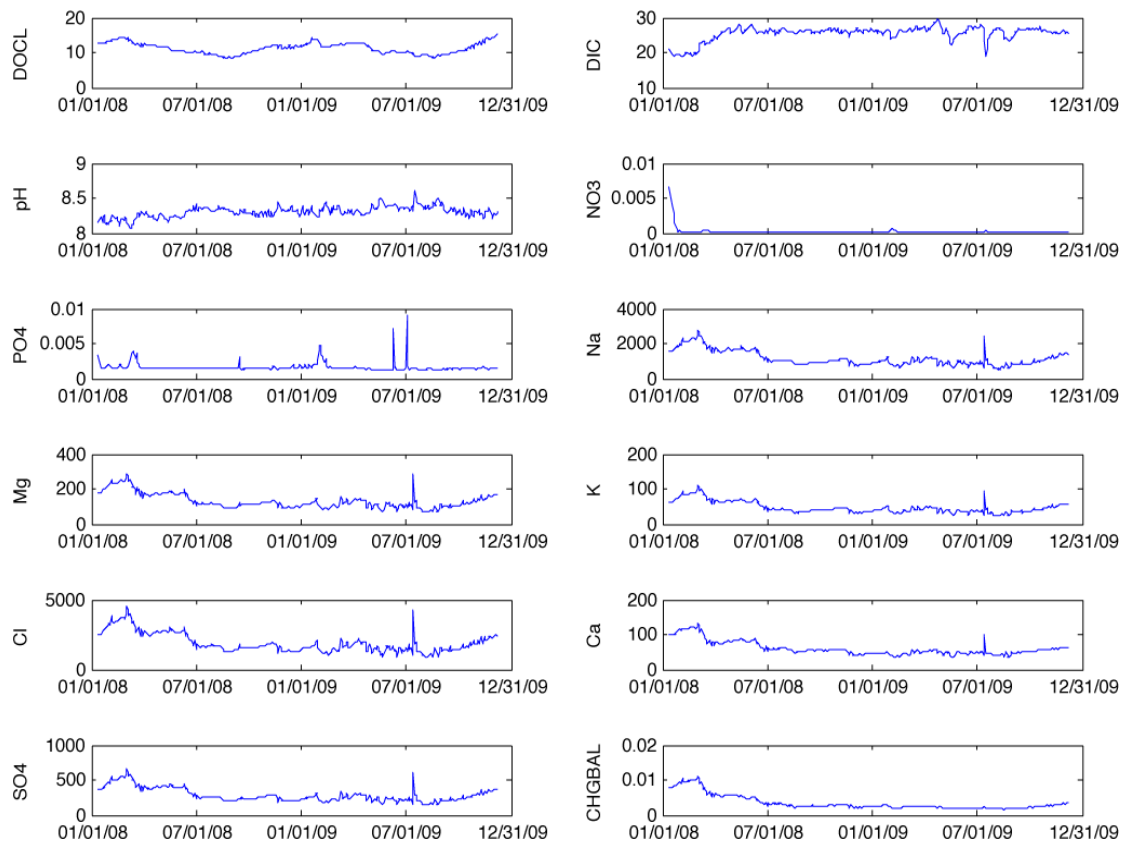


Figure 5.13c: Time-series of water quality attributes used for the open boundary connection with the main lake. Data extracted from profile output point from the Lake Alexandrina (AA) model simulation.

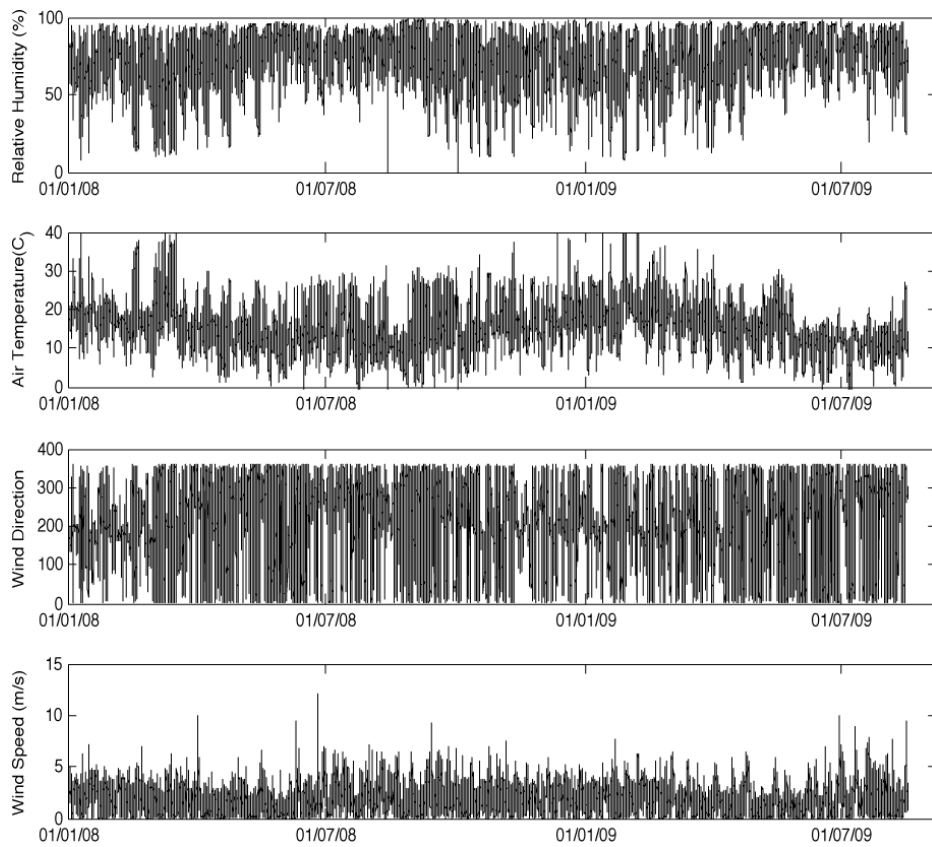


Figure 5.14: Currency Creek meteorological station data used in the validation sub-domain.

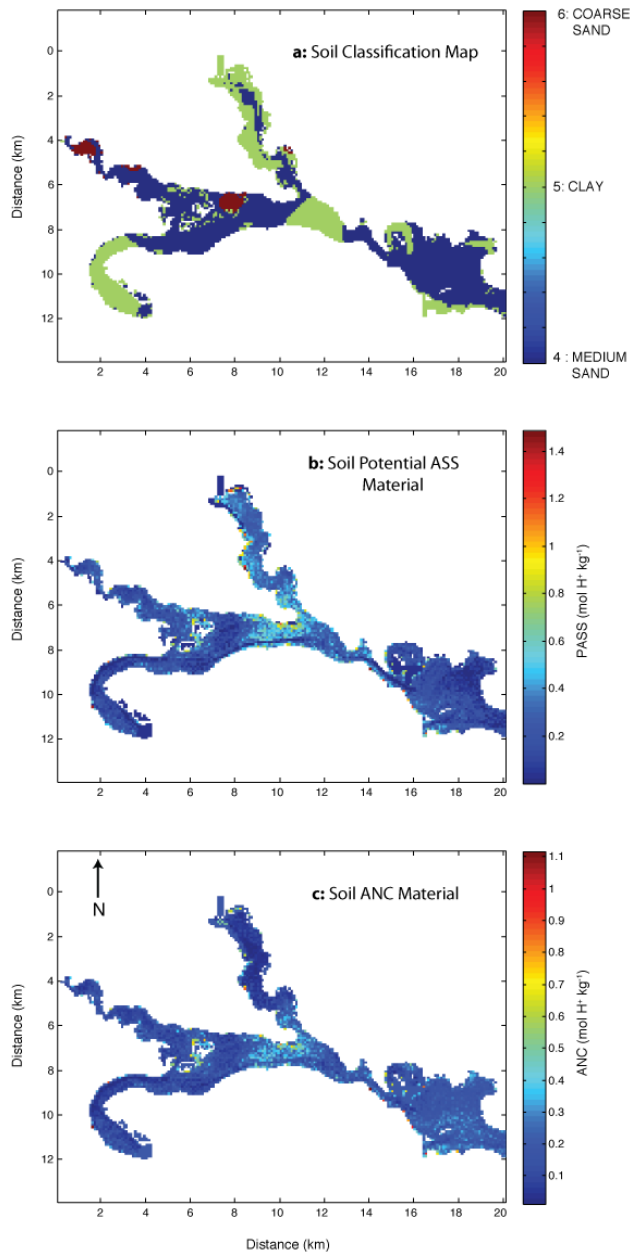


Figure 5.15: Soil property specifications.

The soil characteristics defined for the acid sulfate soil model are shown in Figure 5.15. The lake-bed was configured to have areas of coarse sand, medium sand and clay as outlined in Figure 5.15a, based on the CSIRO mapping data (Fitzpatrick et al., 2010) that has been interpolated onto the ELCOM 100x100m numerical domain.

The simulations were configured to begin at midnight on 1 Jun 2008. Initial values for the lake were estimated from available water level, temperature, salinity (DFW) and water quality data (EPA) collected at that time from various stations, across the site. Initial values of soil properties were input at each grid cell for PASS (Figure 5.15b) and ANC (Figure 5.15c), again by interpolating mapping data from Fitzpatrick et al. (2010) onto the ELCOM 100x100m numerical domain. Vertical profiles of ANC and PASS below the top 20cm were specified based on Figure 5.16.

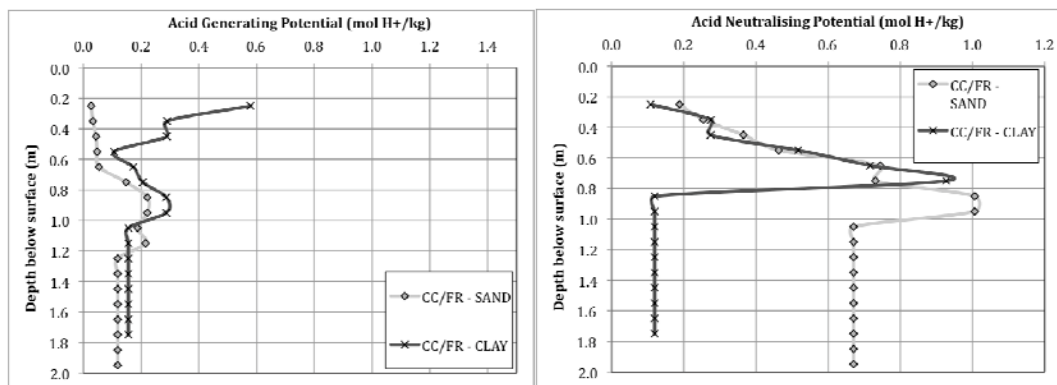


Figure 5.16: Vertical profiles of acid generating potential (AGP, left) and acid neutralising capacity (ANC, right) estimated from available core information from Lake Albert. Data compiled by Earth Systems (2010).

6 Model validation

In this chapter, the results of model hindcast simulations are presented and compared to available lake physical, chemical and biological data from a range of sources. The main data source was the routine data collection stations from the SA Environmental Protection Authority (EPA) (Figure 6.0), and supporting data was also obtained from the SA Department for Water (DFW), SA Water, and the associated Lower Lakes ASS projects.

Due to the acidification that occurred in the Currency Creek region during 2009, the EPA implemented a further intensive monitoring campaign with more high-resolution sampling sites. This data provided important validation data relevant to the high-resolution sub-domain (Section 6.3). The map of the output validation points relevant to the sampling locations is shown in Figure 5.12 along with the model bathymetry.

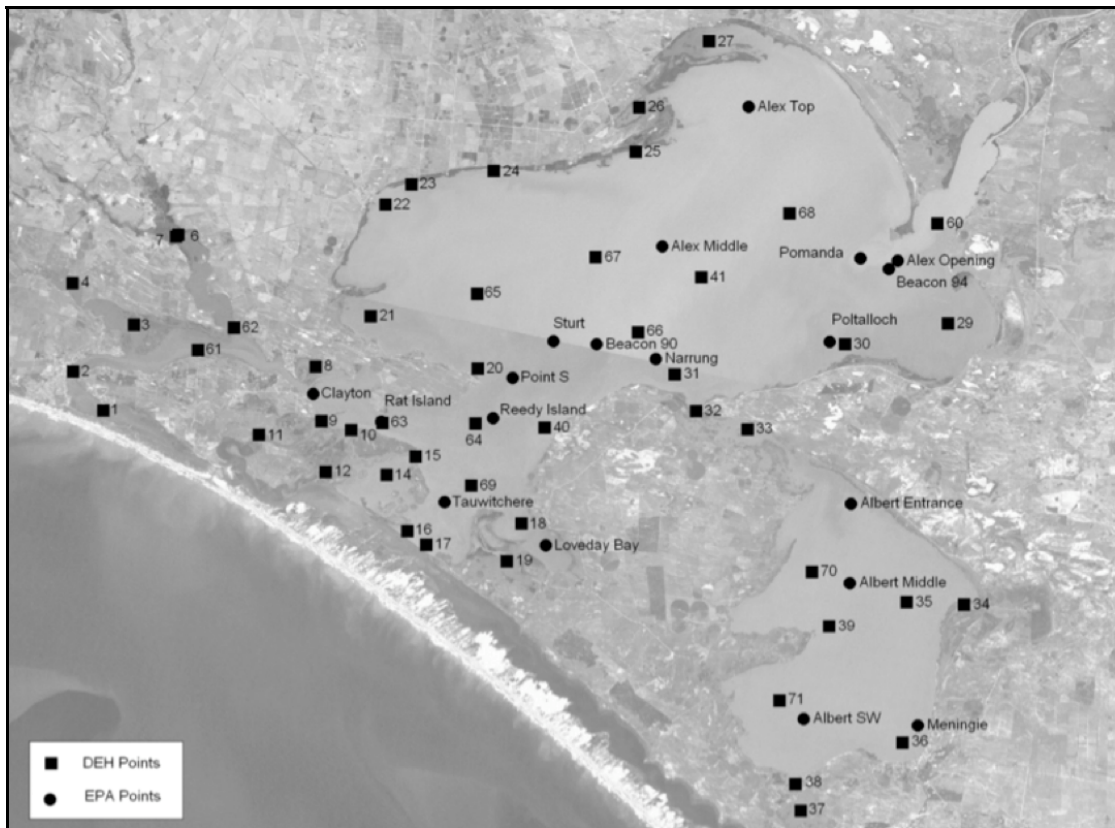


Figure 6.1: Locations of various output reporting locations in Lake Alexandrina and Lake Albert. The EPA points (19 circles) are routine sampling locations for water quality parameters by the South Australian Environmental Protection Authority (EPA) which are the focus of this assessment. The DENR points (squares) are additional output points not presented in this report but have been provided for further ecological risk assessment. Plot adapted from BMTWBM (2010).

6.1 Lake Albert: validation (Jun 2008 – Sep 2009)

Lake physical properties

Initially simulations were conducted with wind speed data from Narrung, however the model was persistently under-predicting evaporation. Pelican Point wind data was trialed instead and gave a better prediction, particularly with the wind drag coefficient set to 0.0014 Nm^{-2} (relative to the default of $0.0010 - 0.0013 \text{ Nm}^{-2}$). As shown in Figure 5.4, the Pelican Pt wind speed was approximately 15% higher than that from Narrung.

The free surface height prediction was also sensitive to the extinction coefficient, through its effect on surface temperature and evaporation. Extinction values below 1.5 m^{-1} allowed penetration of the

solar radiation deep into the water and lower surface temperatures, leading to lower evaporation rates and ultimately an over prediction in water balance. With CAEDYM simulated extinction values were dynamically simulated and tended to be greater than 2 m^{-1} and at times greater than 3 m^{-1} .

With the Pelican Pt wind data and the high extinction coefficients, the daily evaporation from ELCOM was approximately 80% of the theoretical potential evaporation from the Narrung weather station, as calculated from the Penman-Monteith equation. There was some scatter around this relationship but this is expected due to the different calculation methods and since the Penman-Monteith is not ideal for open water. A value of 80% of the potential rate is normally applied as a pan-to-lake correction factor so the predictions are therefore considered to be representative of the observed conditions.

The surface temperatures with the above configuration were well predicted throughout the simulation period (Figure 6.1) and compared well with both the EPA grab data and the real-time DFW temperature loggers. No spatial variability was seen in this data or in the model, as is expected given that the changes are driven by surface meteorological conditions that are set to be uniform across the lake (except for wind). For salinity however (plotted as electrical conductivity at 25°C , Figure 6.1), there is a notable mixing zone between the Narrung region and the main body of the lake (denoted '*AlbertEntrance*'). For the other stations the model captured the seasonal trend in evapo-concentration well, although it did slightly over-predict the salinity in the summer period in the main body of the lake, likely as a result of errors in the water level prediction.

Nutrients and Chl-a

Dissolved Oxygen showed no difference between the simulations and the lake remains fully oxygenated (Figure 6.2); DO varies in line with solubility changes brought about by variable temperature and salinity conditions. The DOC level follows the seasonal trend (Figure 6.2) however the concentration is over predicted in the summer. Since the conservative ions like Cl are predicted well, this would imply evapo-concentration levels are captured well (described in the next section) and that there is rather an under prediction on DOC decay during the warm summer period. NH_4 and NO_3 levels are low throughout the period (Figure 6.4) and it should be noted that as soluble nutrient results were often below detection limit, these are not actual measured values that are plotted and any discrepancy with model outputs may not be as significant. TN is however quite high and is reasonably captured by the model except for some over concentration in the summer, likely for similar reasons as DOC – that is DON mineralization (and subsequent denitrification) is being under predicted. PO_4 is well predicted and TP is similar in trend as TN. Total Chlorophyll-a (Figure 6.5) is high and the model captures the magnitude of the biomass as well as the limited variability in the concentration throughout the year. The data indicates a higher Chl-a concentration at the *AlbertEntrance* location that is under-predicted by the model, suggesting the growth in the Narrung Narrows is too low.

Lake geochemistry

Comparisons of DIC and Ca from simulations with and without mineral phases highlight the role of calcite solubility control on alkalinity buffering during the validation period (Figure 6.6). The validation simulation run without mineral precipitation/dissolution enabled (nPP) shows high concentrations of both DIC and Ca over the summer period, that were not reflected in the field data. The simulation with solubility control enabled (yPP) however showed a great improvement in predictive ability for both these components. Note that this simulation was run several times with variable K_{sp} coefficients for calcite (generally assumed to be -8.48) in order to adjust the model to best fit the data. The original value used for calcite over-predicted the precipitation and loss of Ca and DIC, so it was adjusted towards the aragonite solubility ($K_{sp} = -8.3$), which ultimately gave the best result. Lazar et al. (1983) highlight the behaviour observed here in lab experiments confirming the role of aragonite, and it has been noted in marine chemistry literature that there is slow kinetic of precipitation of calcite in presence of Mg^{2+} .

The remaining geochemical variables (Cl & Na, Figure 6.7; Mg & SO_4 , Figure 6.8; pH and CHGBAL, Figure 6.9) were all predicted accurately by the model. The dissolved metals were also simulated but were zero during the validation period, as expected (Figure 6.10 & 6.11).

The spatial distribution of soil acidity predicted by the model (Figure 6.12) compares favourably with Fitzpatrick et al. (2010) TAA and surface soil pH maps that (not shown) highlight areas of high acidity near the Narrung Narrows opening to Lake Albert, on the western and southern margins, and patches elsewhere around the lake edge.

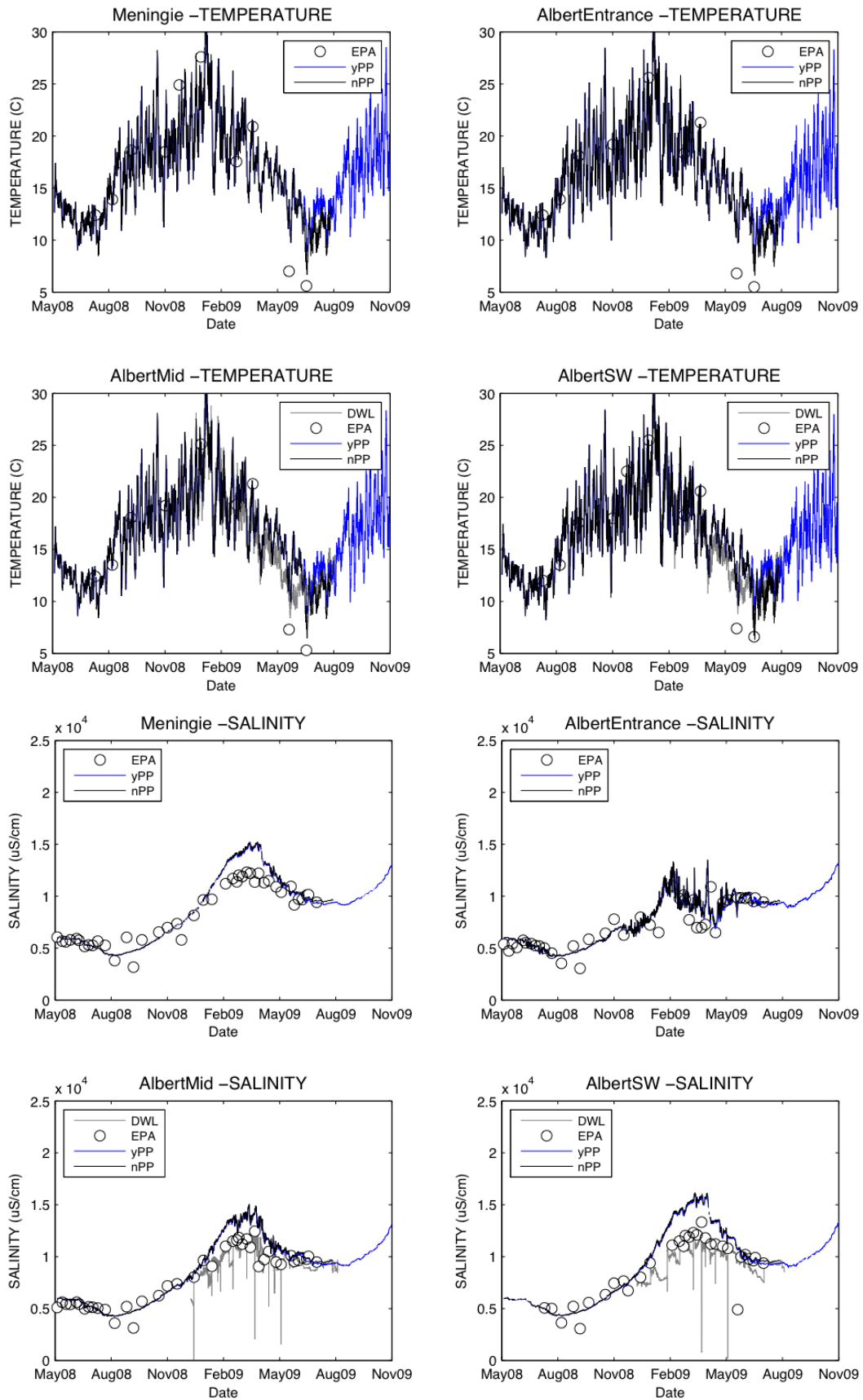


Figure 6.1: Comparison of modelled (yPP and nPP) and measured (EPA and DFW) water temperature and salinity (expressed as electrical conductivity at 25°C) for four stations within Lake Albert.

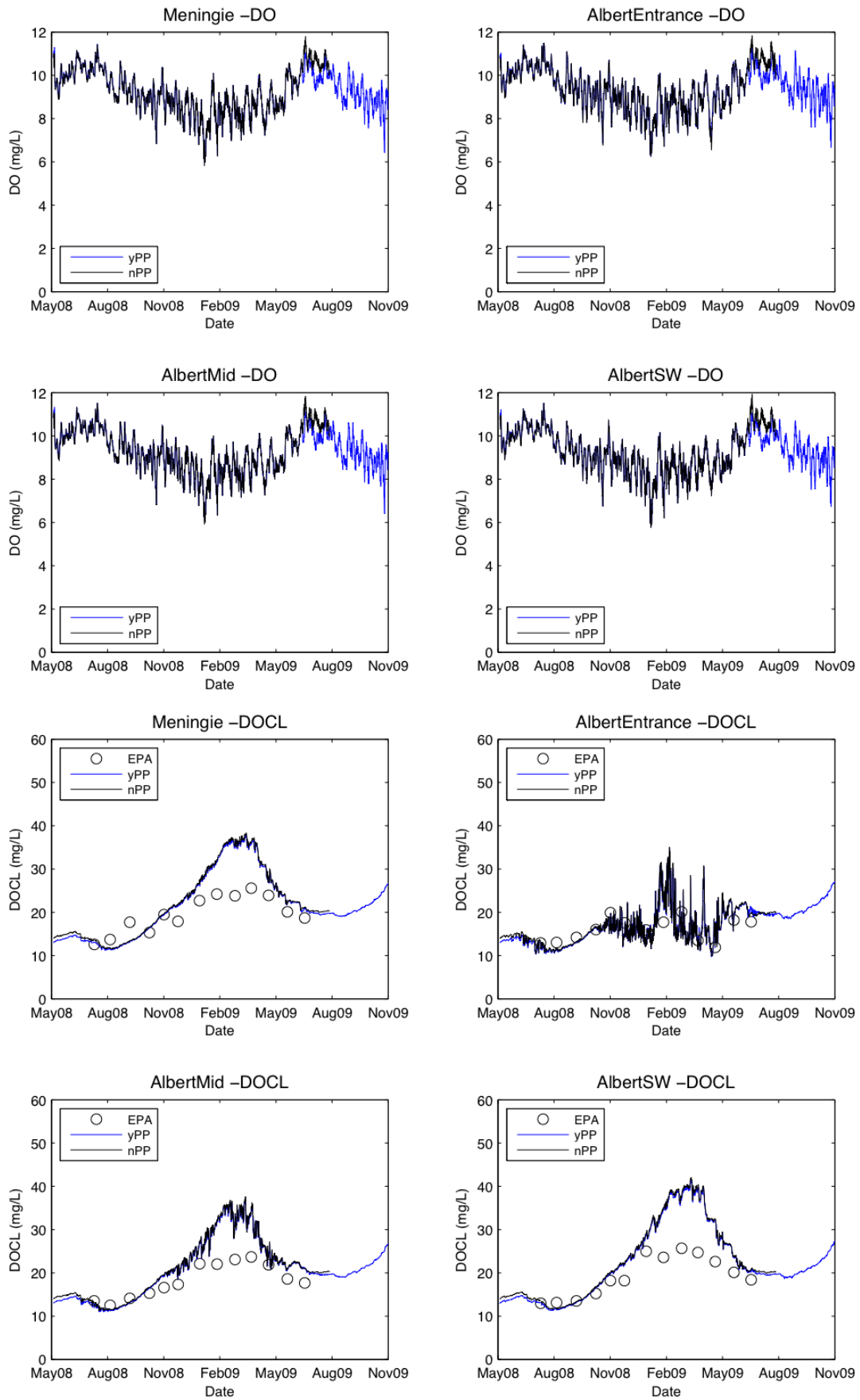


Figure 6.2: Comparison of modelled (yPP and nPP) and measured (EPA) DO (mg L⁻¹) and DOC (mg C L⁻¹) for four stations within Lake Albert.

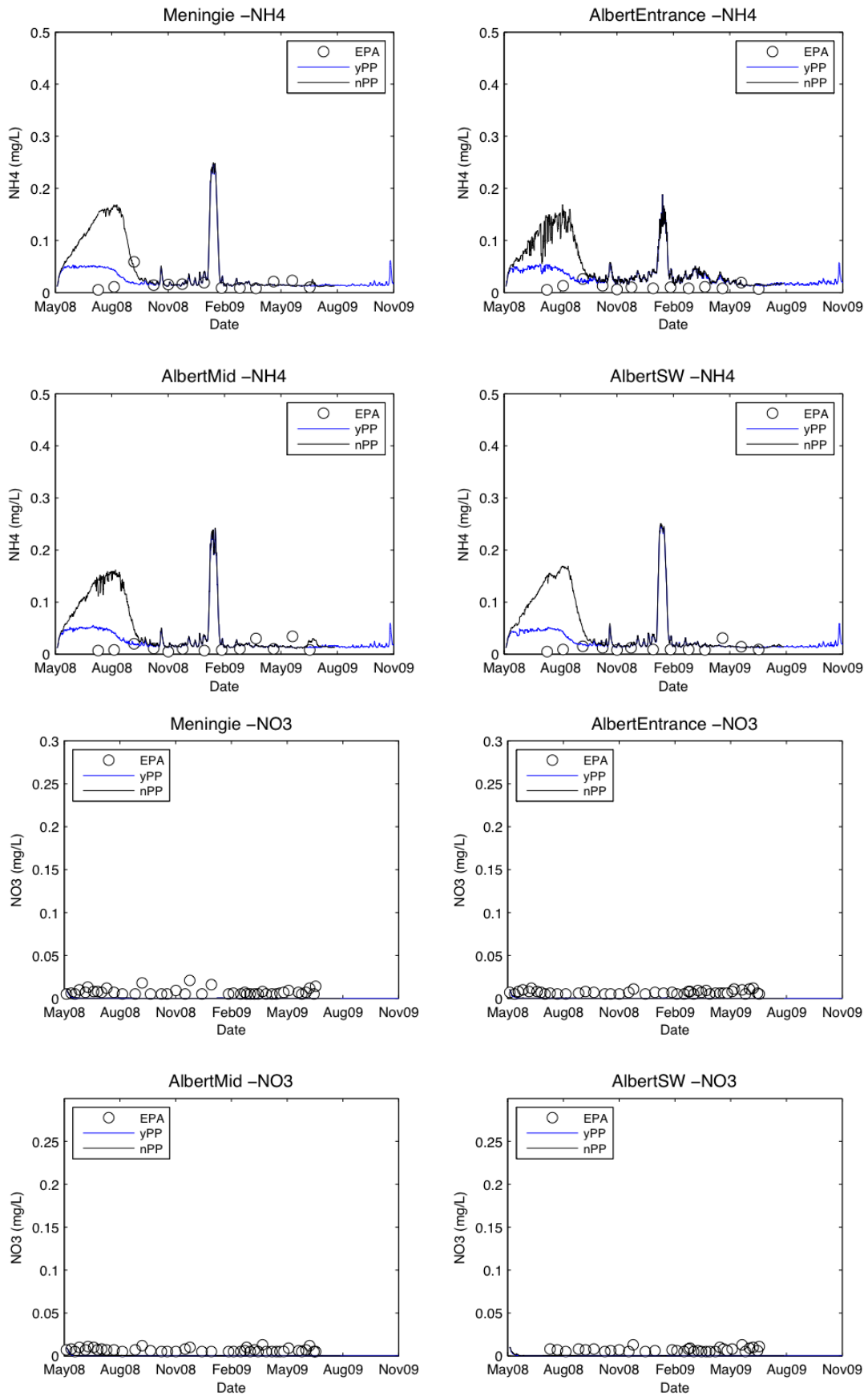


Figure 6.3: Comparison of modelled (yPP and nPP) and measured (EPA) NH₄ (mg N L⁻¹) and NO₃ (mg N L⁻¹) for four stations within Lake Albert. Note that the NO₃/NH₄ results were often below detection limit.

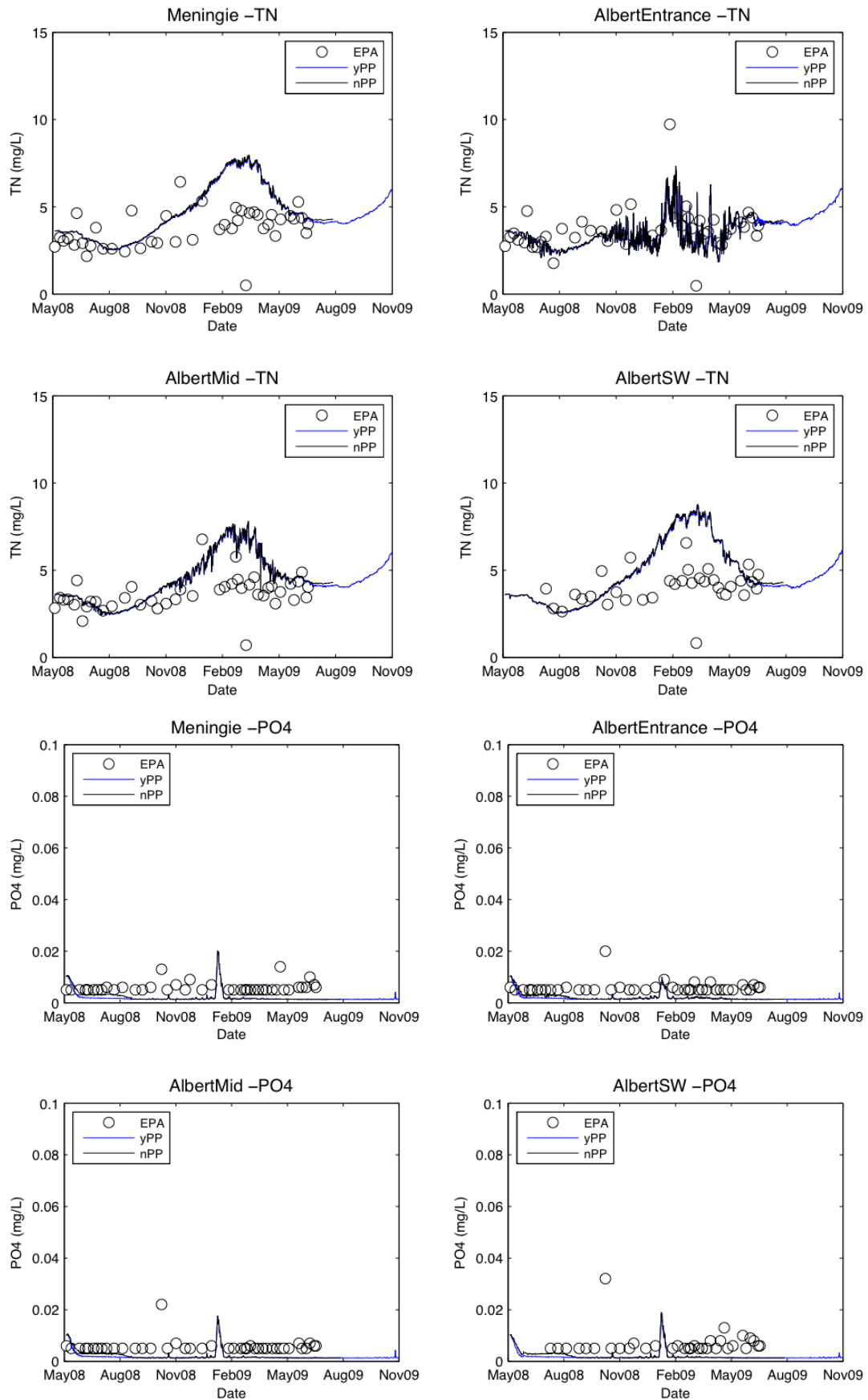


Figure 6.4: Comparison of modelled (yPP and nPP) and measured (EPA) TN (mg N L^{-1}) and PO₄ (mg P L^{-1}) for four stations within Lake Albert. Note that the PO₄ results were often below detection limit.

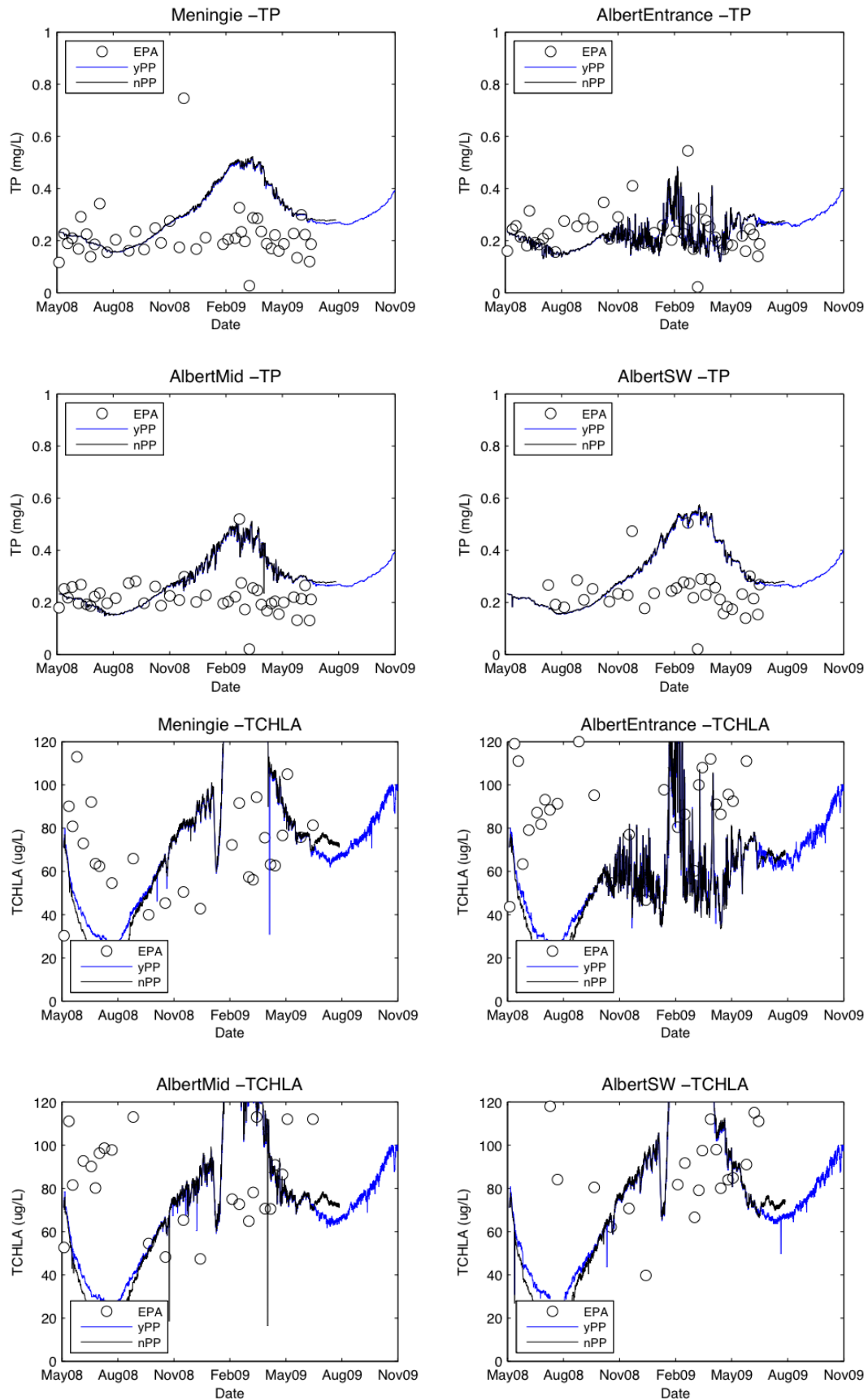


Figure 6.5: Comparison of modelled (yPP and nPP) and measured (EPA) TP (mg P L^{-1}) and total Chlorophyll-a (ug Chla L^{-1}) for four stations within Lake Albert.

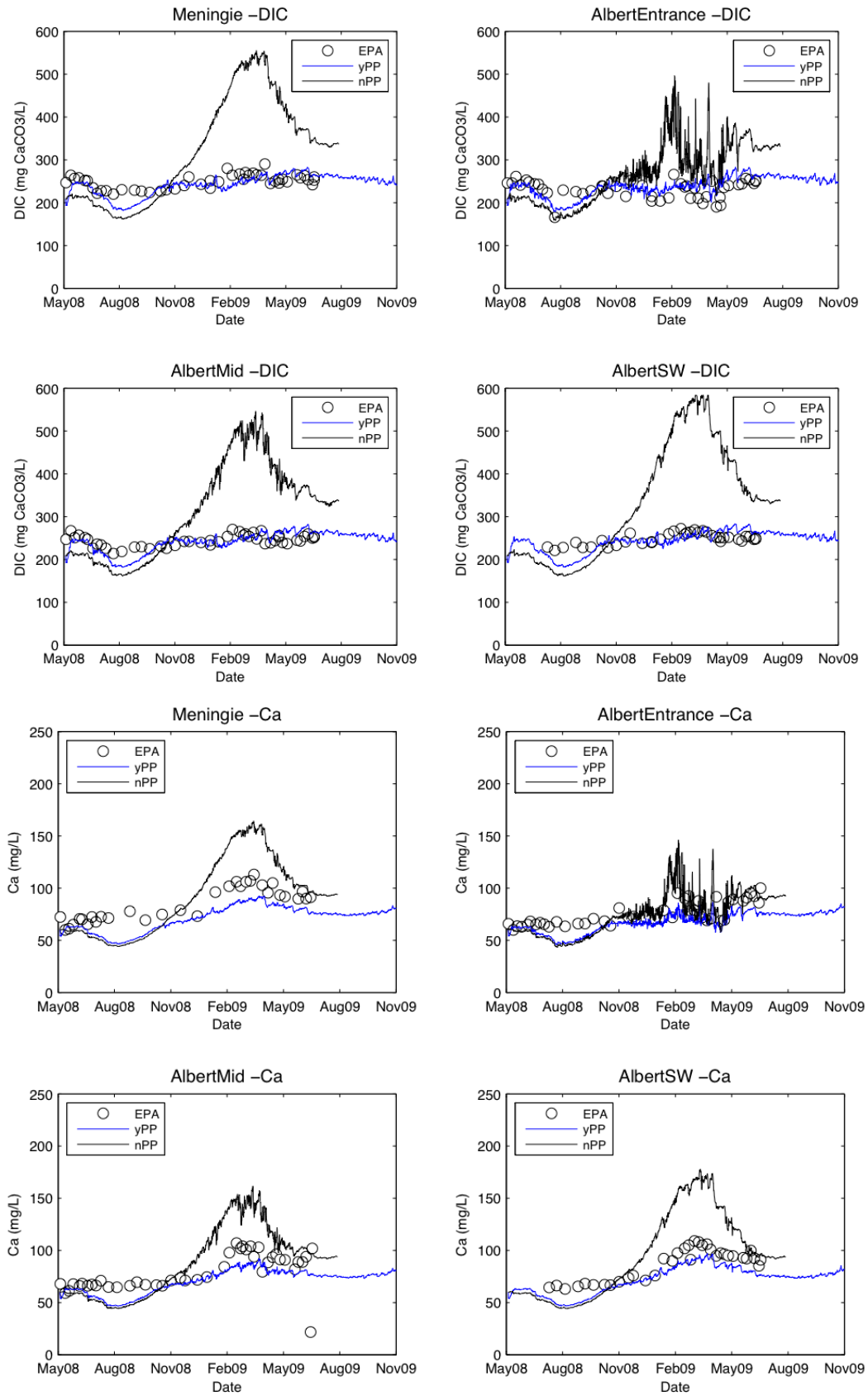


Figure 6.6: Comparison of modelled (yPP and nPP) and measured (EPA) DIC (expressed as alkalinity in terms of $\text{mg CaCO}_3 \text{ L}^{-1}$) and Ca (mg L^{-1}) for four stations within Lake Albert.

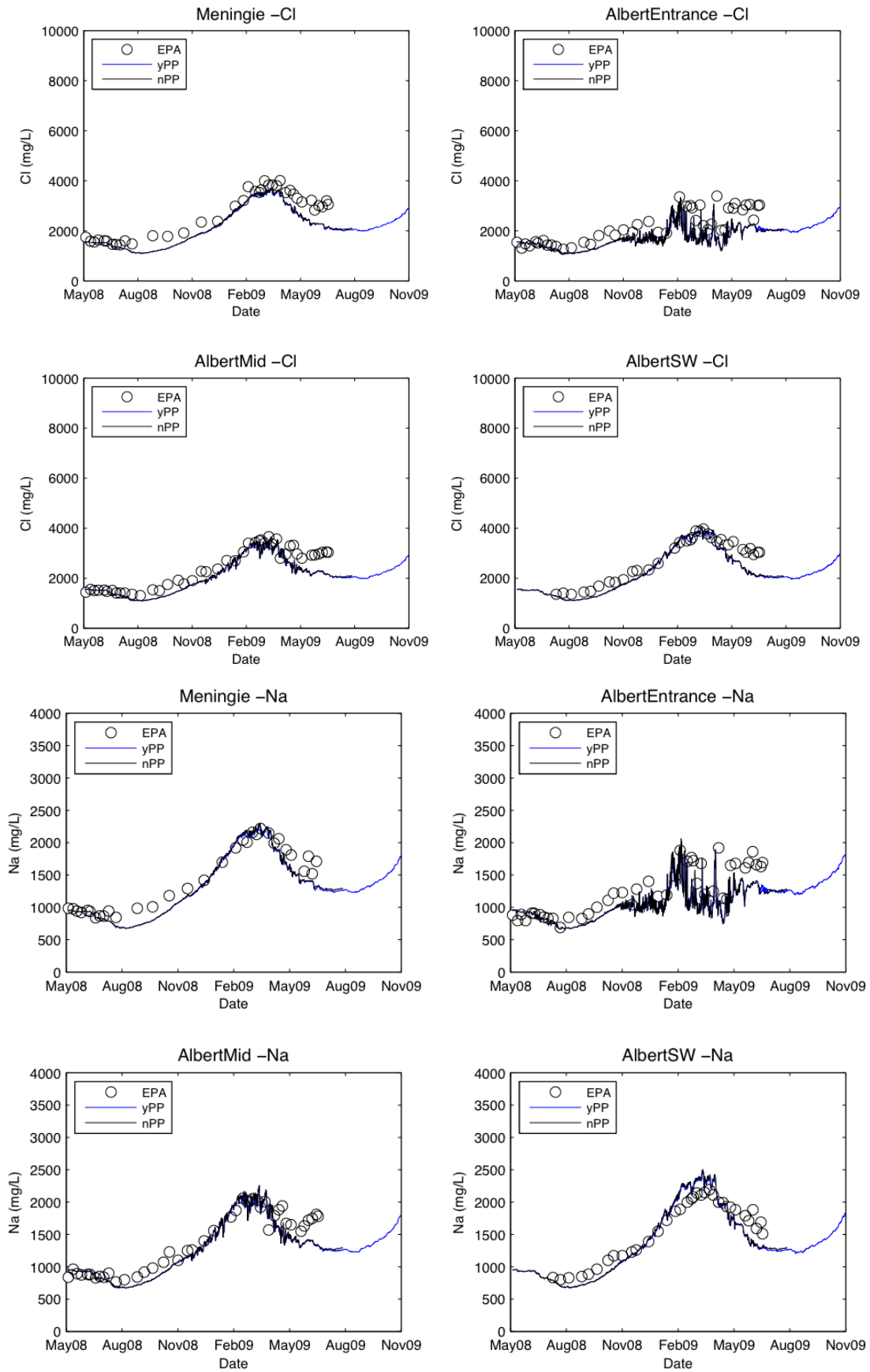


Figure 6.7: Comparison of modelled (yPP and nPP) and measured (EPA) Cl (mg L⁻¹) and Na (mg L⁻¹) for four stations within Lake Albert.

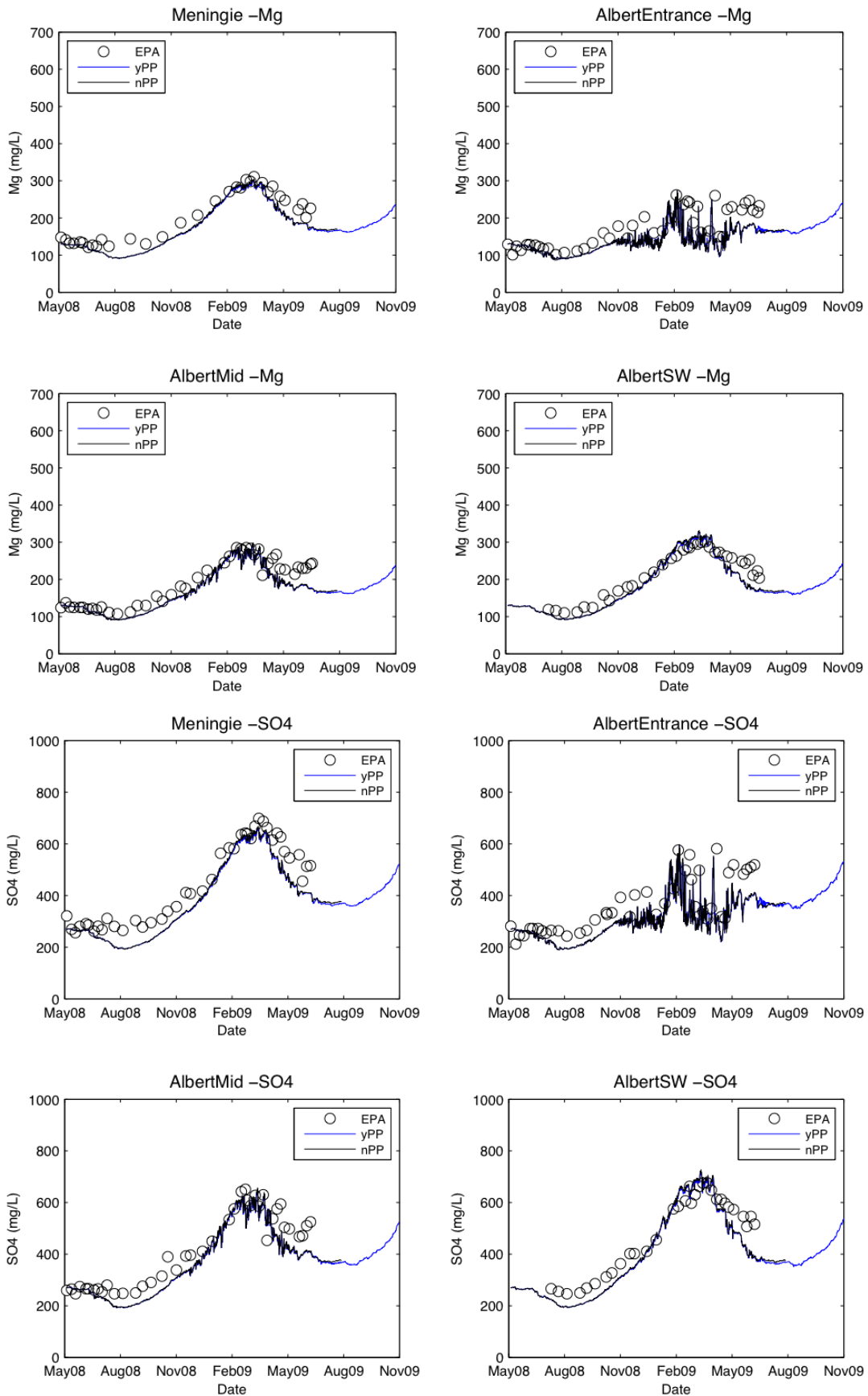


Figure 6.8: Comparison of modelled (yPP and nPP) and measured (EPA) Mg (mg L⁻¹) and SO₄ (mg L⁻¹) for four stations within Lake Albert.

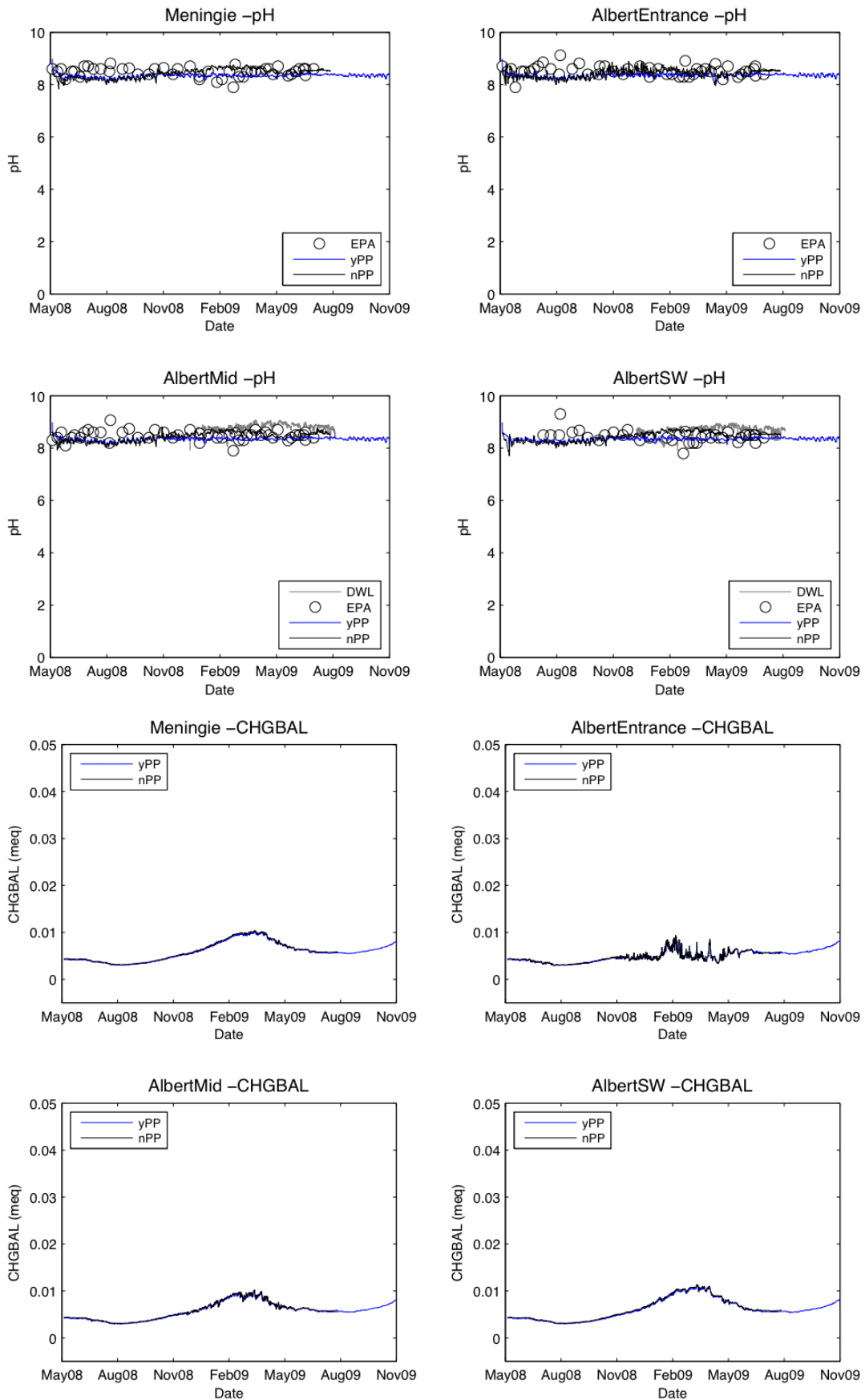


Figure 6.9: Comparison of modelled (yPP and nPP) and measured (EPA and DFW) pH (-) and CHGBAL for four stations within Lake Albert.

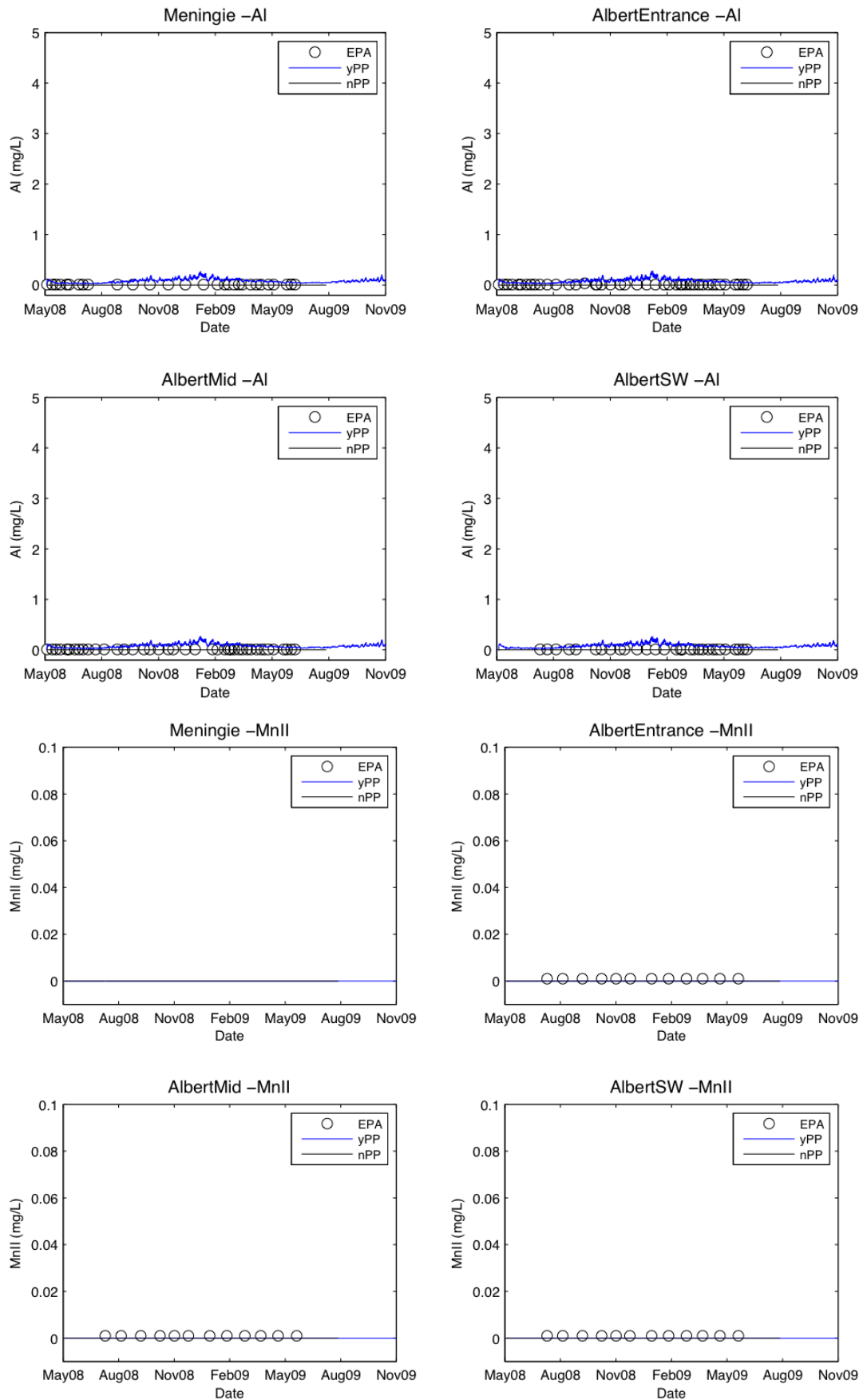


Figure 6.10: Comparison of modelled (yPP and nPP) and measured (EPA) dissolved Al (mg L^{-1}) and dissolved Mn (mg L^{-1}) for four stations within Lake Albert.

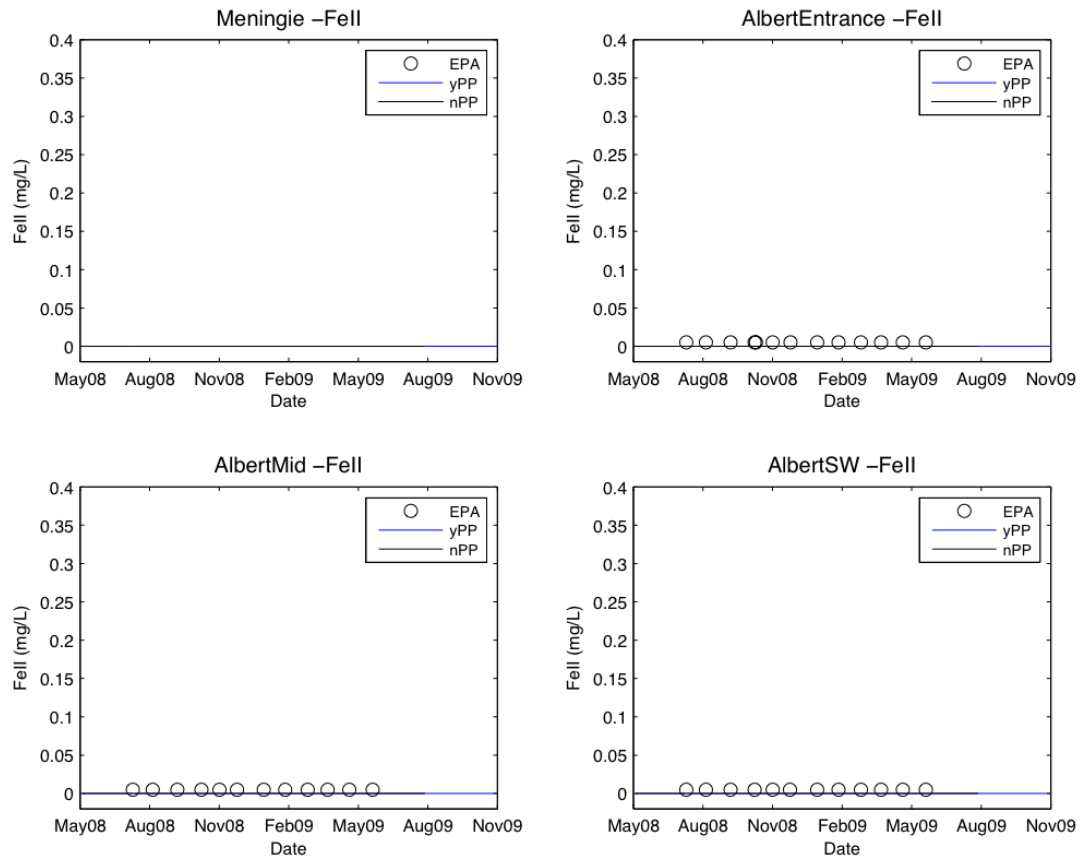


Figure 6.11: Comparison of modelled (yPP and nPP) and measured (EPA) dissolved Fe (mg L^{-1}) for four stations within Lake Albert.

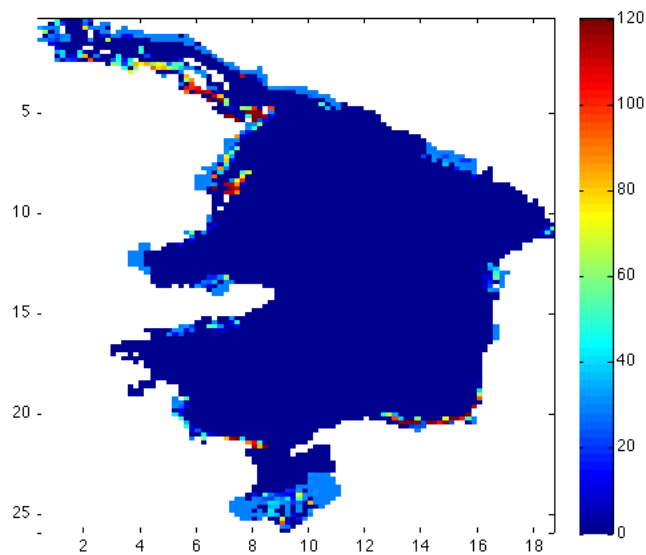


Figure 6.12: Plot of modelled surface acidity ($\text{mol H}^+ \text{m}^{-2}$) taken in Sep 2009. Spatial distribution compares favourably with Fitzpatrick et al. (2010) TAA and surface soil pH maps.

